Counteraction of buoyancy flow in high temperature aquifer thermal energy storage systems by applying multiple partially penetrating wells

80.0

Counteraction of buoyancy flow in high temperature aquifer thermal energy storage systems by applying multiple partially penetrating wells

by

K.S. Marif

In partial fulfilment of the requirements for the degree of

Master of Science

in Civil Engineering
at the Delft University of Technology

Personal information:	**K.S. Marif**	TU Delft, Water Management
		Student number: 4211820
		Tel: +31653291381
		Email: kizjeemarif@gmail.com
Thesis Committee :	**Prof. dr. ir. M. Bakker** Chairman	TU Delft, Water Management
	dr. Ir. J.M. Bloemendal Supervisor	TU Delft, Water Managment & KWR
	dr. N. Hartog Supervisor	Utrecht University & KWR
	dr. R.R.P van Nooijen Supervisor	TU Delft, Water Management
	dr. P. Vardon Supervisor	TU Delft, Geo-technical Engineering

*TU*Delft Delft University of Technology   **KWR**

An electronic version of this report is available at: `http://repository.tudelft.nl/`.

Preface

The document that lies before you contains my Master's thesis, written in fulfilment of the Water Management curriculum. Water Management is one of the master tracks of Civil Engineering at Delft University of Technology.

While this thesis was written as an individual research project I would like to express my gratitude to all people who supported me during my time of conducting this research.

First of all, I would like to thank all members of my thesis committee for their support and guidance. Thank you Prof.dr.ir. Mark Bakker, chairman of the committee. Your feedback, eye for detail and food-for-thought really led to a better research. I would also like to thank Dr. Ronald van Nooijen and Dr. Phil Vardon for their role as university supervisors. Though, we met only a couple of times your feedback was always encouraging and helped me put my work in to perspective.

Furthermore I would like to thank Dr. Niels Hartog, my supervisor at KWR. Our philosophical conversations about heat storage on the "cascade" were inspiring to think out of boxes and investigate new boundaries. The last member of my graduation committee I would like to express my gratitude to is my daily supervisor Dr.ir. Martin Bloemendal. Thank you Martin for our talks in office or in the car during the carpool, your feedback even outside office hours, and your genuine interest in my work.

Furthermore I would like show my appreciation to all people who indirectly contributed to my research. A pleasant working environment has been one of those contributions, for which I would like to thank KWR and all colleagues involved.

To my friends, family and Nathaniel, thank you for keeping things in perspective and reminding me of the fact that it is important to always accompany hard work with some well deserved relaxation

On that note I would like to invite you to read my thesis, I hope you enjoy reading.

Yours sincerely

K.S. Marif

Delft, November 2019

Abstract

The thermal recovery efficiency of High Temperature Aquifer Thermal Energy Storage (HT-ATES) systems can be limited due to the effect of buoyancy flow of the injected hot water. This thesis has researched the application of a Multiple Partially Penetrating Wells (MPPWs) as a well design method to counteract the effect of buoyancy flow and improve the performance of HT-ATES systems (>60°C). A MPPW is a well with more than one screen that allows injection and extraction of water at different depths in the aquifer.

This method to counteract the effect of buoyancy flow was tested through numerical modelling with SEAWATv4. The modelled HT-ATES systems were running for four recovery cycles each including injection-storage-extraction-rest phases. The thermal recovery efficiency was determined over these cycles for 7 different scenarios and four different cases: a) A regular HT-ATES system with a fully penetrating screen, b) a regular HT-ATES system where buoyancy flow is neglected, c) an HT-ATES system with a MPPW with two screens, d) an HT-ATES system with four screens. The latter case was tested for three different control approaches based on data from four different locations in the aquifer.

For the reference scenario where 90°C water was injected, a regular HT-ATES system had a thermal recovery efficiency of 0.61. With the application of MPPWs for both two or four screens this was 0.81 in the fourth recovery cycle, which approaches the case without buoyancy which had a thermal recovery efficiency of 0.88. The application of two or four screens did not show significant difference in thermal recovery efficiency after the first recovery cycle.

A sensitivity analysis showed that the absolute increase in thermal recovery efficiency of an HT-ATES system with a MPPW compared to a regular HT-ATES is higher for larger buoyancy flow (i.e, high injection temperature and high (vertical) hydraulic conductivity), smaller injection volume and larger aquifer thickness. An applicability analysis showed that application of MPPWs is beneficial if the buoyancy flow (which is defined as the vertical hydraulic conductivity times the density ratio of the ambient groundwater and injected water) is greater than 0.1 meters per day.

Keywords

High temperature aquifer thermal energy storage (HT-ATES), counteraction of buoyancy flow, thermal recovery efficiency, multiple partially penetrating well (MPPW), monitoring and control, numerical model.

Table of Contents

I	Analysis

II	Reflection

III	**Appendices**

1. Introduction

This chapter contains the introduction to this research report. An introduction to the topic and related problem description is given in Section 1.1. This is followed by the hypothesis and resulting research objective that is outlined in Section 1.2. The final section of this chapter, Section 1.3 provides the outline of this report.

1.1 Problem Description

In moderate climates like found in the Netherlands, heating accounts for nearly 40% of the total yearly energy consumption (ECN et al. 2016). Developing sustainable heating technology is therefore a key aspect in the energy transition that the Netherlands, and the rest of the world is facing as of 2019. Sustainable energy suppliers such as wind and solar energy undergo seasonal variation just as the energy demand. In general, the demand is high in winter and low in summer while the supply is high in summer and low in winter. Figure 1.1 illustrates the resulting mismatch between the energy demand and supply due to the seasonal variation of the two.
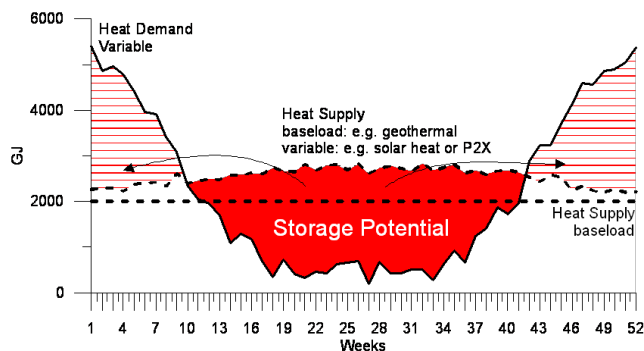

Figure 1.1: Seasonal variation of heat demand and supply (Hartog et al. 2018)

The possibility to store the available heat in summer when demand is low can be at high temperature (>60 °C) used as a buffer for the winter. High Temperature Aquifer Thermal Energy Storage (HT-ATES) is a method to store this heat in the subsurface. When using such high temperatures, the use of heat pumps becomes unnecessary. This makes these systems favorable as heat pumps are relatively energy consuming. Another advantage is that for the same amount of energy storage less space is needed when using higher temperatures.

Despite these advantages, the number of HT-ATES systems are limited. This is because the economic feasibility is mostly determined by the thermal recovery efficiency. Field experiments conducted showed relative low thermal recoveries of only 0.42 (Molz et al. 1983). This is due to loss of energy during the storage period. The total energy loss is the sum of loss by diffusion, conduction, dispersion and flow. Loss due to flow consists of background flow and buoyancy flow. Heat loss due to the effect of buoyancy flow can be significant for HT-ATES systems. The physical property causing the water to float is the

density. There is a non-linear relation between temperature and density, with increasing temperature the density decreases. This results that the injected water will flow in the upward direction which subsequently results in tilting of the hot water front.

Currently, the use of lower storage temperature and aquifers with low permeability are regarded as the main design option for HT-ATES systems to minimize the heat loss due to the effect of buoyancy flow. This limits the range of suitable aquifers and results in overall less energy storage for a certain storage volume. On top of that, the use of low-permeable aquifers decrease the hydraulic capacity of a system and increase the risk of clogging of the well by particles (Olsthoorn et al. 1982).
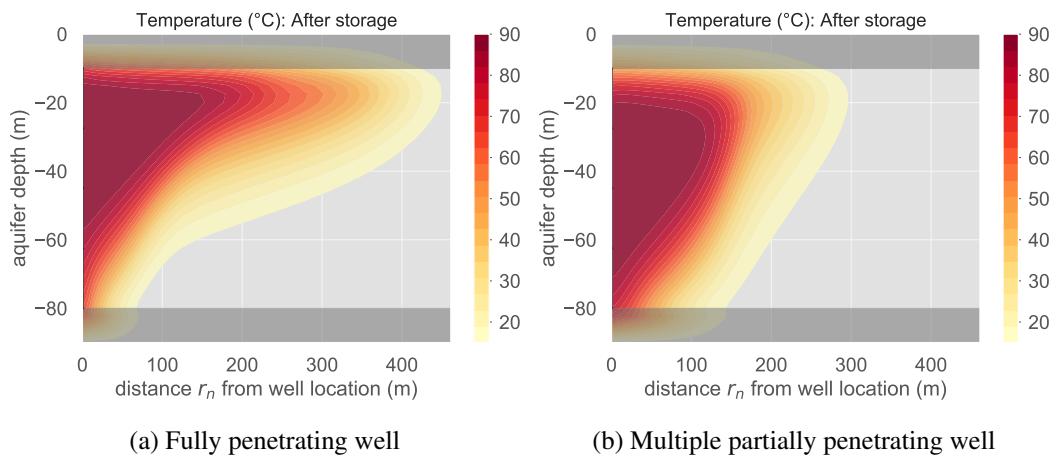

(a) Fully penetrating well   (b) Multiple partially penetrating well

Figure 1.2: Heat spread in the aquifer after storage for a) a fully penetrating well b) a multiple partially penetrating well where water nis injected in the lower half of the aquifer..

The use of multiple partially penetrating wells (MPPWs) is an alternative to deal with the buoyancy effect. The principle of MPPW is that the injection screen is located at a depth that is deeper than that of the recovery screen. By deeper injection, the hot water volume will have more time to reach the top of the aquifer resulting in less tilting of the thermal front after storage (Figure 1.2). By shallower extraction more hot water can be recovered, potentially increasing the thermal recovery efficiency significantly. This enables the use of aquifers with higher permeability and higher storage temperature.

1.2   Research Objective

This study explored the potential of the use of MPPWs to counteract the effect of buoyancy flow in HT-ATES with numerical modelling. The goal of this research was to meet the following objective;

> *"To design, develop, control, and assess the impact of the application of multiple partially penetrating wells on the performance of high temperature aquifer thermal energy storage systems in terms of thermal recovery efficiency."*

To meet this objective the work was carried out by answering the following sub-questions;

1. What are the effects of the application of MPPWs in terms of thermal recovery efficiency for different well configurations; screen lengths, distances between screens?
2. What are the effects in terms of thermal recovery efficiency of controlling HT-ATES systems with MPPWs, based on monitored data in the aquifer?

3. How is the control of HT-ATES system with MPPWs affected by the location of the monitoring points?
4. How is the performance of HT-ATES systems with MPPWs affected by the storage volume, aquifer thickness, and magnitude of buoyancy flow?
5. Under what conditions does application of MPPWs increase the recovery efficiency of HT-ATES systems?

This was done with numerical density-dependent flow simulations of a) regular HT-ATES system with a fully penetrating screen, b) a regular HT-ATES system where buoyancy flow was neglected, which provided an upper bound for the increase in thermal recovery efficiency obtainable by counteracting the effect of buoyancy flow, c) an HT-ATES system with the most basic MPPW design with two screens, and d) an HT-ATES system with MPPW with four screens that were operated by three different control approached based on four different monitoring locations.

1.3 Thesis outline

The thesis is divided in two main parts and 7 chapters. A short explanation of the content of the parts and chapters is given in the overview below and serves as a reader's guide to this thesis.

– **2. Background information:** This chapter provides the background information referred to throughout the research. The information in this chapter is the summarized result of the literature study conducted at the start of this thesis.

• <u>**Part I: Analysis:**</u> This part is the body of the thesis and focuses on proposing, developing, and assessing a MPPW design strategy for the optimization of HT-ATES performance.

– **3. Method and Materials:** In this chapter the research approach is given and discussed for the different MPPW designs and analyses. The proposed scenarios and assessment framework will be given.
– **4. Results:** In this chapter the main results of the simulated scenarios will be presented and discussed.

• <u>**Part II: Reflection:**</u> In part II a reflection on the thesis will be given. This is done by concluding and discussing the work, followed up by a set of recommendations for further research into the subject.

– **5. Discussion:** In the discussion the results of this research will be discussed.
– **6. Conclusion:** The most important findings will be summarized and the central research objective will be reviewed as conclusion to the thesis.
– **7. Recommendations:** Recommendations for future study purposes in the field of HT-ATES systems and MPPWs is given.

• <u>**Part III: Appendices:**</u> All additional information and figures not included in the main body of this thesis document are gathered in the appendices.

2. Background Information

This chapter provides the necessary background information for this research. It is started with the a general description of (HT-)ATES and where it stands within geothermal technologies (Section 2.1). This is followed by Section 2.2 where the processes inducing heat loss in HT-ATES are discussed. In Section 2.3 gives some background information on partially penetrating wells.

2.1 Aquifer Thermal Energy Storage

Aquifer thermal energy storage (ATES) systems is a geothermal technology. ATES is an open system where, groundwater in the water bearing soil layers known as aquifers is pumped up to be heated on spot with available residual heat originating for example from industries. The heated water is injected back into the aquifer and stored until the period where there is demand for heating and the flow direction is reversed and the hot water is extracted to heat buildings. Beside warm water, cold water can be stored which is in excess during winter and extracted in summer to cool buildings. ATES has taken an important role in the energy transition in the Netherlands. Although it can be labelled as a "green" measure, it is not a renewable energy technology but an energy conservation technology. It is different from Borehole Thermal Energy Storage (BTES) which is a closed system that stores the heat in a network of pipes in the subsurface.
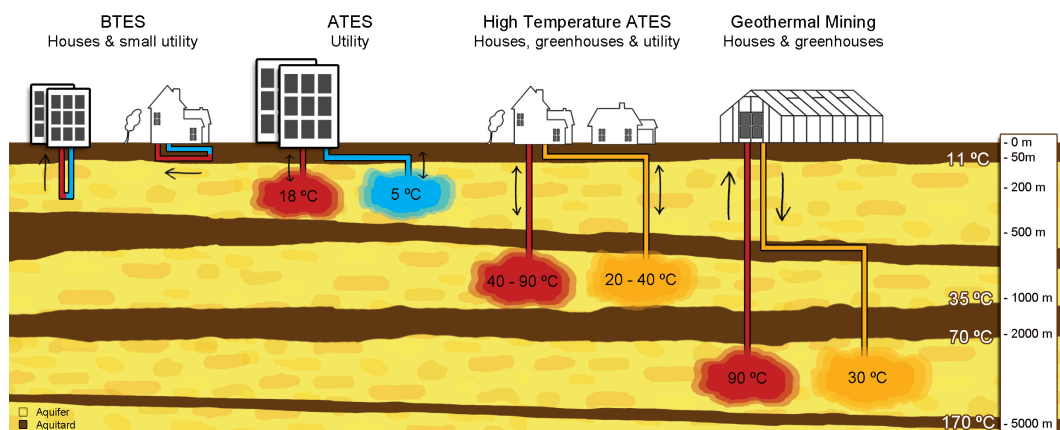

Figure 2.1: Geothermal energy systems as applied in the Netherlands (Bloemendal 2018)

2.1.1 System Types

There are different types of this technology that are categorized based on storage temperature, location in the aquifer and number of wells. First, a distinction can be made between Low Temperature Aquifer Thermal Energy Storage (LT-ATES) and High Temperature Energy Storage (HT-ATES). The first type is already widely used in the Netherlands. As of 2018, there are over 2,500 LT-ATES systems present in the Netherlands and the number is increasing. This type is usually referred to as ATES.

5

The injected hot water of these systems has a maximum temperature of 25 °C and are usually situated in shallow depths (50-250m). When extracting this water, it is not directly usable to heat up buildings and a heat pump is always used to get the water at the required temperature. These heat pumps need energy to function. When using HT-ATES systems, the use heat pumps can be minimized or even diminished. HT-ATES systems inject water that has a temperature above 60 °C. and are usually situated in deep aquifers deeper than 250m. Figure 2.1 shows a representation of the different geothermal energy systems in the Dutch subsurface.

Another distinction can be made on the number of boreholes. A system is called a monowell when only one borehole is drilled in the subsurface. The extraction and injection is done in two different screens that are separated in vertical direction. A doublet well is when two boreholes are drilled and are separated horizontally. Monowells are mostly used for small buildings while doublet are used for large utility buildings. A schematic presentation is shown in Figure 2.2
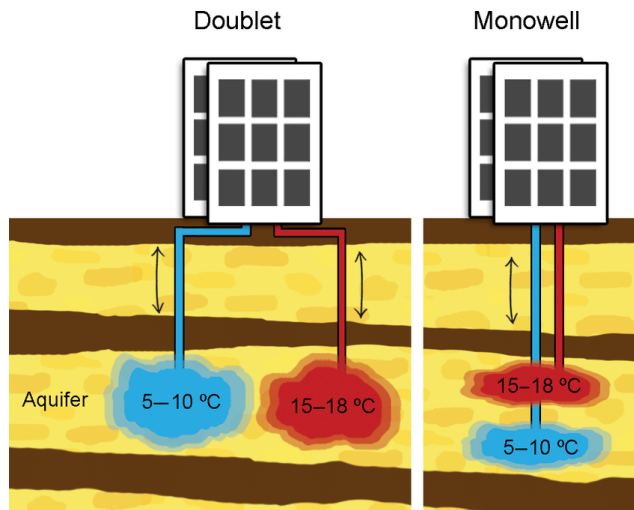

Figure 2.2: Schematic representation of ATES Doublet and Monowell (Bloemendal and Olsthoorn 2018)

It is interesting to note that mono-wells in principle can be categorized as multiple partially penetrating wells. There are in fact two screens in one borehole at different depths in the aquifer. Available mono-well systems can therefore be used as reference projects and their design guidelines can serve as base for guidelines HT-ATES systems with MPPW.

While conventional ATES systems are used for both cooling and heating, HT-ATES systems are usually used for only heating.

Table 2.1 gives the overall geohyrological characteristics and permit storage volume at the location 204 ATES systems in the Netherlands (Bloemendal and Hartog 2018). These values can be used as initial conditions to represent a case which is suitable in the Netherlands for the assessment of an HT-ATES design.

Table 2.1: Ranges in geohydrological characteristics of the 204 ATES systems and permit storage volume range. (Bloemendal and Hartog 2018)

Aquifer thickness (m)	Hydraulic conductivity (m/d)	Storage volume (m^3)
30-180	5-45	50,000 - 5,000,000

2.2 Heat loss in High Temperature-ATES

In (HT)-ATES systems heat is lost through conduction, diffusion, dispersion and flow. The total loss due to flow consist of thermal loss due to background flow and buoyancy flow. The first one occurs when there is a natural hydraulic gradient that is capable of moving a water body in the storage time. The part that fall out of range of the well is lost. In this study it is assumed that there is no background flow and will therefore not be further discussed. Loss due to buoyancy flow is dominant in HT-ATES systems and will therefore be extensively discussed in Subsection 2.2.1. The conduction and dispersion losses are described in Subsection 2.2.2. The shape of the storage volume is described in Subsection 2.2.3.

2.2.1 Buoyancy flow

Buoyancy flow is a flow that occurs when the injected water and ambient groundwater have a different density. Looking at HT-ATES systems, the fact that the injected water with a higher temperature has a lower density, leads to flow in the upward direction. This flow induces tilting of the thermal front. The thermal front is the transition zone between the injected hot water and the colder ambient groundwater. Normally, this zone is vertical but tilts with a certain rate after injection has started.

The tilting of the thermal front causes that the geometry of the stored volume changes. Hereby will the contact surface between the stored warm water volume and the upper confining layer increase leading to conduction losses. On top of that, the thermal front has more surface area inducing more buoyancy flow. If the tilting of this front is large enough, the cold ambient groundwater can reach the well screen before extraction, leading to low extraction temperatures. Figure 2.3 displays these consequences. Beside the density, the viscosity is also dependent on the temperature. This makes that infiltration of warm water is less resistant in areas where there is already heat present.
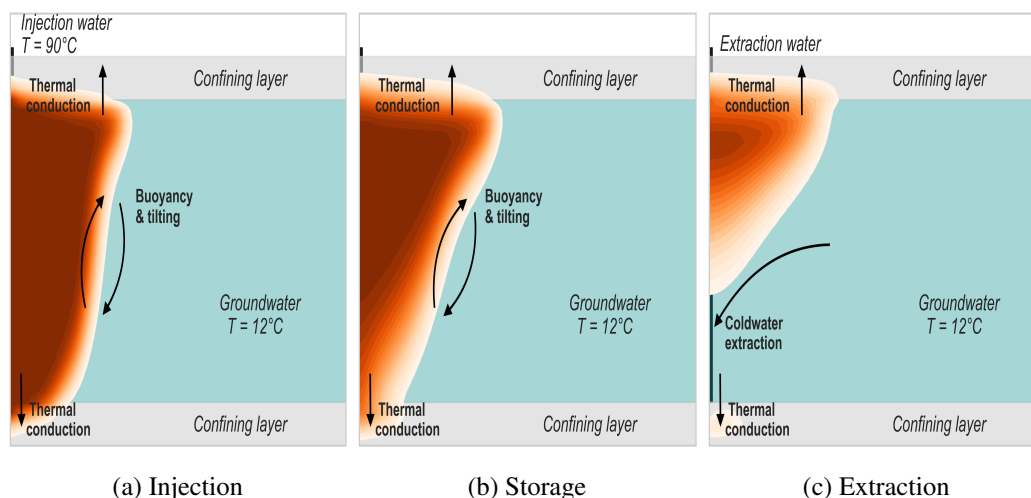

Figure 2.3: Schematic overview of a full HT-ATES recovery cycle in a confined aquifer for (a) injection, (b) storage and (c) extraction periods.

Tilting time

A method to describe the rate of tilting is by the characteristic tilting time (t_0) (Hellström et al. 1988). It is defined as follows

$$t_0 = \frac{H}{\sqrt{k_a^H k_a^V}} \frac{C_a \pi^2 (\mu_a + \mu_i)}{C_w 32 G(\rho_a - \rho_i) g} \tag{2.1}$$

where H is the aquifer thickness (m), k_a^H and k_a^V are the horizontal and vertical permeability of the aquifer (m/d), C_a and C_w are the volumetric heat capacities of the aquifer and water $(J/(m^3 K))$, μ_a and μ_i are the dynamic viscosity of the ambient groundwater and the injected water (kg/(m *s)), ρ_a and ρ_i are the densities of the ambient ground water and injected water (kg/m^3), G is Catalan's constant and g is the acceleration of gravity (m/s^2).

The tilting time is the time it takes till the thermal front is rotated $60°$. This applicable for a situation where the water is only stored and no pumping occurs. It gives a first order approximation for the buoyancy effect that is expected for certain scenarios.

Mixed convection ratio

Buoyancy flow is also known from Aquifer Storage Recovery where the density difference is induced by density difference due to salinity. A distinction can be made between two types of convection: Forced and free convection. Forced convection is water flow caused by a hydraulic gradient which occurs when there are pumping activities or a regional hydraulic gradient. This type of convection acts in horizontal direction. Free convection is water flow caused by the density difference and acts in the vertical direction. The significance of free convection is ASR system resulted in a definition of mixed convection ratio, see Equation 2.2 (Ward et al. 2007). The mixed convection ratio (M) defines the ratio between the forced (v_{forced}) and free convection (v_{free}).

$$M = \frac{v_{free}}{v_{forced}} = \frac{2\pi r H}{Q} K_v * \frac{\rho - \rho_0}{0} \tag{2.2}$$

where, H is the aquifer thickness (m), Q the pumping rate (m^3/d), r the hypothetical radius of the storage volume (m) K_v the vertical hydraulic conductivity of the aquifer (m/d), and ρ_0 and ρ the density of the ambient groundwater and injected water (kg/m^3). Equation 2.2 reads that if forced convection is dominant, i.e. M « 1 free convection is negligible (see Figure 2.4a). Values of approximately 1 for M indicate that there is a balance and if M » 1 free convection is significant and therefore can not be neglected (see Figure 2.4b).
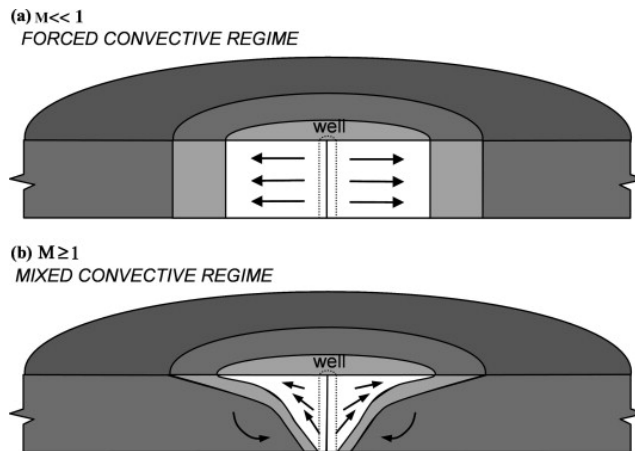

Figure 2.4: Concept of two convective regimes: (a) where forced convection greatly exceeds free convection, the interface will remain largely vertical; (b) where both forced convection and free convection are of similar magnitude, the result is a truly mixed convective regime.(Ward et al. 2007)

2.2.2 Conduction and dispersion

Conduction is the process where heat moves from higher temperatures to lower temperatures. This process occurs whether or not the water is stagnant. It causes a decrease of the thermal gradient. Dispersion is the process where local variation in flow velocity result in mixing of water. Heterogeneity of the soil matrix and the variation of the velocity in the direction of the flow in the pores causes dispersion. Near the well, the dispersion has found to be dominant because of high flow velocity. Moving more away from the well, conduction losses become more significant. Both conduction and dispersion occurs at the boundary of the storage volume. When the storage volume is increased, the absolute conduction loss at the boundaries will also increase. However, the relative loss will be smaller.

2.2.3 Spreading of the water

When there is no buoyancy flow, the shape of the storage volume is cylindrical. When water is infiltrated in the aquifer it is assumed that the infiltrated water is stored in the shape of a cylinder. The diameter of this cylinder is called the hydraulic radius. The dimensions of the volume can be expressed in the aquifer thickness and the thermal radius. The thermal radius is the maximum radial extent of the hot water. There will be an equilibrium of heat between the soil and water. Therefore the thermal front is moving slower than the water which is described as the thermal retardation. This leads to a smaller zone where the temperature is equal to the temperature of the well, also called the thermal zone (see Figure 2.5. The radius of the thermal zone is called the thermal radius. The thermal radius is expressed is Equation 2.3 and the thermal retardation in Equation 2.4.

$$R_{Th} = \left(\frac{V}{\pi H \theta R_T} \right)^{\frac{1}{2}} \tag{2.3}$$

where V represents the storage volume (m^3), H is the aquifer thickness (m). θ is the porosity of the aquifer (-) and R_T is the thermal retardation factor (-). This is defined as

$$R_T = 1 + \frac{\rho_{bulk}}{\theta} \frac{c_{ps}}{\rho_f c_{pf}} \tag{2.4}$$

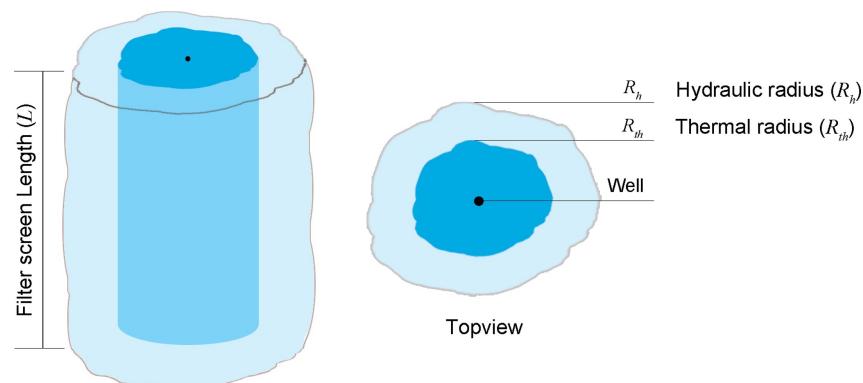where c_{ps} and c_{pf} the heat capacity of the soil and water (J/kg °C).

Figure 2.5: Cylinders representing the hydraulic radius (Rh) of water around the well and the thermal radius (Rth) of the thermal zone around the well. The height of the cylinder is the wells screen length L.(Bloemendal and Hartog 2018)

This is valid for a case with a cylindrical shape. Figure 2.3 showed that when there is buoyancy, there is tilting and the cylindrical shape of a storage volume is disrupted. So, this will not be valid for this research where buoyancy flow is considered. But this can be used to describe the shape superficially as a first order description.

2.3   (Multiple) Partially Penetrating Wells

Before pumping starts, the water level in the well is at the static water level. When a well starts extraction, water around the well is removed and the water level decreases. This is called the pumping water level. The difference between the static water level and the pumping water level is the drawdown.
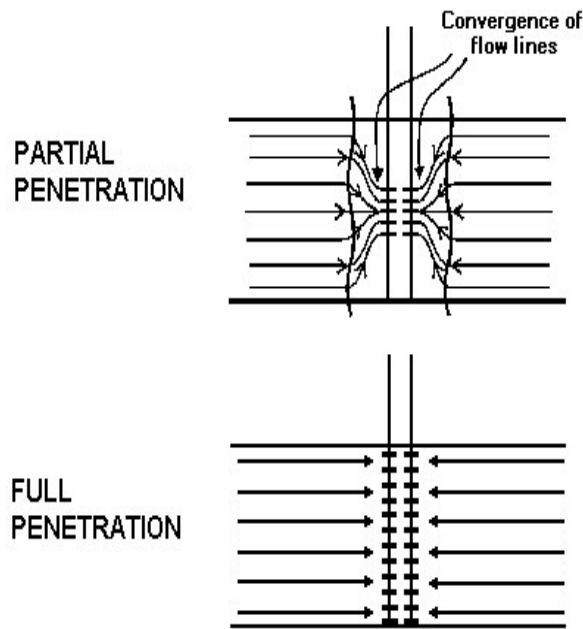
Figure 2.6: Fully and partially penetrating well.

A fully penetrating well is open over the entire aquifer thickness. When aquifers have a large thickness it is not favorable to use a fully penetrating well. Partiality penetrating wells are screened over only a part of the aquifer. This induces vertical flow close to the well. The flow velocity increases and so does the drawdown.

$$s_p = s + \Delta s \tag{2.5}$$

where, s is the drawdown of a fully penetrating well and Δs is the additional drawdown for a partially penetrating well and defined as Equation 2.6 with the screen bounding the top or bottom of the aquifer and Equation 2.7 if the screen is centered in the aquifer (Todd and Mays 1980).

$$\Delta s = \frac{Q_p}{2\pi T} \frac{1-p}{p} \ln\left(\frac{(1-p)L_{sc}}{r_w}\right) \tag{2.6}$$

$$\Delta s = \frac{Q_p}{2\pi T} \frac{1-p}{p} \ln\left(\frac{(1-p)L_{sc}}{2r_w}\right) \tag{2.7}$$

where Q_p is the well discharge (m^3/d), T the aquifer transmisitvity (m^2/d), p the penetration fraction L_{sc}/H (-), L_{sc} the screen length (m) and r_w the radius of the well (m).

A multiple partially penetrating well (MPPW), is a well in a single borehole with different screens that can be operated independently. Mono-wells in ATES systems

2.3.1 Practical Regulations

There is design velocity that is recommended on the surface of a well. This is formulated for infiltration (Equation 2.8) and extraction (Equation 2.9). When the hydraulic conductivity and storage volume per year is known, the corresponding required screen length can be determined.

$$v_{design_{infiltration}} = 1000(\frac{K}{150})^{0.6}\sqrt{\frac{V_{clogging}}{2MFIu_{eq}}} \tag{2.8}$$

where, v_{design} is the design velocity (m/h), K the hydraulic conductivity of the aquifer (m/d). $v_{clogging}$ the specific clogging velocity (m/y), MFI (Membrane Filter Index) is an indication of the sludge perseverance of a water volume (s/l^2), u$_{eq}$ the number of equivalent full load hours per year (h).

It is recommended to take 0.1 m/y as a regular clogging speed per year. When groundwater is infiltrated a value of 2 can be assumed for MFI.

$$v_{design_{extraction}} = \frac{K}{12} \tag{2.9}$$

Boreholes diameters are usually between 0.4-0.8 m but can be drilled up to a diameter of 1 m. The diameter and the screen length of a well determines the area where the velocities are at the design velocities expressed in Equation 2.8 an Equation 2.9. With these guidelines it can be determined how may boreholes are needed for a certain screen length and desired storage capacity.

Analysis

This part consist of two chapters that present the analysis of this study. The aim of this part is 1) to elaborate and reason on how the research objective and the research questions as presented in Chapter 1 are approached, 2) to present and discuss the results of the proposed research steps.

In Chapter 3 the method and materials that were used in this study are presented.

This is followed by Chapter 4, which contains the results of the conducted analysis.

3. Method and Materials

In this chapter it is explained and reasoned what method is applied and what material is used to meet the research objective. This chapter starts with a general research approach (Section 3.1). The following Section 3.3, Section 3.4, Section 3.5 and Section 3.6 are extensive presentations of the steps in the research approach. An overview of the researched scenarios is given in Section 3.7 and the corresponding assessment framework in Section 3.8.

3.1 General research approach

The performance of an HT-ATES system is sensitive to multiple factors such as hydraulic conductivity, aquifer thickness and injection volume and temperature. The use of MPPW brings additional factors that affect the performance of the system like number of screens, screen length and control approach of the screens. The research approach was set-up such that these factors were assessed. Figure 3.1 illustrates the general overview of the research approach with the steps and desired outcome.
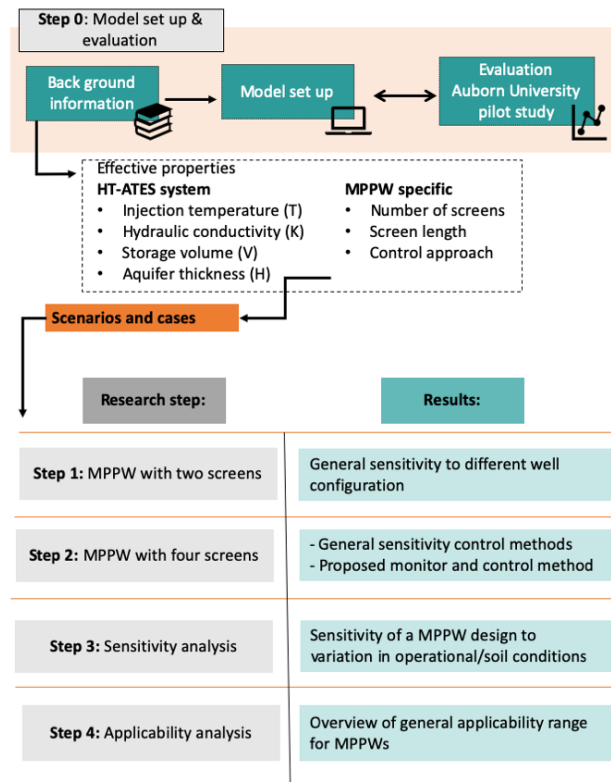

Figure 3.1: Overview scheme of research approach

3.2 Numerical model for heat transport

As this was a synthetic study, it relied heavily on numerical modelling. The simulations are done in the python based SEAWATv4. It uses MODFLOW-2000 and MT3DMS to simulate variable density groundwater flow and heat transport during the HT-ATES recovery cycles (Langevin 2008). The construction of the input files and the process of the output of SEAWATv4 are done via the open FloPy package in Python (Bakker et al. 2013). In this section, the setup and the relevant settings of the model are presented. The model was evaluated with results from the study by Lopik et al. 2016 whom evaluated his model by the data from the *Auburn University Pilot Study* ((Buscheck 1984) (Molz et al. 1983)). The results of the evaluation can be found in Appendix A.

3.2.1 MODFLOW

MODFLOW is a groundwater simulation program (Harbaugh et al. 2000). It is able to simulate groundwater flow in a mulit-layer aquifer system. An operating HT-ATES system extracts water from one well and simultaneously infiltrates the groundwater in another well after it has been heated. Pumping causes flow of the water in the aquifer by changing the hydraulic head. The groundwater flow through porous media is described by the following equation (Harbaugh et al. 2000)

$$S\frac{\partial h}{\partial t} = \nabla q + W \tag{3.1}$$

where S is the specific storage coefficient (m^{-1}), h the hydraulic head for a constant density (m), ∇ the gradient vector in x,y,z direction (-), q the specific discharge vector (m/d), W the volumetric flux per unit volume (d^{-1}), and t the time (d). The specific discharge is described by the Darcy equation

$$q = -K\nabla h \tag{3.2}$$

where K is the hydraulic conductivity (m/d). The hydraulic conductivity is temperature dependent since it is defined by the density and viscosity of the water, see Equation 3.3.

$$K = \frac{\kappa \rho_w g}{\mu} \tag{3.3}$$

where, μ is the viscosity of the water (kg/m/s), ρ the density of the water (kg/m^3), g the gravitational constant (m/s^2) and κ the intrinsic permeability (m^2).

3.2.2 MT3DMS

MT3DMS is a simulation program for multi-species mass transport. MT3DMS is able to simulate the processes of advection, disperion, sorption and reactions of solute specie in the groundwater. The equation that describes these processes and is solved by MT3DMS is as follows ((Thorne et al. 2006), (Zheng and Wang 1999), (Langevin et al. 2008)),

$$\left(1 + \frac{\theta_s \rho_s K_d}{\theta}\right)\frac{\partial(\theta C^k)}{\partial t} = \nabla(\theta D \nabla C^k) - \nabla(q_w C^k) + q_{src} C_{src}^k \tag{3.4}$$

where C^k is the concentration of a solute k (kg/m^3), K_d is the sorption coefficient (m^3/kg), C_{scr}^k is the concentration of solute k in source (kg/m^3) and D is the sum of dispersion and diffusion ($D = D_{disp} + D_{dif}$) (m^3/d). The dispersion term D_{disp} is formulated as

$$D_{disp} = \alpha \frac{q}{\theta} \tag{3.5}$$

where α is the dispersivity tensor (m). Equation 3.4 can be translated to describe the process of heat transport. Thorne et al. 2006 showed that the equation describing heat transport is similar to the solute transport equation.

$$\underbrace{\left(\frac{\rho c_{bulk}}{\theta c_w \rho_w} \right)}_{\text{Retardation}} \frac{\partial(\theta T)}{\partial t} = \nabla \left(\theta \left[\underbrace{\frac{k_{bulk}}{\theta c_w \rho_w}}_{\text{Conduction}} + \underbrace{D_{diff}}_{\text{Dispersion}} \right] \nabla T \right) - \nabla \underbrace{(q_w T)}_{\text{Advection}} + q_{src} \frac{\rho_{src} c_{src}}{\rho_w c_w} T_{src}$$

$$\tag{3.6}$$

In both equations (Equation 3.4, Equation 3.6) the advection and dispersion terms are the same mathematically. The adaptions that are applied to Equation 3.4 in order to get Equation 3.6 are done to include the process of heat conduction and thermal retardation. Molecular diffusion of solute (D_{diff}) is described by Fick's law and is mathematically similar to heat conduction described by Fourrier's law. The molecular diffusivity term needs to be replace by the bulk thermal diffusivity which is defined as

$$D_{temp} = \frac{k_{bulk}}{\theta c_w \rho_w} \tag{3.7}$$

The process of solute sorption to the soil is replaced by the temperature equilibrium between the soil particles and water resulting in thermal retardation. To account for this process, the distribution coefficient of solute is replaced by the thermal distribution coefficient $K_{d,temp}$ defined as

$$K_{d,temp} = \frac{c_s}{\rho_w c_w} \tag{3.8}$$

Langevin (2008) translated the differential equations for solute transport in SEAWATv4 to allow for heat transport.

The bulk density and the soil density are related by the water content;

$$\rho_b = \rho_s (1 - \theta) \tag{3.9}$$

3.2.3 SEAWAT

SEAWAT couples MODFLOW and MT3DMS to calculate the heat and flow each time step. This is done by solving the following form of variable-density groundwater flow equation.

$$\nabla \left[\rho \frac{\mu_0}{\mu} K_d \left(\nabla h_0 + \frac{\rho - \rho_0}{\rho_0} \right) \right] = \rho S_{s,0} \frac{\partial h_0}{\partial t} + \theta \frac{\partial \rho}{\partial C} \frac{\partial C}{\partial t} - \rho_s q_s' \tag{3.10}$$

with ρ the fluid density, ρ_0 the fluid density at reference temperature and concentration, ρ_s the density of the source and sink (m^3/kg), μ the dynamic viscosity and μ_0 the dynamic viscosity at reference concentration and temperature (kg/m/d), K_0 the hydraulic conductivity tensor. of material saturated by the reference fluid (m/d), h_0 is the hydraulic head measured in terms of reference fluid of specified concentration and temperature (m), the porosity (-), z is the elevation (m), $S_{s,0}$ is the specific storage defined as the volume of water released from storage per unit volume per unit decline of h_0 (m^{-1}) and t is the time (d).

SEAWAT is designed to simulate three dimensional variable- density ground-water flow. Modelling in three dimensions can be computationally demanding. In this study the flow is reduced by on dimension as it assumed that there is axial symmetry.

Axial Symmetric

When there are homogeneous conditions, and there is no groundwater flow to an extraction well or from an injection well exhibits radial symmetry. With this occurring radial symmetry, the flow equations can be reduced by one dimension. This is beneficial for the duration of the running time of the numerical simulations. However when aquifers don't have the properties as explained above this assumption cannot be justified. Nonetheless, it is reasonable to use this when there is no conflicting evidence.
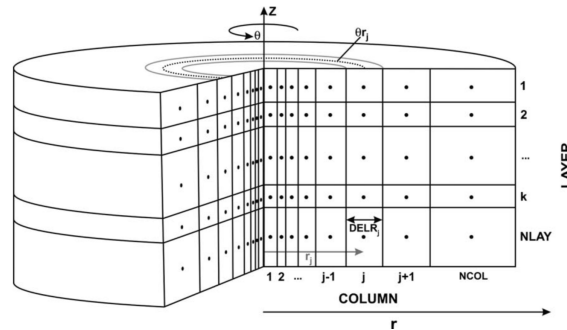

Figure 3.2: Schematic of an axially symmetric profile model (Langevin 2008)

The method of Langevin 2008 proves to be accurate in the simulation of groundwater flow, flow and transport and coupled variable-density flow and transport in both radially homogeneous and heterogeneous aquifers. In this approach, a slice out of the axisymmetric flow domain is extracted and translated into the terms of MODFLOW (see Figure 3.2. This slice is a representation of the full cylinder. To simulate the increasing volume area and storage volume with radial distance, a number of flow and transport parameters P are function of the radial distance from the node of a cell to the well.

For flow simulation, the specific storage S_s (/m), the vertical hydraulic conductivity K_v (m/d) and horizontal hydraulic conductivity K_h are adjusted. For the heat transport, the parameters porosity θ (-) and bulk density ρ_b are scaled (Vandenbohede et al. 2014).

3.2.4   Equations of State

When the density is constant throughout the entire aquifer Equation 3.2 is applicable. However, the density will change as temperature is changing. Therefore, pressure gradients are used instead of head gradients.

$$q = -(\frac{K}{\rho_w g})(\rho_w g \nabla z + \nabla P) \tag{3.11}$$

where P is the water pressure (N/m^2).

Equation 3.11 is rewritten for the three components of the Cartesian coordinate system in terms of freshwater head and results in;

$$q_x = -K_x \frac{\partial h_f}{\partial x} \tag{3.12}$$

$$q_y = -K_y \frac{\partial h_f}{\partial y} \tag{3.13}$$

$$q_z = -K_z \left(\frac{\partial h_f}{\partial z} + \frac{\rho_w - \rho_{w,f}}{\rho_{w,f}} \right) \tag{3.14}$$

where ρ_w is approximated as

$$\rho_w = \rho_{w,f} + \frac{\partial \rho}{\partial T}(T - T_f)^2 \tag{3.15}$$

The density term reflects the direct action of gravity on a fluid element at the calculation point and only affects the component of specific discharge in the vertical direction. It should be kept in mind, however, that the overall pressure distribution in a porous medium is controlled, in part, by the overall fluid density distribution, and thus, horizontal components of specific discharge also are affected by density variations in the system.

The density and viscosity are important properties of water to be considered as they are temperature, concentration and pressure dependent. In the following equations of state the value of these properties can be defined given it's state parameters. In this study only fresh water is considered meaning that the concentration is ignored.

Density-Temperature relation

The density of water is dependent on the temperature. The relation between these two is non-linear and is presented in Figure 3.3.

However, the standard version of SEAWATv4 uses a linear relationship between density and temperature. For small temperature ranges this can be done without very large over- or underestimations. However, for larger temperature ranges this can cause some inaccuracy. Therefore a new SEAWATv4 is developed with a non-linear density-temperature relation to accurately take into account the range of temperature. The equation of this is presented in Equation 3.16 and plotted in Figure 3.3. The blue dots represent the values of the density that are measured through experiments (Engineering 2003).

$$\rho(T) = 1000 - 2.9758 \cdot 10^{-3}(T + 15.31)^2 \tag{3.16}$$

The relation in Equation 3.16 is found by a second order least squares polynomial fit through the data points. This method is part of the NumPy package for Python (Oliphant 2006–). To show the effect of the use of a linear density equation, the conventional SEAWATv4 is used to simulate the Auburn pilot study (Buscheck et al. 1983) and compare this with the result of a non-linear density equation for 20 recovery cycles.
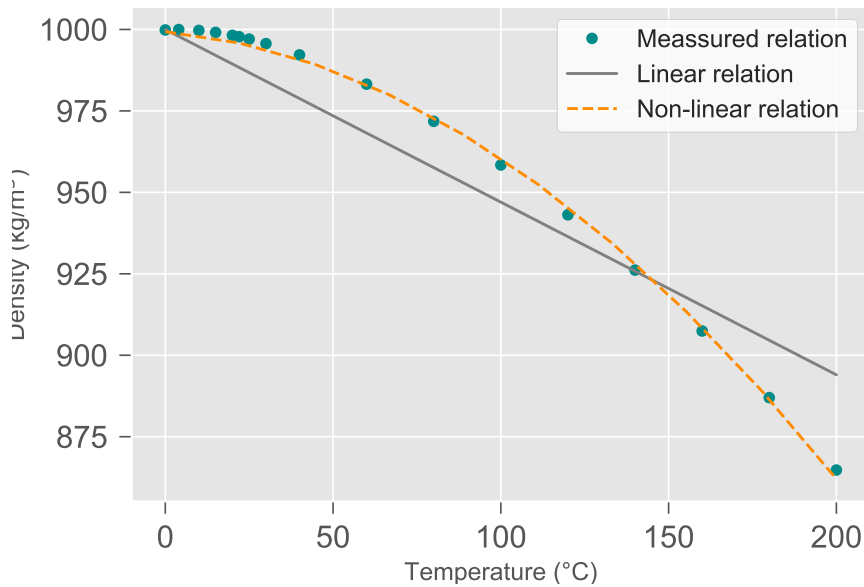
Figure 3.3: Different density temperature relationships

The linear density equation is derived by linear interpolation of the minimum and maximum density values for the range of temperature.

$$\rho(T) = 1000 - 0.53T \tag{3.17}$$

Equation 3.17 presents the linear interpolation over the range of 10-150 °C and is also plotted in Figure 3.3. The evaluation of the model based on the results of Lopik et al. 2016 are compared for both linear and non-linear density temperature relation. This comparison can be found in Appendix A.

Super-heated water

The density temperature relation as presented in Equation 3.16 is for a temperature range from exceeding 100 °C. Liquid water above boiling point can also be stored if the pressure is above the saturated vapor pressure. This is called super-heated water and is considered in this research. The saturation pressure for water till 100 °C is at atmospheric pressure. The saturation pressure is increasing with the temperature (The saturation pressure-temperature relation can be found in Figure E.2. For water with a temperature of 120 °C, the saturation pressure is 199 kPa. This means that to store water of this temperature in liquid form. a water column of 20m with a density of 1000 kg/m^3 is needed above the injected water. As the depth of HT-ATES systems reach > 200 along with high water tables, this is not considered as a limitation.

Viscosity-Temperature relation

Fluid viscosity can be expressed as a function of temperature by the following equation (Voss et al. 1984).

$$\mu(T) = 2.394 \cdot 10^{-5} \cdot 10^{\frac{248.37}{T+133.15}} \tag{3.18}$$

The viscosity is relatively more sensitive to changes in temperature compared to the density Figure 3.4. Though, the decrease in flow resistance eases the flow in all directions including the flow in the upward direction.
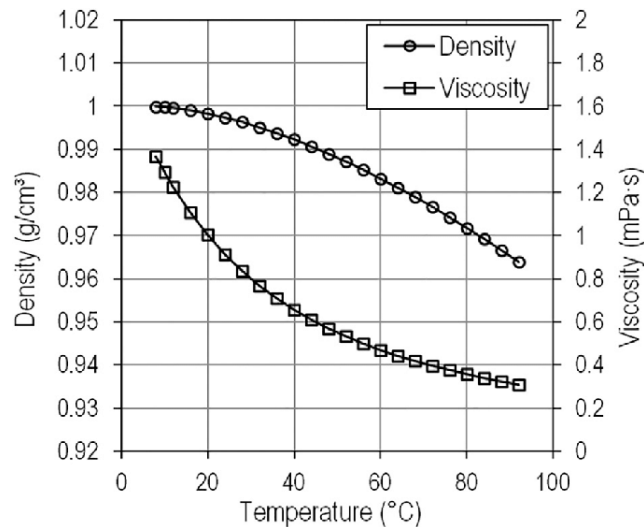

Figure 3.4: Relation between temperature and the density and the viscosity of fresh water (Schout et al. 2016)

Hence, the density difference induces the density driven flow but the viscosity confines the ease by which this flow appears and therefore needs to be considered.

Temperature dependent properties

It should be noted that other properties like heat capacity, of the water change as well with changing temperature, especially for super-heated water. This is very small in the range that is considered in this research and therefore was neglected (ToolBox 2004b). The viscosity decreases exponentially with increasing temperature. Figure 3.4 shows that the viscosity is stabilizing and becoming less variable for higher temperatures, and therefore wont limit the use of super-heated water.

The thermal distribution factor $d,temp$ and thermal diffusivity D_T are dependent on the water density which is temperature dependent. In the simulations these values were updated for density difference. Simulations without the update showed negligible difference in results and was verified by other studies (Lopik et al. 2015).

3.2.5 Simulation environment

The model uses a logarithmic scale with a domain to 3000m. The smallest cell size is 0.5m and increases to the largest cell size of 50m in at least 100 steps. The grid layer thickness Δz is dependent on the aquifer thickness and well screen. It is determined such that a grid layer is never part of two screens in most cases 2.5m. Constant head, temperature and concentration boundaries were pointed to the outer, upper and lower boundary of the model (Buscheck et al. 1983). The convergence criterion is set to 10^{-10} °C to simulate heat transport accurately (Vandenbohede et al. 2014). The well has a radius of 0.2m. The preconditioned Conjugate Gradient 2 (PCG2) is applied to solve the groundwater flow. The Modified Method Of Characteristics (MMOC) with a courant number of 0.5 is used.

Flow regime

A block function is used to represent the course of the discharge over one recovery cycle. Each recovery cycle is 360 days function with four phases of 90 days. A time step of $\Delta t = 5d$ is used. Figure 3.5 shows the discharge scheme for one recovery cycle with the appurtenant phases.
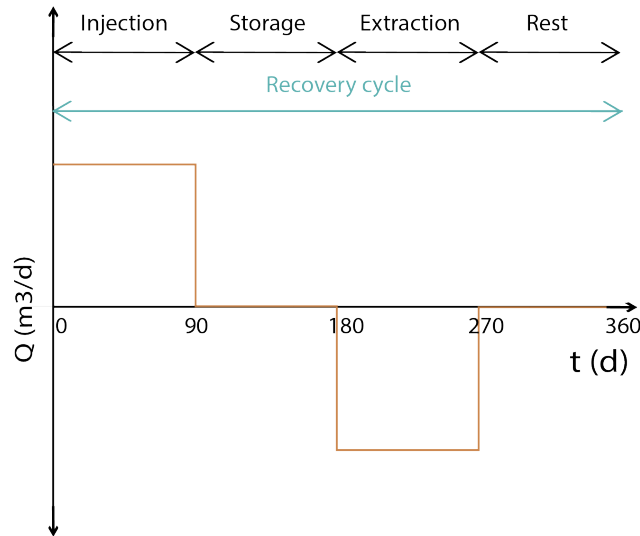

Figure 3.5: Discharge scheme for one recovery cycle

The injection volume V_{inj} is equal to the extraction volume V_{ex} for all the conducted simulations. It is therefore referred to as the storage volume V.

3.3 MPPW with two screens

This research is started with the most basic type of MPPW that has two screens. The two screens are refereed to as the injection screen and the extraction screen. This reference is made since both screens only operate in a specific phase of the recovery cycle. During this first part of the research the focus was laid on evaluating the effect different screen length combinations have for a well with two screens. The aim of this research step is to answer the following research question;

What are the effects of the application of MPPWs in terms of thermal recovery efficiency for different well configurations; screen lengths, distances between screens?

To do so, sixteen different well screen combinations for three different scenarios that represent variation in the buoyancy flow were simulated. The result of this analysis is a optimal extraction/injection screen length combination for all three scenarios and a general sensitivity to different well configurations.

The lengths were varied from penetration over 100% of the aquifer thickness (fully penetrating well), 75%, 50% and 25% of the aquifer thickness.

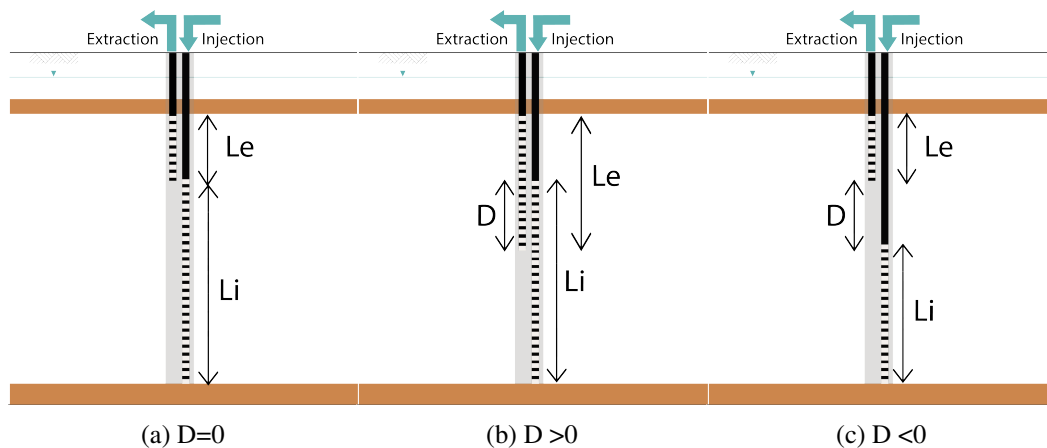(a) D=0   (b) D >0   (c) D <0

Figure 3.6: Schematic representation of screen length variations and the resulting gap or overlap "D" between the two screen

The different combinations of the screen lengths are categorized based on 1) the ratio of the length of the extraction screen over the length of the injection screen Le/Li, 2) the length of overlap or gap between the bottom of the extraction length and top of the injection length. This gap or overlap is labeled as "D". In Table 3.1 all the simulated combinations are presented. The value of the cells is the ratio Le/Li. The color indicates the length of overlap or gap between the two screens (D). A negative value means that there is gap, a positive value means that there is an overlap and when there is neither of the two, the two screens are bounded and is formulated as D=0 (grey).

Table 3.1: Overview of the screen length combinations. The left column represent the injection screen lengths (Li), the top row represents the extraction screen length (Le).

	Le/Li			
	H	0.75H	0.5	0.25
H	1	0.75	0.5	0.25
0.75H	4/3	1	2/3	1/3
0.5H	2	1.5	1	0.5
0.25H	4	3	2	1

Overlap (positive) / Gap (negative) D						
H	0.75H	0.5H	0.25H	0	-0.25H	-0.5H

3.4   MPPW with four screens

In this part of the research different scenarios are simulated for an HT-ATES with MPPW that has four screens. As for four screens it is not straightforward how the discharge is distributed over the screens, these screens were operated based on measuring points at a distance r from the well. Three types of operation methods were tested. In this way the first research question of this research step was addressed;

What are the effects in terms of thermal recovery efficiency of controlling HT-ATES systems with MPPWs, based on monitored data in the aquifer

As this distance r has effect on the temperature, it is likely that it also has effect on how the system is operated. That is why the control approaches were tested for four different

monitoring locations ($r = R_{th}$, $r = 0.75R_{th}$, $r = 0.50R_{th}$ and $r = 0.25R_{th}$). This was done two answer the second research question corresponding to this research step.

How is the control of HT-ATES system with MPPWs affected by the location of the monitoring points?

The vertical location of these measuring points were located halfway each screen and were not adjusted throughout all the simulations. This location is chosen as it is expected that halfway the screen, the average temperature is measured. A schematic representation for a system with four screens is presented in Figure 3.7.
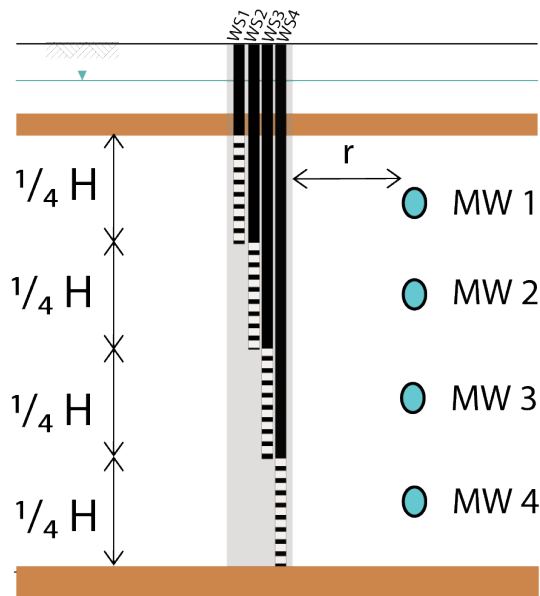
Figure 3.7: System layout for monitor and control with four well screens (WS) and four monitoring points (MW)

The measured temperatures are used to operate the four screens. In this research three different control approaches were tested for the different scenarios. The description and motive behind this approach are explained in the following Subsection 3.4.1, Subsection 3.4.2 and Subsection 3.4.3. All the approaches have in common that they strive to maintain a vertical thermal front, what is regarded as the optimal shape of the storage volume that is found for cases without buoyancy flow.

3.4.1 Control Approach 1 (Case d.1): Discrete presume buoyancy

When the system starts operating (t=0), the discharge is equally divided over the screens. Throughout the simulation, the temperature is measured at the monitoring points (Figure 3.7). The average of the value of these points are used as a threshold. During injection, the system counts how many monitoring points are above the threshold temperature. As the design of the well aims to counteract buoyancy flow, it is assumed that the monitoring points that are above the threshold temperature belong to the top screens. The discharge rate that belonged to these top screens are added to the bottom screen. For example; if two out of four monitoring point are above the average temperature of all four monitoring points, screen 1 and screen 2 are turned off. The initially equally distributed discharge rate becomes 0 (screen 1), 0 (screen 2), 0.25 (screen 3) and 0.75 (screen 4). So, the bottom screen (screen 4) gets the parts of the screen that are closed. The same procedure is done during the extraction phase. The

difference is that the screens that are below the average temperature of the monitoring points are closed off. The part of the discharge that belonged to these screens are added to the top screen.

The main reason for this type of approach is handling beforehand as it is expected that the water will flow to the top of the aquifer during injection and storage, ending in the upper part of the aquifer during extraction. There is no control during storage, injecting deeper in the aquifer helps to delay the tilting time Equation 2.1. This reduces the thermal losses.

Circulation during storage

When there is a very large buoyancy flow, circulation of the water can be considered to reduce the heat loss due to the effect of buoyancy flow during the storage period.
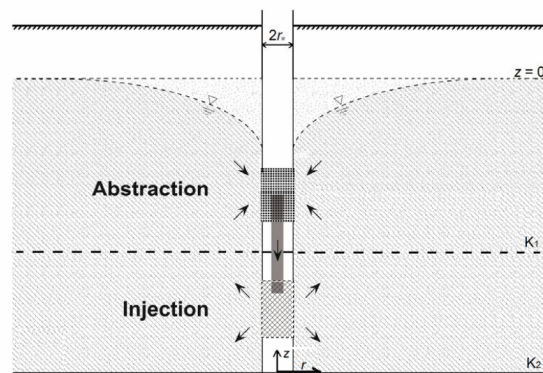
Figure 3.8: Sketch of the single borehole extraction and injection concept. (Schaffer-Jin 2014)

A method that is commonly used for de-watering of construction site is the so called vertical circulation well. Figure 3.8 shows the principle of this method. Groundwater is extracted from higher parts of the aquifer and re-injected at a greater depth in the aquifer. So, no volume is lost. In HT-ATES systems with MPPWs implemented, this can be used to circulate the warm water in the storage period to counteract the effect of buoyancy flow. This hypothesis has been tested for one scenario with very high injection temperature. A fixed volume of 40% of the total storage volume is circulated during the storage period. The distribution is such that the extraction happens in the upper half of the aquifer and the injection in the lower half of the aquifer. The circulation approach reads,

1. The portion of each monitoring temperature in the total of all monitoring temperatures is calculated. This gives the initial discharge ratios.
2. The absolute difference between MW1 and MW4 and between MW2 and MW3 is calculated. (see Figure 3.7)
3. The portion of MW1 is multiplied by the difference calculated in step 2. The portion of MPW4 is divided by this difference.
4. The same is done for MW 2 and 3.
5. The portions are re-calculated based on the scaling done in step 2 and 3.

NOTE: it is explicitly mentioned if the storage water is circulated during storage.

3.4.2 Control Approach 2 (Case d.2): Equal discrete division

The second operational approach handles only on measurements. It is a simple approach that only acts on concurrent measurements.

During injection, the temperature at the monitoring points are measured. The average of the temperatures of all monitoring points was used as threshold. If the value of a monitoring point is above the threshold, the corresponding screen is closed. The discharge is then redistributed equally. For example; if monitoring point 3 (MW3 in Figure 3.7) has a temperature above the average of all four monitoring points, screen 3 is closed and the discharge division over the screens becomes (1/3,1/3,0,1/3) During extraction, a temperature below the threshold is the criteria to turn off the corresponding screen.

For scenarios where the water is not moving faster than the timeframe that is used to review the system and change screen operations, it was expected that this way of approach would be beneficial.

3.4.3   Control Approach 3 (Case d.3): Continuous division

The last operational approach is the same as the previous approach (Control Approach 2). The difference is found in the way of redistributing the discharge. The discharge is equally divided over the screens that are running without taking into account differences in temperature between the corresponding monitoring points. In this operational approach, the discharge is re-distributed over the operating screens based on the ratio of the monitored temperature values. During injection, this results in a discharge distribution where the screen with the lowest ratio (of the monitored temperature) gets the highest discharge rate. During extraction, the screen with the highest ratio gets the biggest discharge rate. The difference with control approach 2, is that when dividing the discharge based on the relative difference it creates possibilities for a screen to compensate more. This type of control might be less practical in reality as the pumps need to be able to run in a large capacity range.

3.5   Sensitivity Analysis

The third step in this research was dedicated to study the sensitivity of the performance of a MPPW design to variation in aquifer thickens, storage volume, and magnitude of buoyancy. The aim of this research step was to answer the following research question.

How is the performance of HT-ATES systems with MPPWs affected by the storage volume, aquifer thickness, and magnitude of buoyancy flow?

In Section 3.3 and Section 3.4 the focus is mainly on finding the potential of MPPW as a method to counteract the effect of buoyancy flow. This was among other things done by simulating different magnitude of buoyancy flow for different well design. In this sensitivity analysis the result of both sections were compared to each other, to a regular HT-ATES system and a system where buoyancy flow is neglected. The best well design for both two and four screens are tested on their sensitivity to aquifer thickness and injection volume. The injection temperature, ambient groundwater temperature and hydraulic conductivity are not varied as this effects the buoyancy flow (see Equation 3.14 and the effect of buoyancy flow is extensively tested in the previous research steps.

The effect of the vertical hydraulic conductivity is expected to be very similar to the injection temperature because both induce buoyancy flow. However other anisotropy values of the aquifer can have effect if the buoyancy flow is large. Four cases with different K_v and K_h were assessed. The findings and elaboration of these cases can be found in Appendix B.

3.6 Applicability Analysis

The last step of this research was dedicated to finding generic relation of geo-hydrological and operational conditions in which it is useful to consider MPPWs as design for an HT-ATES well. The research question for this step was expressed as

Under what conditions does application of MPPWs increase the recovery efficiency of HT-ATES systems?

The applicability was analyzed by simulating two types of HT-ATES systems. A regular HT-ATES with a fully penetrating screen and a system with two screens. The layout of the latter one is illustrated in Figure 3.9. This can be regarded as the most basic type of MPPW where two screens are stacked on top of each other with both a screen length of half the aquifer thickness. The upper one is used for extraction, and the lower one for injection.
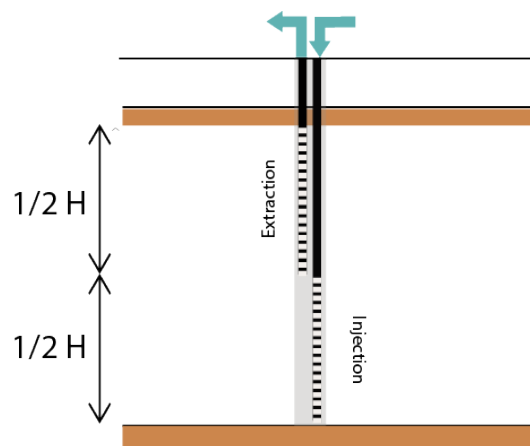
Figure 3.9: System layout for applicability analysis

To incorporate all the relevant geo-hydrological and operational parameters the buoyancy flow and the dimensionless H/R_{th} parameter were varied and simulated. As can be recalled from Equation 3.14, the buoyancy flow is dependent on the vertical hydraulic conductivity, the injection temperature and the ambient groundwater temperature. The thermal radius as expressed in Equation 2.3 is dependent on the injection volume and aquifer thickness. These are the main properties affecting the performance of the system in terms of thermal recovery. The goal of this analysis was to find a general applicability expression for MPPW in HT-ATES systems.

3.7 Simulated scenarios and cases

The aquifer and aquitard properties used for the simulations are given in Table 3.2. The reference scenario (scenario 1) had an aquifer thickness H of 70 m. This aquifer was bounded by two aquitards of 10 m. The ambient groundwater had a temperature of 12°C. The surface temperature was set to be constant to simulate an infinite long top confining layer to prevent heating up of the boundary. A schematic representation of the whole system is given in Figure 3.10. The temperature of the injected storage volume V of 900,000 m^3 was 90°C.

Table 3.2: Overview of model simulation parameter values (Caljé 2010)

Properties	Parameter value
Aquifer properties	
Specific storage S_s	$6 \cdot 10^{-4}$ (m^{-1})
Porosity θ	0.3 (-)
Bulk density ρ_b	1,855 (kg/m^3)
Heat capacity c_{ps}	880 (J/kg °C)
Thermal conductivity λ_s	2.55 (W/m °C)
Thermal distribution coefficient $K_{d,Temp}$	$2.1 \cdot 10^{-4}$ (m^3/kg)
Thermal retardation factor R_T	2.3 (-)
Bulk thermal diffusivity D_{temp}	0.158 (m^2/d)
Horizontal hydraulic conductivity K_H	25 (m/d)
Vertical hydraulic conductivity K_V	5 (m/d)
Aquitard properties	
Specific storage S_s	$6 \cdot 10^{-4}$ (m^{-1})
Porosity θ	0.4 (-)
Bulk density ρ_b	1,590 (kg/m^3)
Heat capacity c_{ps}	880 (J/kg °C)
Thermal conductivity λ_s	2.55 (W/m °C)
Thermal distribution coefficient $K_{d,temp}$	$2.1 \cdot 10^{-4}$ (m^3/kg)
Bulk thermal diffusivity D_{temp}	0.131 (m^2/d)
Horizontal hydraulic conductivity K_H	$25 \cdot 10^{-5}$ (m/d)
Vertical hydraulic conductivity K_V	$5 \cdot 10^{-5}$ (m/d)
Groundwater properties	
Heat capacity c_{pf}	4,186 (J/kg °C)
Thermal conductivity λ_f	0.58 (W/m °C)
Solute properties	
Longitudinal dispersion α_l	0.5 (m)
Transversal dispersion α_t	0.05 (m)
Molecular diffusion D_m	$1 \cdot 10^{-10}$ (m^2/d)

Table 3.3 gives the overview of the simulated scenarios. In the additional scenarios to the reference scenario, HT-ATES and aquifer characteristics were varied. In scenario 2 the injection temperature is increased such that the buoyancy flow as described in Equation 3.14 is 50% larger than the reference scenario. For scenario 3 50% less buoyancy flow is simulated with respect to the reference scenario. The following scenarios 4-5 are for changing aquifer thickness. Scenario 6 simulated a case with 50% less storage volume.

Table 3.3: Overview of the simulated scenarios (* indicates the deviated parameter from the reference scenario).

Scenario	T_{inj} (°C)	K (m/d)	H (m)	V (m^3)
1 (Ref)	90	25	70	$90 \cdot 10^4$
2	112*	25	70	$90 \cdot 10^4$
3	61*	25	70	$90 \cdot 10^4$
4	90	25	105*	$90 \cdot 10^4$
5	90	25	35*	$90 \cdot 10^4$
6	90	25	70	$45 \cdot 10^4$*
7	150*	25	70	$90 \cdot 10^4$

The last scenario represents a large system with a large buoyancy flow by injecting water of very high temperature. The effect of vertical circulation in the storage period was assessed for this scenario were the injectuin temperature was set to be 150°C..
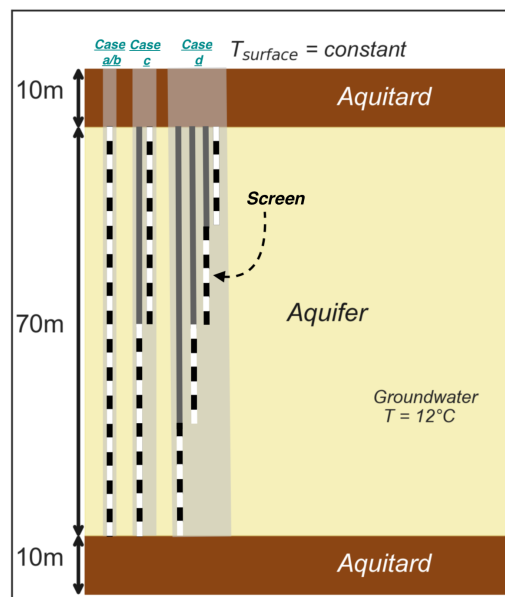
Figure 3.10: Schematic overview of the simulated systems.

Four types of HT-ATES systems (Case a,b,c,d) were simulated for the scenarios as presented in Table 3.3. A regular HT-ATES system with a fully penetrating screen (Case a), a theoretical regular HT-ATES system where no buoyancy flow was considered (Case b), an HT-ATES system with MPPW that had two screens (Case c), and an HT-ATES system with four screens that were operated based on monitoring points in the aquifer (Case d). A detailed description of the cases can be found in the previous sections of this chapter. The following Table 3.4 gives an overview of the cases and the simulated scenarios (Table 3.3) for each case.

Table 3.4: Overview of the different simulated cases

Case	Number of screens	Buoyancy flow	Monitor and control during injection and extraction	Monitor and control during storage	Tested scenario
a	1 (Fully penetrating)	Yes	No (only on and off)	No	1-7
b	1 (Fully penetrating)	No	No (only on and off)	No	1-7
c	2 (Partially penetrating)	Yes	No (only on and off)	No	1-6
d.1	4 (Partially penetrating)	Yes	Yes, presume buoyancy flow	No	1-7
d.2	4 (Partially penetrating)	Yes	Yes, discrete division	No	1-6
d.3	4 (Partially penetrating)	Yes	Yes, continuous division	No	1-6
d.1x	4 (Partially penetrating)	Yes	Yes, presume buoyancy flow	Yes	7

Applicability Analysis

For the applicability analysis 8 H/R_{th} (aquifer thickness over the thermal radius) values were simulated over a buoyancy flow range. The thermal radius R_{th} is defined as presented in Equation 2.3. An HT-ATES system with a regular fully penetrating screen was compared to a MPPW with two screens of half the aquifer thickness. An overview of the proposed simulations are presented in Table 3.5.

Table 3.5: Overview of the simulations for the applicability analysis.

	Buoyancy flow (m/d)		H/R_{th} (-)	
Case	Lower	Upper	Lower	Upper
a) Regular fully penetrating	0.03	0.7	0.3	1.1
c) MPPW with two screens	0.03	0.7	0.3	1.1

The simulations of this analysis were done over two recovery cycles to prevent that the results will be influenced by the unstable performance of the first recovery cycle.

3.8 Assessment Framework

For the evaluation and comparison of the different simulation results, an assessment framework is required. In this research two performance indicators were used. The first performance indicator is the thermal recovery efficiency (Subsection 3.8.1). This can be derived after a certain recovery cycle. During the recovery cycle the performance can be expressed in the slope of the thermal front. This is the second performance indicator that is described in Subsection 3.8.2.

3.8.1 Thermal Recovery Efficiency

The feasibility of HT-ATES systems is mostly controlled by the thermal recovery efficiency. It is one of the main parameters that is used to determine the overall energy saving. It is defined as the ratio of the extracted energy over the injected energy (see Equation 3.19).

$$\eta_{th} = \frac{E_{out}}{E_{in}} = \frac{\sum (V_{ex}\rho_{ex})c_{pf}(T_{ex} - T_a)}{\sum (V_{in}\rho_{in})c_{pf}(T_{in} - T_a)} \tag{3.19}$$

with V_{im}/V_{ex} the injected and extracted volume (m^3), ρ_{in}/ρ_{ex} the density of the injected and

extracted water (kg/m^3), c_{pf} the heat capacity of the water (J/kg °C), T_{in} and T_{ex} the injected and extracted water temperature (°C) and T_a temperature of the ambient groundwater (°C).

Counteraction of buoyancy flow

The thermal loss due to buoyancy flow is defined as the thermal recovery efficiency of a system without buoyancy flow (Case b), minus the thermal recovery efficiency of a regular system with a fully penetrating screen where buoyancy is present (Case a). This value is used to define the maximum counteractable thermal recovery loss. The thermal recovery efficiency of a system with MPPW (Case c/d), minus the thermal recovery efficiency of a regular HT-ATES system (Case a) is defined as the loss due to buoyancy flow that is counteracted. The counteraction of buoyancy flow by applying MPPW is defined as

$$Counteraction = \frac{\eta_{MPPW} - \eta_{REG}}{\eta_{MAX} - \eta_{REG}} 100\%$$
(3.20)

with η_{MAX} the thermal recovery efficiency of a system without buoyancy flow, η_{REG} the thermal recovery efficiency of a regular fully penetrating well and η_{MPPW} the thermal recovery efficiency of an HT-ATES system with MPPW.

3.8.2 Slope of the thermal front

The thermal recovery efficiency is a performance indicator that can be determined after a recovery cycle. During the recovery cycle the slope of thermal front can serve as a performance indicator. When there is a large tilt of the thermal front, this results in low thermal recovery efficiency as more heat is lost (Figure 2.3). With the use pf monitoring wells the temperature distribution over the aquifer can be logged and translated into a slope of the thermal front. The use of MPPWs in general and in particular the designed control approaches as described in Section 3.4 strive to minimize the tilting of the thermal front by using monitoring data in the aquifer.

Determination of the thermal slope by numerical model

For the determination of the slope of the thermal front, the thermal front is assumed to be linear. The distance to the thermal front r is determined over the entire aquifer with steps of dz, see Figure 3.11. The slope is calculated by fitting a linear line through the points according to Equation 3.21.

$$slope = \frac{\sum_{i=1}^{n} r_i(z_i - z_{mean})}{\sum_{i=i}^{n} z_i(z_i - z_{mean})}$$
(3.21)

where z_i is the vertical location of where r_i is determined. z_1 is at dz from the top of the aquifer. n is the total number of points used and is determined by $n = H/d_z$.
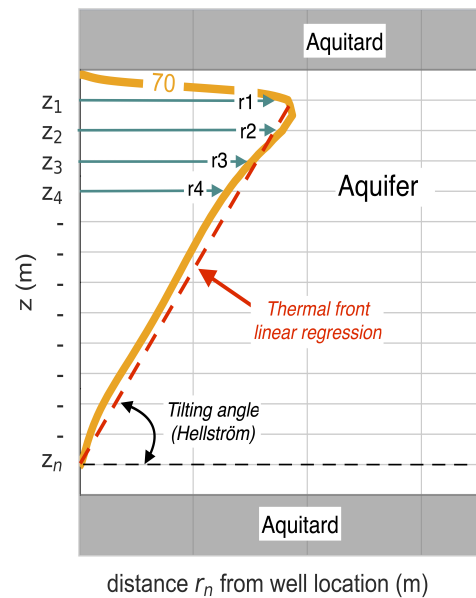
Figure 3.11: Schematic representation of the approach to determine the slope of the thermal front for a certain temperature contour (70°C in this representation)

Evaluation of approach

This approach was evaluated by comparing the results with the tilting time expressed in Equation 2.1 (Hellström et al. 1988). Equation 2.1 is only valid for a fully penetrating well in a homogeneous aquifer. The tilting time is defined as the time where the tilting angle is 60 °. This is measured from the horizontal of the aquifer to the thermal front. This angle is translated in to a slope of -0.58 in terms how the slope of the thermal front is expressed in this research.

Determination of slope by monitoring points

The way the slope is determined by the model is practically not possible. Therefore the slope was also approached by using the monitoring points in the aquifer as presented in Figure 3.7. The temperature value and vertical location were used as data for the regression of a linear line representing the slope of the thermal front

For a large range of aquifer and operational parameters the slope and the thermal recovery was assessed for the first recovery cycle. The approach and result of this assessment can be found in Appendix D.

4. Results

In this chapter the results of the proposed simulations as described in **??** are presented. First, the effect of different screen lengths on the thermal recovery efficiency is presented in Section 4.1. This is followed by Section 4.2 where the resulting effect on the thermal recovery efficiency of monitor and control of four screens is given and elaborated. The goal of MPPWs is to maintain a vertical thermal front to minimize heat loss due to effect of buoyancy flow. In Section 4.3 the assessment of the optimal MPPWs designs on the slope of the thermal front is presented and discussed for the reference scenario. In Section 4.4 the outcome of the sensitivity analysis is presented by comparing the performance of a MPPW with two and four screens for different aquifer and operational parameters. Lastly, the result of the applicability analysis is given in Section 4.6. All sections are closed by a sub-conclusion summarizing the main findings of that section.

4.1 MPPW with two screens

In this section the results are presented for the most basic MPPW with two screens. This section aims to provide a general sensitivity of the configuration of a two screened MPPW for different magnitude of buoyancy flow. The screens were varied length to asses the effect on the thermal recovery efficiency in order to answer the following research question

What are the effects of the application of MPPWs in terms of thermal recovery efficiency for different well configurations; screen lengths, distances between screens?

Two types of characteristics of the combinations were used to evaluate the results. The extensive presentation of these two characteristic can be found in Section 3.3 and are briefly listed below. The two screens are referred to as the injection screen with corresponding length *Li* and extraction screen with corresponding length *Le*.

- **Le/Li**, this the ratio of the extraction screen length over the injection screen length. *Le/Li* < 1, the extraction screen length is smaller than the injection screen length. *Le/Li* > 1, the extraction screen length is larger than the injection screen length.
- **D**, this is the overlap or overlap length between the bottom of the extraction screen and top of the injection screen. *D* > 0, overlap. *D* < 0, gap. *D*=0,

The thermal recovery efficiency as was found for the regular HT-ATES system with and without buoyancy flow (Case a and b) are given in Table 4.1. The maximum increase in efficiency that is possible by counteracting the buoyancy flow with MPPW is the net difference of the thermal recovery efficiency of Case a and b.

Table 4.1: Thermal recovery efficiency (-) of the fourth recovery cycle for a regular HT-ATES system (Case a) and a system without buoyancy flow (Case b).

Scenario	Regular HT-ATES (Case a)	No buoyancy flow (Case b)	Max. counteract-able with MPPW (b-a)
1: T_{inj} = 90 °C	0.61	0.88	0.27
2: T_{inj} = 112 °C	0.51	0.88	0.37
3: T_{inj} = 61 °C	0.77	0.88	0.11

The results of scenario 1-3 are respectively presented in Subsection 4.1.1, Subsection 4.1.2 and Subsection 4.1.3.

4.1.1 Scenario 1: T_{inj} = 90 °C

The use of two screens to operate the HT-ATES system for scenario 1 shows promising results (Figure 4.1). To clarify the figure, each square represents the thermal recovery efficiency for a particular injection screen and extraction screen length combination. The top left corner indicates a regular fully penetrating well (Case a). When reading from left to right, the extraction screen length is decreased for a certain injection screen length. When reading from top to bottom, the injection screen length is decreased for a particular extraction screen length. All the lengths are a function of the aquifer thickness H,70 m in this scenario.
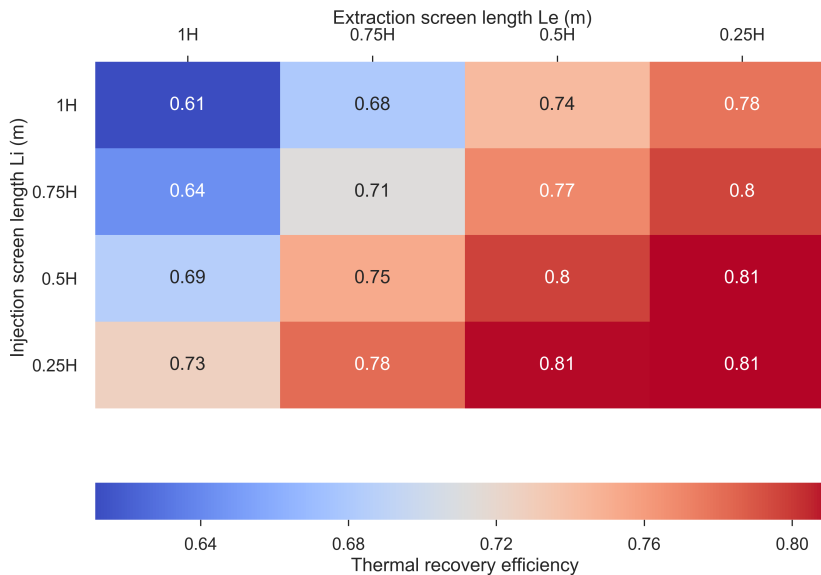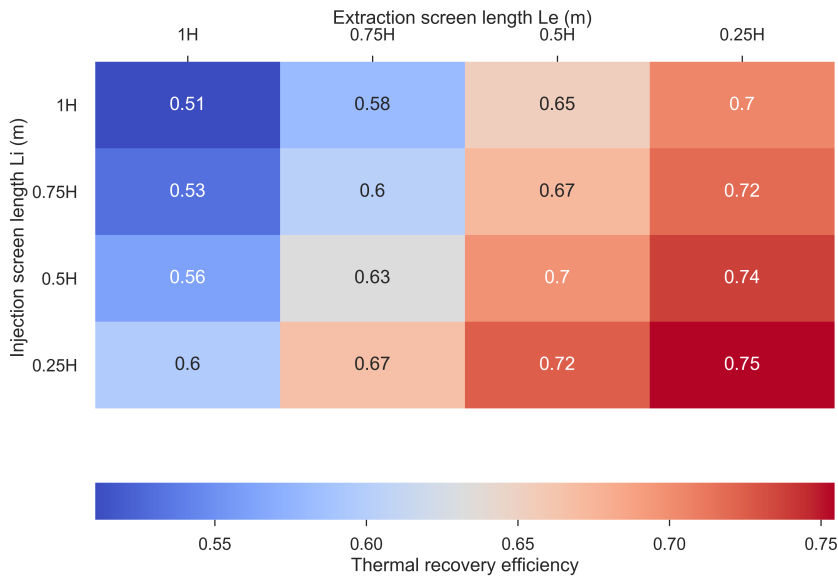

Figure 4.1: Thermal recovery efficiency for the fourth recovery cycle of varied injection screen length (Li) and extraction screen length (Le) combinations for an injection temperature of 90°C,

The first column of Figure 4.1 depicts the results of a two screened MPPW where the extraction screen is kept constant and is a fully penetrating screen, while the injection screen length is steps wise decreased meaning that the overlap D decreases. This creates a situation that the buoyant water has more distance to travel until reaching the top of the aquifer. This results in a absolute increase of thermal recovery efficiency of 0.12 for the shortest injection

screen lengths of 25% of the aquifer thickness (bottom left value in Figure 4.1). This means a counteraction of $\frac{0.12}{0.27}100\% = 44\%$,

The top row is the thermal recovery efficiency for a fully penetrating injection screen and varied extraction screen length. This also creates a decrease in the overlap length D but in this case this is created by Le/Li smaller than 1. The thermal recovery efficiency increase is 0.17 for a extraction screen length of 25% of the aquifer thickness. This means a counteraction of $\frac{0.17}{0.27}100\% = 63\%$. This indicates that the effect of a smaller extraction screen length is more profitable than that of the injection screen length.

The last column shows the result for the case where the extraction screen length is 25% of the aquifer thickness and the injection screen length is varied. The maximum absolute gain that is observed is 0.03. It shows an convergence where continuation of the decrease of the injection screen length wont have any additional benefit. The same holds for the last row, where the thermal recovery efficiency is found for an injection screen length of 25% of the aquifer thickness while decreasing the extraction screen length. A gap of $D = 0.25H$ between the two screens shows it is sufficient to counteract $\frac{0.20}{0.27}100\% = 74\%$ of the loss due to effect of buoyancy flow. This convergence can be the result of that the added efficiency by counteraction of the buoyancy when increasing the gap D is not more than the loss that is gained by other heat transport processes like conduction and dispersion. As more surface area with the ambient ground water is created and the velocity of the water is increased when injecting with the same discharge over a smaller area.

Best design for scenario 1

There are three combinations that result in the best performance for scenario 1 namely:

- Le/Li = 0.5 (Le = 0.25H, Li = 0.5H) and D = -0.25
- Le/Li = 2 (Le = 0.5H, Li = 0.25H) and D = -0.25
- Le/Li = 1 (Le = 0.25H, Li = 0.25H) and D = -0.5

When using these configurations 74% of the loss due to buoyancy is counteracted, leaving a difference in thermal recovery efficiency with the theoretical maximum (Case b) of an absolute value of 0.09. These three well design options represent three different well configuration but end up with the same result. The gap between the bottom of the extraction well and top of the injection screen length (D) needs to either be 0.25H or 0.5H.

There is a clear trend that the system performance is improved when creating less overlap between the screens. However, the corresponding length ratios Le/Li indicate that the effect of the decreased overlap is more effective when this is caused by a decrease in extraction screen length, so smaller Le/Li.

4.1.2 Scenario 2: T_{inj} = 112 °C

The results of scenario 2 where 50% more buoyancy (with respect to the reference scenario) that was simulated by injecting water of 112 °C, shows the same trend as for scenario 1 (See Figure 4.2). The application of MPPWz results in an increase of the thermal recovery efficiency.
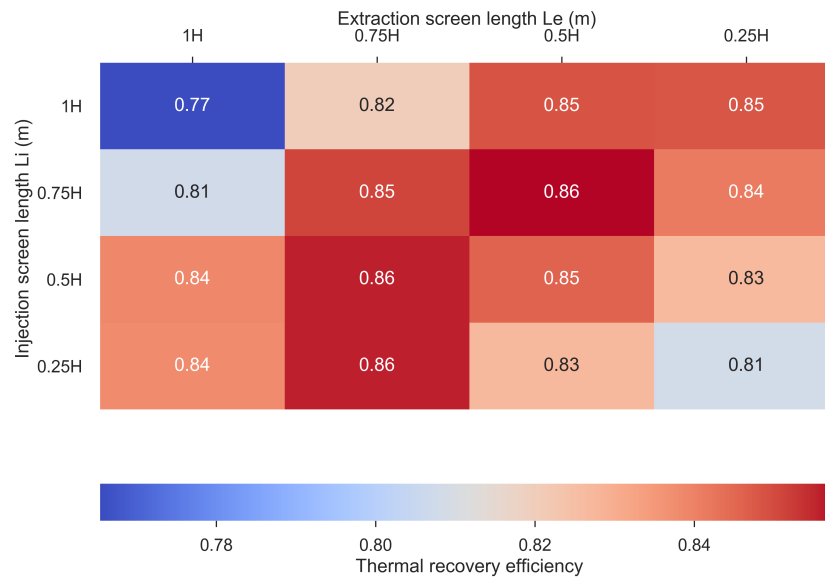
Figure 4.2: Thermal recovery efficiency for the fourth recovery cycle of varied extraction screen length (*Le*) and injection screen length (*Li*) combinations for an injection temperature of 112 °C.

The result of the previous scenario (Figure 4.1) showed that the performance of the system in terms of thermal recovery efficiency is more sensitive to the extraction screen length (*Le*) than to the injection screen length (*Li*), The results as presented in Figure 4.2 indicates that this effect is more dominant when there is more buoyancy flow.

The net increase in thermal recovery efficiency when the extraction screen is fully penetrating ($Le = H$) and the injection screen length is decreased to 25% of the aquifer thickness ($Li = 0.25H$) is 0.09. This is a counteraction of only $\frac{0.09}{0.37}100\% = 24\%$. While in the case where only the extraction screen length is decreased ($Le = 0.25H$ and $Li = H$) there is a counteraction of $\frac{0.19}{0.37}100\% = 51\%$. This indicates that in case of large buoyancy flow deep injection is less effective than shallow extraction The effect of deep injection is spread over the rest of the recovery cycle, while the effect of shallow extraction is concentrated to the corresponding phase of the recovery cycle.

It can also be noted that more gap (*D*) between the two screens is beneficial. There is a convergence of the thermal recovery efficiency where the net increase for smaller screen lengths is decreasing. This convergence is not as convincing like in scenario 1 (Figure 4.1).This suggests that for this scenario smaller screen lengths and thus more gap between the screens are predicted to have effect and increase the thermal recovery efficiency. This can for example be created by choosing a larger aquifer or using smaller screen lengths (>25% of the aquifer thickness).

Best design for scenario 2

There is one well configuration that the results present as the optimal for this scenario, namely:

- Le/Li = 1 (Le = 0.25H, Li = 0.25H) and D = -0.5

When using this configuration, 65% of the thermal energy loss due to buoyancy is counteracted.

It is clear that the system performance is improved when creating more gap between the screens. The effect that this has on the thermal recovery efficiency is more beneficial when this gap is created by smaller extraction screen length.

4.1.3 Scenario 3: T_{inj} = 61 °C

Figure 4.3 depicts the results for scenario 3, where 50% less buoyancy flow was simulated with respect to the reference scenario (scenario 1) by injecting water with a temperature of 61 °C.

Figure 4.3: Thermal recovery efficiency for the fourth recovery cycle of varied injection screen length (*Li*) and extraction screen length (*Le*) combinations for an injection temperature of 61 °C.

The observation of the first column and the first row, shows that the effect of variation in solely injection screen length or solely extraction screen length are almost identical with a small difference of 0.01 lead by the extraction screen length. So, both measures have similar effect when the buoyancy flow is low. It can be observed that when decreasing both screens in length such that a gap is created, the thermal recovery efficiency is not optimal. In this scenario the magnitude of the buoyancy is not enough to supply the extraction screen length with warm water in the same rate as it is extracted.
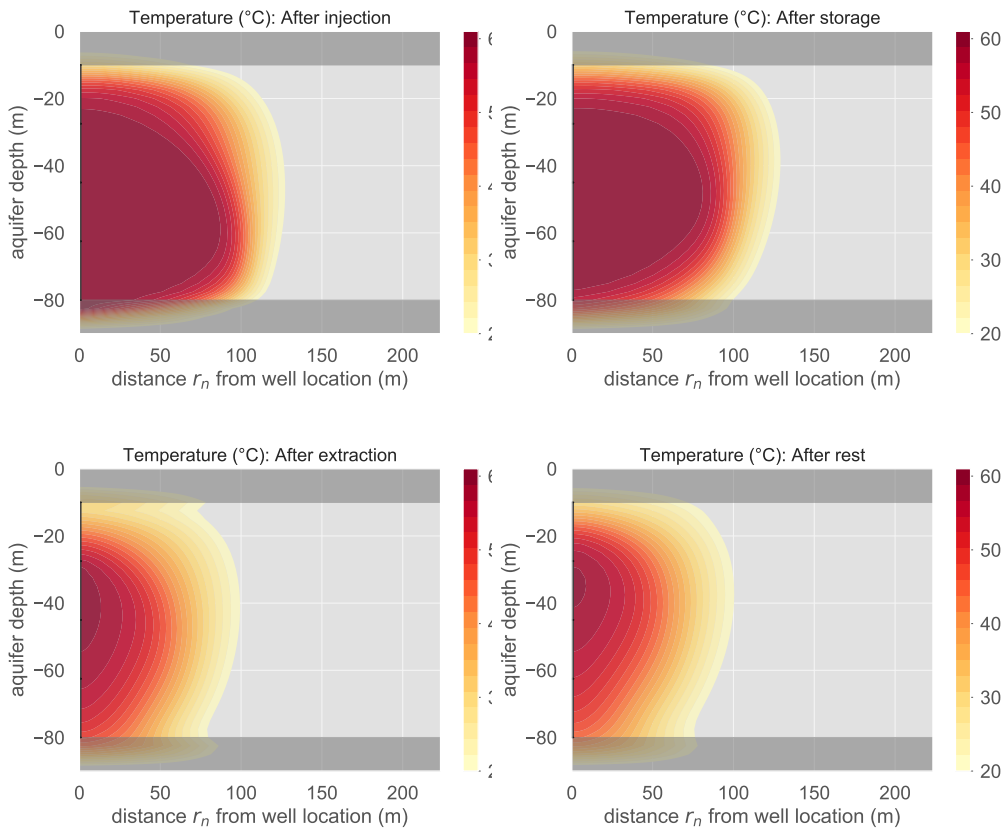
Figure 4.4: Temperature spread in the aquifer for scenario 3 (T=51°C) of the fourth recovery cycle with Li=Le=0.25H.

When observing the temperature spread in the aquifer for the case with $Le = Li = 0.25H$ (Figure 4.4). it shows that the heat is left in the aquifer after the extraction period. It can also be noted that after the storage period, the volume shows a cylindrical shape without tilting of the thermal front which indicates the optimal shape for a storage volume found when there is no buoyancy flow.

Best design for scenario 3

There are three combinations that result in the best performance for scenario 3 namely:

- Le/Li = 2/3 (Le = 0.5H, Li = 0.75H) and D = 0.25
- Le/Li = 1.5 (Le = 0.75H, Li = 0.5H) and D = 0.25
- Le/Li = 3 (Le = 0.75H, Li = 0.25H) and D = 0

These screen length combinations counteract 82% of the buoyancy flow. The effect of a two screen MPPW is beneficial for the performance of an HT-ATES system with small buoyancy flow with respect to the reference scenario. As the buoyancy flow is smaller, no gap between the screens is needed and overlap is beneficial for certain combinations.

4.1.4 Conclusion: MPPW with two screens

One research question corresponded to this section. Analyzing the thermal recovery efficiency for variations in screen length combinations shows that in all simulated scenarios the performance is improved with a maximal counteraction in the range of 65%-82% with

respect to a fully penetrating well for the fourth recovery cycle. It should be noted that beside the optimal combinations that were found there are many other combinations that approach these maximum. Meaning that there are ranges of combinations for each scenario that significantly (>50% counteraction) improve the performance of the system in terms of thermal recovery efficiency. All the different well configurations that counteract more than 50% of the thermal loss due to buoyancy flow for all three scenarios are illustrated in Figure 4.5.
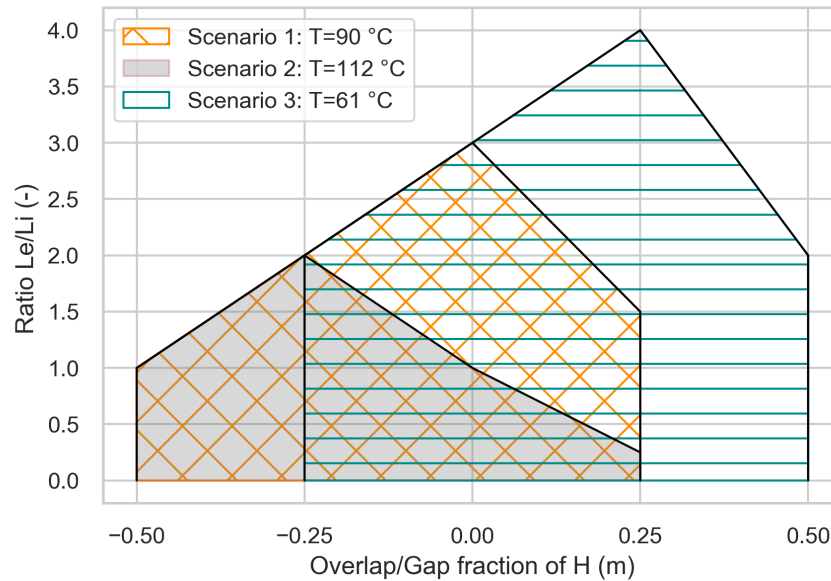
Figure 4.5: Screen length combinations for scenario 1-3 that at least counteract 50% of the loss due to the effect of buoyancy flow.

The magnitude of the buoyancy determines how much overlap or gap is needed and what the screen length ratio *Le/Li* should be to counteract this flow. Figure 4.5 shows that the sensitivity to the well design is higher when there is more buoyancy as less screen length combinations are possible. This figure should be carefully interpreted as it is based on percentages. The absolute increase in thermal recovery efficiency is higher when there is more buoyancy flow. It can be concluded that a MPPW with two screens is an effective design of the well to increase the performance in terms of thermal energy recovery.

4.2 MPPW with four screens

In this section the results are given for the simulations of a MPPW with four screens. The results of this section were produced to answer the following research questions:

1. *What are the effects in terms of thermal recovery efficiency of controlling HT-ATES systems with MPPWs, based on monitored data in the aquifer?*
2. *How is the control of HT-ATES system with MPPWs affected by the location of the monitoring points?*

The four screens are stacked on top of each other and have all a screen length of 25% of the aquifer thickness. This MPPW design was applied with three different control approaches.

- **Control Approach 1 (Case: d.1):** Discrete Premeditate, buoyancy flow is assumed and taken into the control approach (see for a detailed description Subsection 3.4.1)
- **Control Approach 2 (Case: d.2):** Discrete, the system only acts on monitored data of at that moment and the discharge is equally divided over operating screens (see for a detailed description Subsection 3.4.2)
- **Control Approach 3 (Case: d.3):** Continuous, the system only acts on monitored data of at that moment and the discharge is divided based on the measured temperature (see for a detailed description Subsection 3.4.3)

The control approaches were tested for input data that were delivered by four different radial locations ($0.25R_{th}$, $0.5R_{th}$, $0.75R_{th}$ and R_{th}) of the monitoring points. A detailed description of the layout and the control approaches can be found in Section 3.4.

The aim is to find a control method of a MPPW to optimize the performance of HT-ATES system in terms thermal recovery efficiency. The results of scenario 1-3 are subsequently presented in Subsection 4.2.1, Subsection 4.2.2 and Subsection 4.2.3. Per scenario the different cases are compared and discussed in terms of thermal recovery efficiency and discharge distribution. Each section is closed with a resulting sub-conclusion.

4.2.1 Scenario 1: T_{inj} = 90 °C

In this subsection the results are presented for a MPPW with four screens that were controlled based on three different approaches and four different monitoring location r (Section 3.4) for scenario 1. Firstly, the resulted thermal recovery efficiency is presented and discussed. Secondly, the discharge distribution over the fourth recovery cycle is given and compared for the different control actions when measuring at $r = R_{th}$. Thereafter, the effect of the monitoring location is granted and elaborated on for Case d.1. This section ends with a proposed well design.

Thermal recovery efficiency

For the reference scenario (scenario 1) the results for the three different control actions are depicted in Figure 4.6. The different lines in each sub-graph represent the result of the monitoring location that is used for that control approach. The values in the plot are the difference in thermal recovery efficiency between a regular HT-ATES system and a MPPW. The red line in the plot is for the difference between an HT-ATES system where buoyancy flow is neglected (Case b) and a regular HT-ATES system (Case a). This difference is the absolute maximum recoverable thermal recovery efficiency by buoyancy flow counteraction.
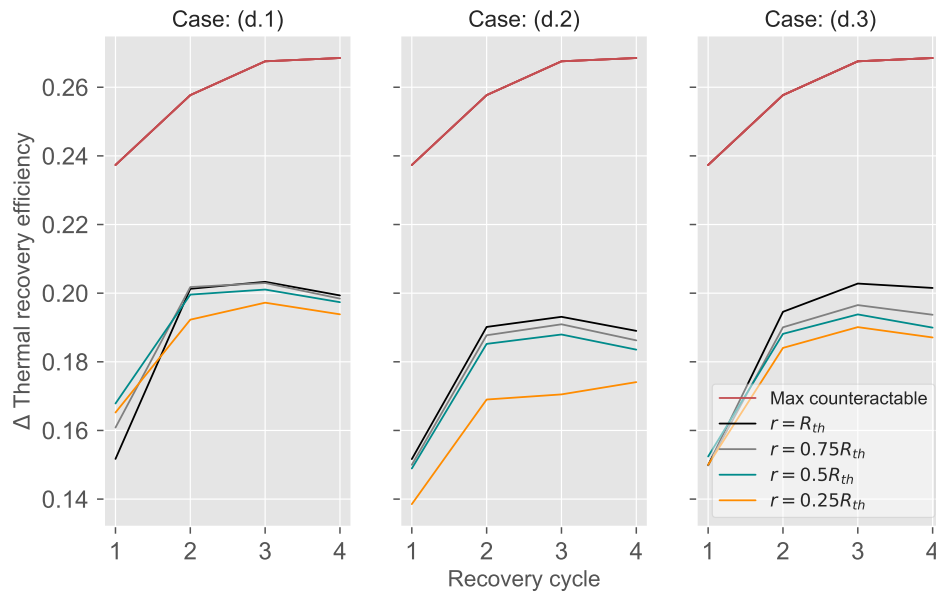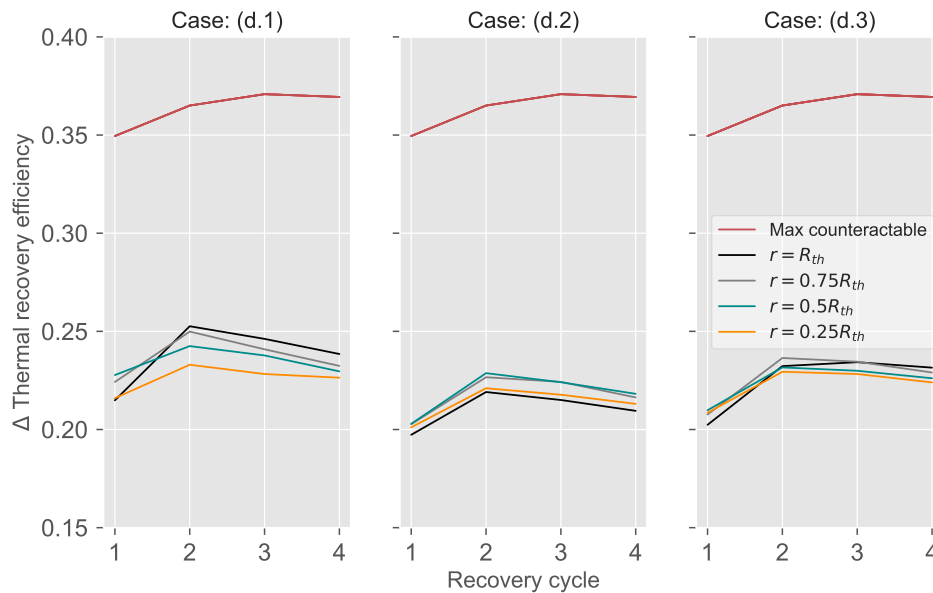
Figure 4.6: Difference in thermal recovery efficiency for scenario 1 (T_{inj}=90 °C)) between a MPPW and a regular HT-ATES (d-a), and maximum counteract-able thermal recovery efficiency (Case b-a), over the first four recovery cycles for control approach 1-3, with different monitoring locations.

For all three control approaches the result show improvement in the performance of the system in terms of thermal recovery efficiency. All three approaches show the same trend that measuring farther away from the well presents the best results after the first recovery cycle. This is explained by the fact that there is a greater temperature gradient over the aquifer thickness further away from the well during the recovery cycles. While very close to the well there will be especially in the injection phase barely a temperature gradient as the injected water temperature is measured. However, the absolute difference between the results of the monitoring location are very small. The largest difference of 0.02 is found for control approach 2 between the thermal recovery efficiency of $r = 0.25R_{th}$ and $r = R_{th}$ in the third recovery cycle.

Discharge distribution

The discharge distribution for each control action (Case d.1-3) based on monitoring at $r = R_{th}$ is shown in Figure 4.7. It can be noted that the way the system is controlled does not have influence on the screens that are used during extraction. In all three cases this is solely screen 1 and screen 2, meaning that the heat is mainly in the upper half of the aquifer. During injection the distribution shows more variation for the different control actions. This indicates a similar state when the extraction period starts regardless of the injection scheme. This is in accordance of the previous found solution for a MPPW with two screens where it was concluded that the system is less sensitive to the injection screen length than the extraction screen length. Case d.1 (Figure 4.7a) shows a constant discharge distribution throughout the entire cycle. while for Case d.2 screen 2 is closed after 2/3 of the extraction period (Subsection 4.2.2) and for Case d.3 the share of screen 2 gradually decreases till it s 0 eventually (Figure 4.7a). This insinuates the attempt to correct for more shallow injection as a result of the control approach where buoyancy flow is not pre-assumed like in Case d.1.

(a) Case d.1

(b) Case: d.2

(c) Case: d.3
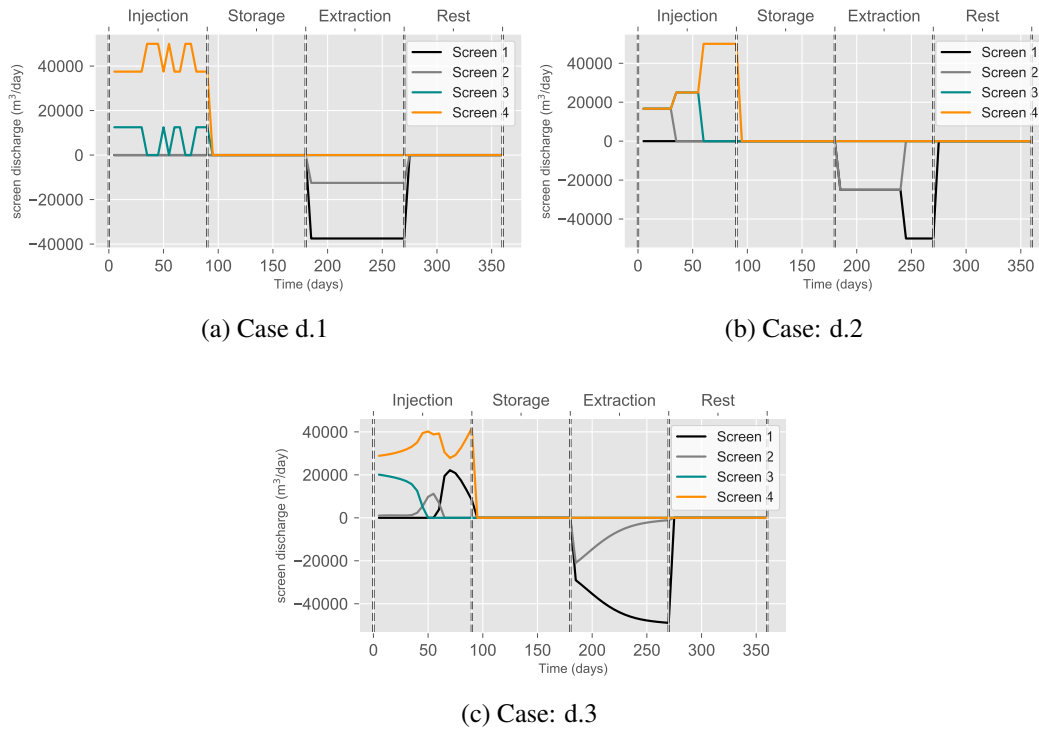
Figure 4.7: The discharge distribution over the fourth recovery cycle for control approach 1-3 for the monitoring location $r = R_{th}$.

Monitoring location

Measuring farther away from the well does not perform best in the first recovery cycle for control approach 1 (Case d.1) (see Figure 4.6). This is because during this cycle the water needs more time to get to these monitoring points. So it takes more time before control is applied as there is no temperature gradient till the water reaches the monitoring point. In the following cycles there is an initial gradient due to residual heat from the previous cycle. So control is applied throughout the entire cycle.

The total discharge contribution per screen for the fourth recovery cycle of control approach 1 (Case d.1) is depicted in Figure 4.8 for the different monitoring location. The negative values in the chart represent the extraction volumes and the positive values represent the injection values.
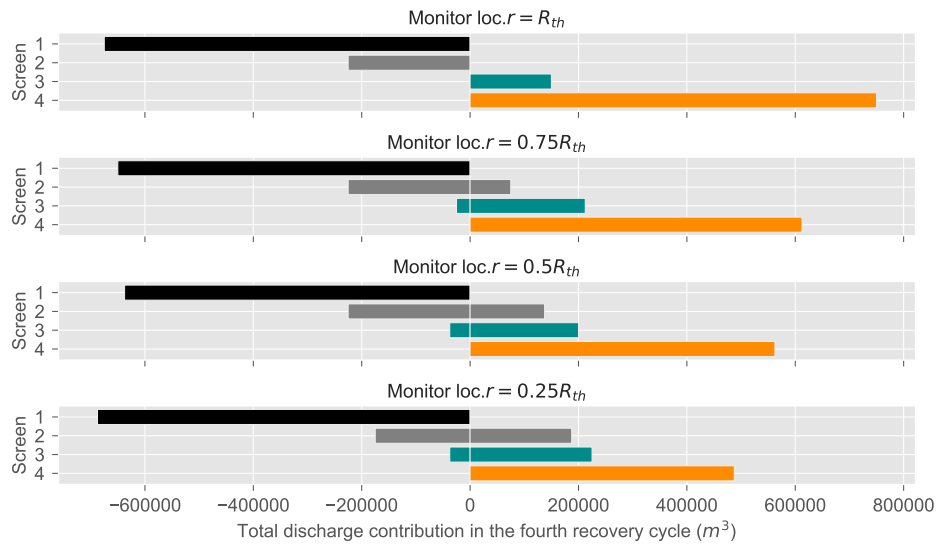
Figure 4.8: Total discharge contribution per screen for scenario 1, Case d.1, for different monitoring locations r.

It can be noted that the extraction distribution is very similar for all monitoring locations. The contribution for injection however shows variance such that there is more distribution over the screens when measuring close to the well. This can be a consideration during a design process as there will be less load on a particular screen if it more evenly distributed.

When observing how the discharge is distributed over the screens in the fourth recovery cycle for control approach 1 for $r = R_{th}$ (Figure 4.9a) and $r = 0.25R_{th}$ (Figure 4.9b), it can noted that for the injection phase more control is applied when the monitoring points are located at $r = R_{th}$. But in the extraction phase measuring close to the well ($r = 0.25R_{th}$) there is more control while in the injection phase it shows a steady distribution after day 10. This is the result of small temperature differences close to the well as the injected water is measured.

(a) Monitoring location $r = R_{th}$

(b) Monitoring location $r = 0.25R_{th}$
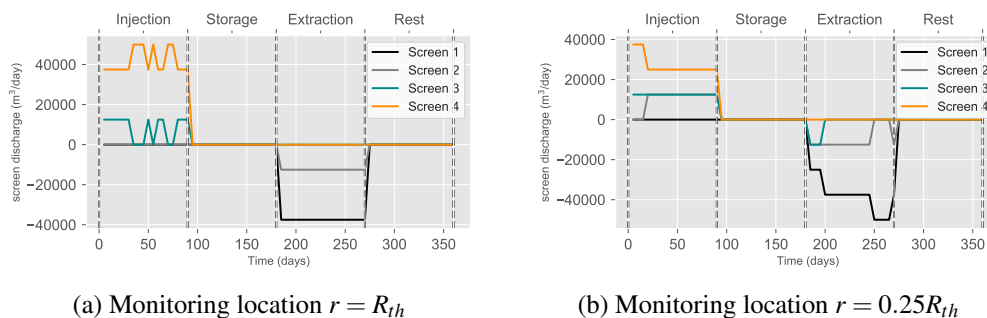
Figure 4.9: The discharge distribution of the fourth recovery cycle for control approach 1, scenario 1

Best well design

For all control approaches the performance of the system is at best when measuring at $r = R_{th}$. The control approaches 1 and 3 show the largest effect on the thermal recovery efficiency (+0.20) with respect to a regular HT-ATES system with a fully penetrating well (Case a). This improvement leaves an absolute thermal recovery efficiency of ± 0.07 that is

not counteracted. This concludes that for this scenario it is effective to assume buoyancy or distribute the discharge based on the ratio of the measured temperatures.

4.2.2 Scenario 2: T_{inj} = 112 °C

In this subsection the results are given for scenario 2, where the injection temperature is 112°C instead of 90 °C as in the reference scenario. The MPPW in the simulations had four screens that were controlled based on three different approaches and four different monitoring location r (Section 3.4). Primarily, the resulted thermal recovery efficiency is presented and discussed. Next, the discharge distribution over the fourth recovery cycle is given and compared for the different control actions when measuring at $r = R_{th}$. To continue, the effect of the monitoring location is granted and elaborated on for Case d.1. This subsection is closed with a brief conclusion.

Thermal recovery efficiency

The absolute recovered thermal recovery efficiency by using MPPW with four screens, which is the thermal recovery efficiency of an HT-ATES system with MPPW with four screens (Case d.1-d.3) minus the efficiency of a regular HT-ATES system with one fully penetrating screen are depicted in Figure 4.13. The red line represents the absolute maximum possible increase in thermal recovery efficiency which is the result of the case where buoyancy flow is neglected (Case b) minus the a regular HT-ATES system (Case a).
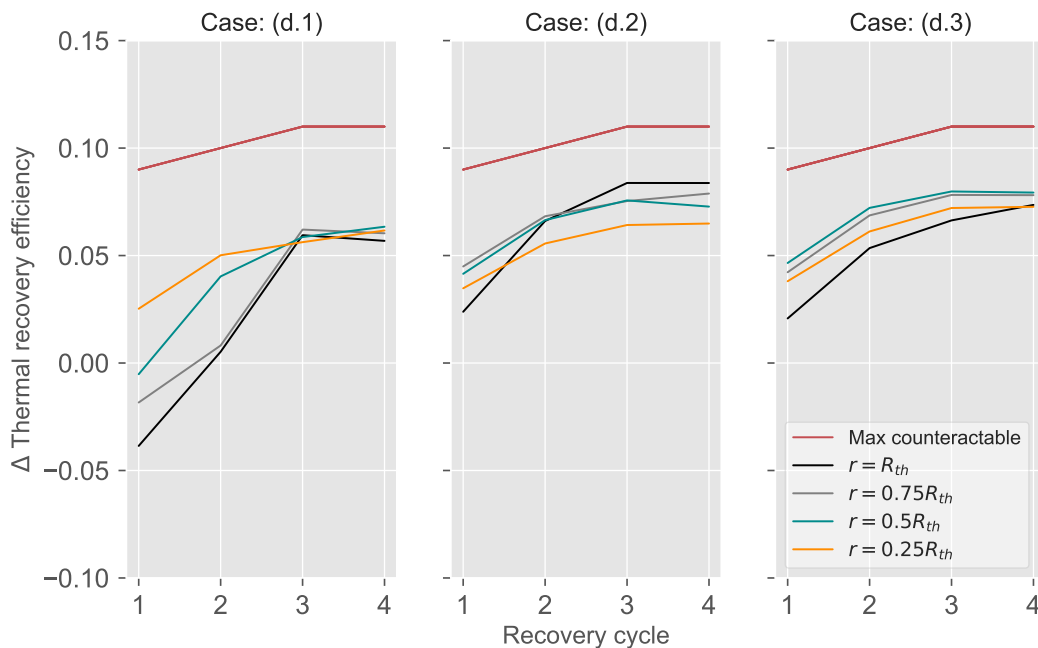

Figure 4.10: Difference in thermal recovery efficiency for scenario 2 (T_{inj} = 112°C)) between a MPPW and a regular HT-ATES (d-a), and maximum counteract-able thermal recovery efficiency (Case b-a), over the first four recovery cycles for control approach 1-3, with different monitoring locations.

All the different cases show a minimum absolute increase of 0.20 of the thermal recovery efficiency. However, it is clear that for scenario 2, control approach 1 (Case d.1) performs best. This result is independent of where the input data for the control method is measured. This suggest that for this scenario it is beneficial to assume that there is a buoyancy flow. The largest counteraction is achieved in the second recovery cycle. The following recovery

cycles show that the increase in thermal recovery efficiency by using MPPW is decreasing. This is explained by the fact that a regular HT-ATES takes more time to stabilize, so there is still improvement in the thermal recovery efficiency. While an HT-ATES with monitored and controlled MPPW is designed to optimize the system and therefore stabilizes faster.

Discharge Distribution

The resulting discharge distribution over the fourth recovery cycle of the different control approaches are presented in Figure 4.11 for monitoring at $r = R_{th}$. During extraction only screen 1 and 2 are used for all three control approaches. This is similar to the result of scenario 1 (Section 4.2.1), but screen 2 is turned off earlier in this scenario as a result of more buoyancy flow.

An interesting difference is found during injection for control approach 1 and 3 (Case d.1 and Case d.3). The distribution over time indicates that when applying Case d.1, the initial temperature gradient is larger than at the end of the recovery cycle because screen 3 is turned on. For Case d.3 (Figure 4.11c this is the opposite where the distribution is decreasing and only screen 4 operates at the end of the injection phase.

(a) Case d.1

(b) Case: d.2

(c) Case: d.3
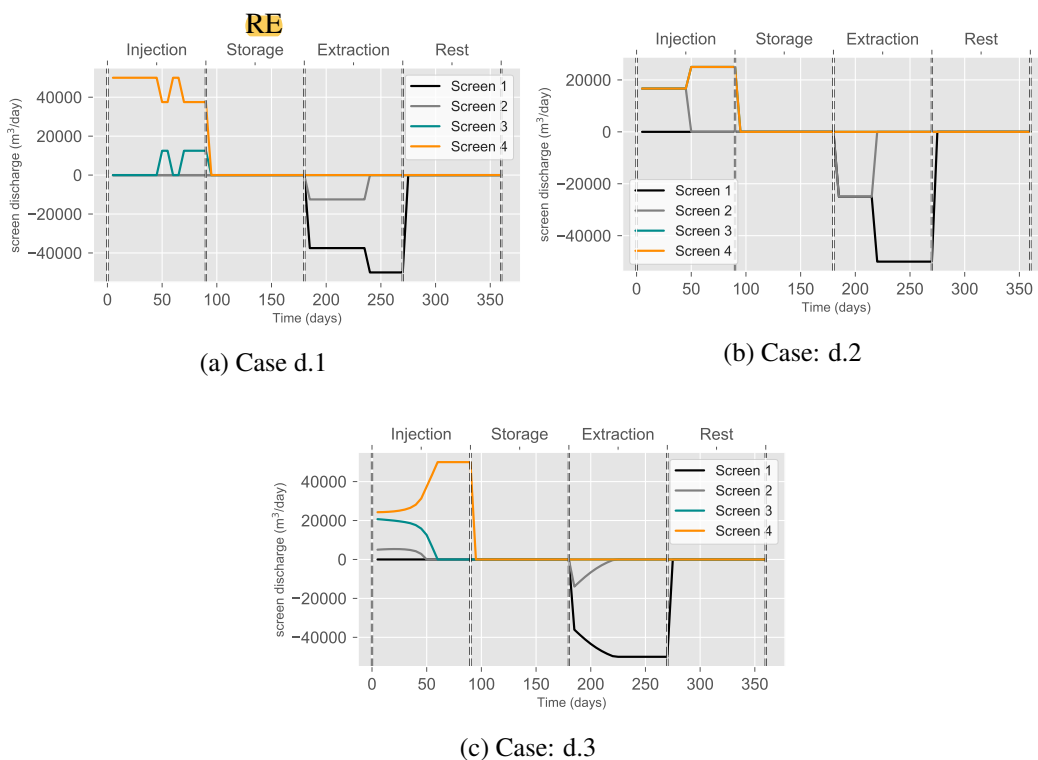
Figure 4.11: The discharge distribution of the fourth recovery cycle for control approach 1-3 for the monitoring location $r = R_{th}$.

Monitoring location

When zooming into the results of control approach 1 (left graph Figure 4.13), it can be noted that for the first recovery cycle measuring at a distance $r = R_{th}$ performs at last. This backlog is however quickly resumed in the second recovery cycle. This is due to the fact that it takes the hot water more time till it reaches the monitoring points at a distance of $r = R_{th}$. This seems to be contradicted by the results of $r = 0.25R_{th}$ (closest monitoring points to

the well) which performs slightly worse than $r = R_{th}$. However, the explanation in this Case is that when measuring really close to the well during the injection phase there is less temperature gradient because the temperature of the injected water is measured and therefore less control is applied. This effect holds throughout all four recovery cycles and therefore the thermal recovery efficiency is not resumed as for $r = R_{th}$. This was also found for scenario 1 Subsection 4.2.1. This is an important finding for the set-up of a design approach for HT-ATES systems with MPPW.
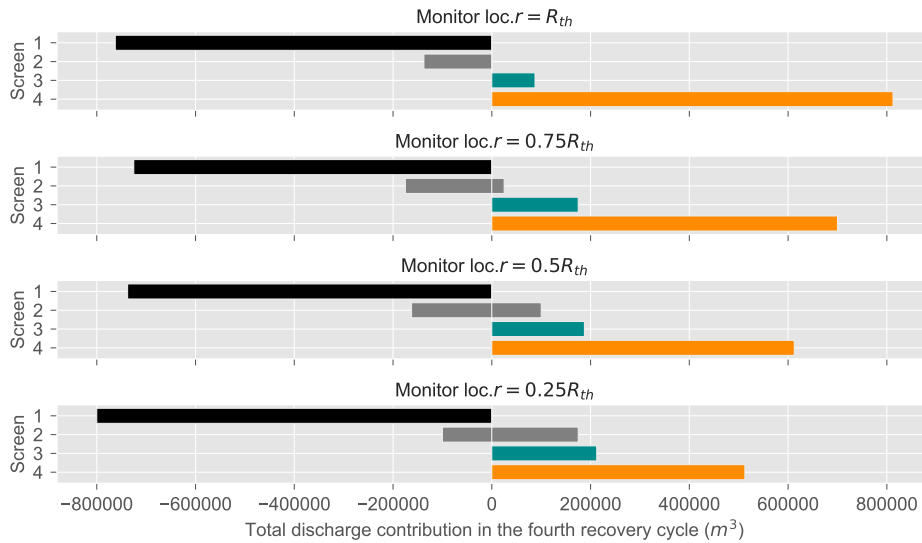
Figure 4.12: Total discharge contribution per screen for scenario 2, Case d.1, for different monitoring locations.

The discharge contribution per screen shows the same trend as for scenario 1 (see Figure 4.12) but with less distribution over the screens. The contribution per screen during extraction is exactly the same for $r = 0.75R_{rth}$ and $r = 0.5R_{th}$. However, when $r = 0.5R_{th}$ less load is applied on screen 4 during injection and the total discharge is more distributed. This indicates that the performance of HT-ATES with MPPW is less sensitive to the way the water is injected.

In terms of practicality, the use of monitoring at $r = 0.75R_{th}$ or r= 0.5Rth show most distribution over the screens when considering both the injection as the extraction phase. As described in Subsection 2.3.1, a certain screen length has a maximum capacity, and one borehole can have up to four screens. So, when the discharge is more distributed over more screens less boreholes will be needed. This has effect on the total cost of a project and should therefore be considered.

Best well design

The thermal energy recovery for scenario 2 is increased by applying monitor and control. The best way of controlling is pre-assume that there is buoyancy flow and take this into account in the control approach. The location of the monitoring points have initially large effect on the thermal recovery. However, this evens out for continuing recovery cycles. The main effect of the location of the monitoring points is how the discharge is distributed over the screens mainly in the injection phase. In this scenario, 1/5 of the load on screen 1 and

1/4 of the load on screen 4 can be reduced by measuring at $r = 0.5R_{th}$ and $r = 0.75R_{th}$. This is important to take into consideration when developing a design strategy.

4.2.3 Scenario 3: T_{inj} = 61 ℃

For scenario 3 control approach 2 resulted in the best performance followed closely by control approach 3. As there is indeed less buoyancy the presumption in a control method that there is buoyancy flow does not benefit the performance in this Case (Control approach 1). With monitoring at $r = R_{th}$, $r = 0.75R_{th}$, and $r = 0.5R_{th}$ the performance is worse than that of a regular HT-ATES system with a fully penetrating well in the first recovery cycle.

Figure 4.13: Difference in thermal recovery efficiency for scenario 3 (T_{inj} = 61°C)) between a MPPW and a regular HT-ATES (d-a), and maximum recoverable efficiency and regular HT-ATES (d-a), and maximum counteract-able thermal recovery efficiency (Case b-a), over the first four recovery cycles for control approach 1-3, with different monitoring locations..

The sensitivity of the performance of to monitoring location for the cases of this scenario is very small for recovery cycle 4. The shape of the volume has a cylindrical shape, creating symmetry. Thus, the ratio between the monitoring points is nearly the same for each location.

4.2.4 Conclusion: MPPW with four screens

In this section the research question corresponding will be answered. Overall, the results showed that by controlling the screens with the assumption that there is buoyancy flow (Case d.1) the performance of an HT-ATES system is at it's best. However, when buoyancy is becoming smaller this is not a right method to control the system. The way to control systems with small buoyancy flow, is by controlling based on at the concurrent temperature data in the aquifer because the buoyancy flow is small. Close monitoring ($r = R_{th}$) has shown to be not optimal as less control is applied during the injection phase. Measuring very close to the well the injected water will be measured which means that temperature gradients are harder to detect in this phase. It can be concluded that measuring at a distance $r = R_{th}$ presents the best overall results in terms of thermal recover efficiency after the first recovery cycle. The

temperature gradients are higher farther away from the well resulting in more control of the system. The absolute difference in thermal recovery efficiency are however not significant. For most cases around 1% compared to $r = 0.75R_{th}$ and $r = 0.5R_{th}$. However, the discharge distribution in the injection phase particularly is significantly different for the different monitoring locations. This should be weighted in the design of MPPWs for HT-ATES systems since the hydraulic capacity is dependent on the screen length (Subsection 2.3.1).

4.3   Slope of the thermal front

The developed control approaches and MPPWs in general strive to a minimal slope of the thermal front as this is regarded as the optimal shape of the storage volume minimizing losses due to the effect of buoyancy flow. On top of that, it can be used as a performance indicator during a recovery cycle as it can be approached by measuring points in the aquifer. In this section the assessment of the slope of thermal front is presented for the reference scenario.

When there is a regular HT-ATES with a fully penetrating screen, the slope of the thermal front decreases linearly in the injection and storage phase. During extraction the slope of the thermal front increases until the rest phase starts. During the rest phase the thermal front also increases but to a lesser extent. The course of the slope for the reference scenario is presented in Figure 4.14. It was researched if the calculated slope is dependent on which temperature contour is used. Figure 4.14 shows that the course of the slope for different temperature contours are similar. This is because the contours are symmetric in the radial direction (Tsang et al. 1981). However, part of the heat is left in the aquifer after extraction in the form of mainly water at lower temperature. This results in that after extraction the initially vertical thermal front is not completely restored and the following cycle starts with an initial slope.
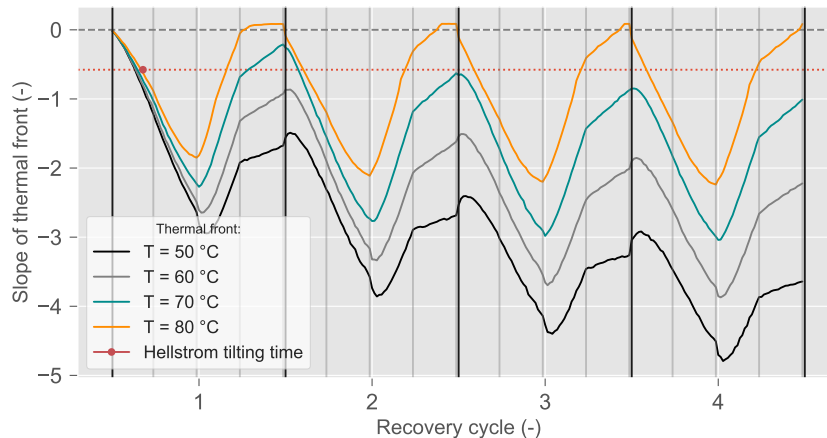
Figure 4.14: Slope of thermal front of different contour temperature for regular HT-ATES system over the first recovery cycle for scenario 1.

The red dot in Figure 4.14 represents the tilting time determined by Equation 2.1 for the reference scenario. Table 4.2 presents the values for the tilting time for scenario 1-3. It can be noted that the slope determined by the model is in agreement with the tilting time.

Table 4.2: Tilting time determined by Hellströms expression (Equation 2.1) and the tilting time determined by the model as presented in (Equation 3.21) for a regular HT-ATES system (Case a).

Scenario	Hellström tilting time (d)	Modelled tilting time (d)
1: $T_{inj} = 90$ °C	68	65
2: $T_{inj} = 112$ °C	54	50
3: $T_{inj} = 61$ °C	105	110

The application of MPPW changes the course of the slope in two ways. First, there is an increase in slope as a result of deep injection. Usually the slope decreases as a result of the buoyancy flow. Positive slope means there is more heat in the bottom of the aquifer. After a certain maximum slope is reached, the slope decreases linearly till extraction starts. This increase in the slope results in extension of the tilting time. Second, the slope is increasing faster during the extraction period for all temperature contours. This increase results in that after extraction the slope is mostly restored.

(a) Deep injection (b) Shallow extraction
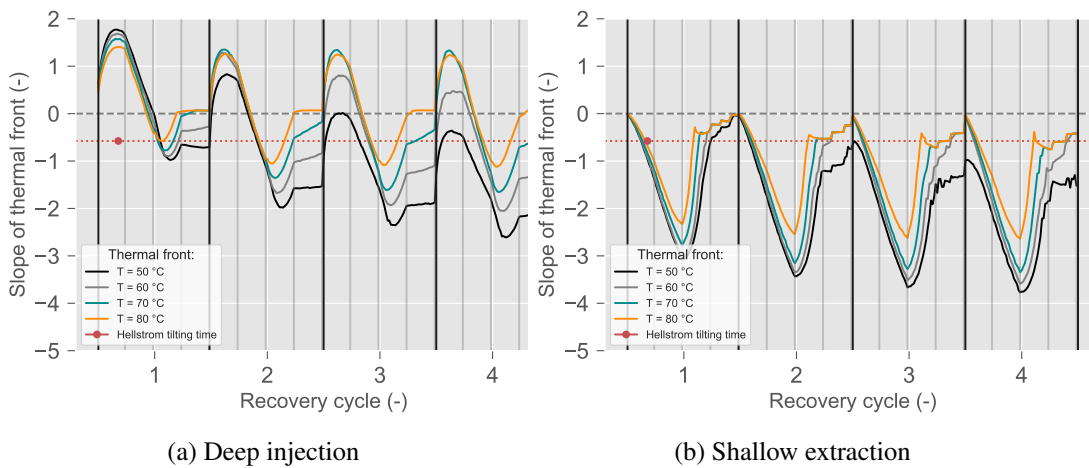
Figure 4.15: The slope of the thermal front for different temperature contours.

This explains why shallow extraction is more beneficial as more heat is recovered.
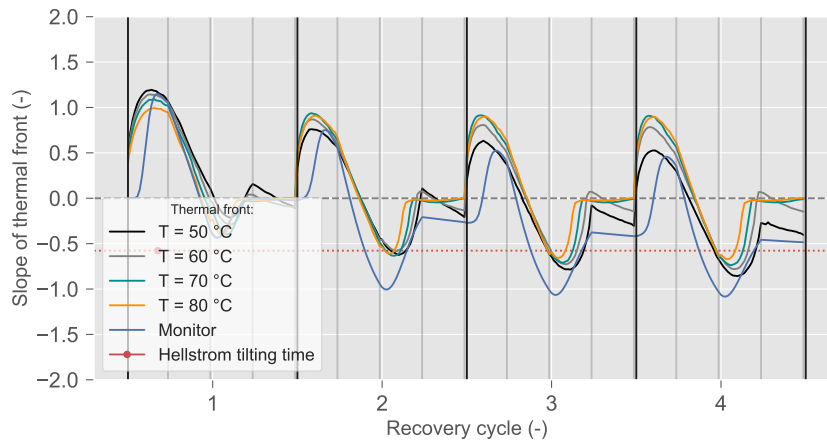
Figure 4.16: Slope of thermal front of different contour temperature for an HT-ATES system with a MPPW with two screens ($Le = Li = 0.25H$).

Figure 4.16 present the result if both deep injection and shallow extraction is applied by using an injection and extraction screen length of 25% of the aquifer thickness ($Li = Le = 0.25H$). It shows that the tilting time is increased and the residual slope is closer to zero after extraction. An interesting remark is the decrease in slope during the rest phase. This insinuates that the body of 50°C and 60°C are still flowing in the upward direction as result of the buoyancy flow.

(a) After extraction

(b) After rest
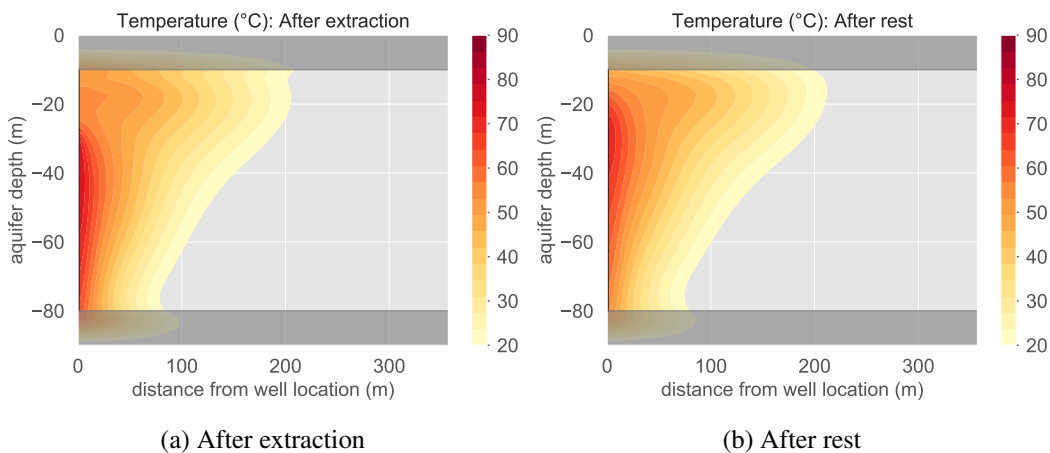
Figure 4.17: The temperature distribution in the aquifer for scenario 1 and Case c ($Li = Le = 0.25H$).

This is indeed the case when observing the temperature distribution in the aquifer as depicted in Figure 4.17. Part of the heat that is left in the aquifer is still buoyant and flows towards the top of the aquifer. This heat is extracted in the next recovery cycle.
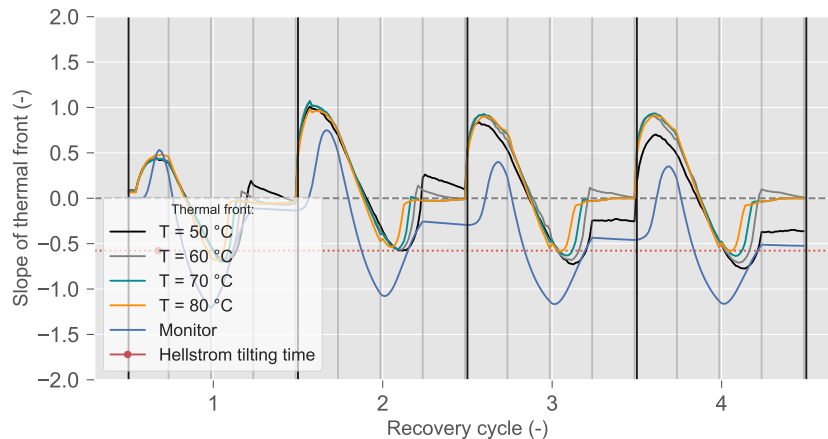
Figure 4.18: Slope of thermal front of different contour temperature for an HT-ATES system with a MPPW with four screens Case d.1 with monitoring at $r = R_{th}$

The slope over time for Case d.1 where a MPPW with four screens was implemented and controlled based on monitoring points at $r = R_{rth}$ is presented in Figure 4.18. It shows a almost identical course as Figure 4.16 but with a main difference in the first cycle. Both well designs result in a recovery efficiency of 0.81 in the fourth recovery cycle. This implicates that the slope of the thermal front is indeed representative to the performance of HT-ATES systems.

The blue line in Figure 4.18 and Figure 4.16 represents the slope of the thermal front determined by measuring points in the aquifer at a distance $r = R_{th}$ from the well. It shows strong similarities with the slope determined by the model. These similarities are in terms of both the course and maximum/minimum values of the slope of the thermal front. This suggests that the monitoring at $r = R_{th}$ is representative of what happens in the aquifer. The residual slope after the rest phase indicates the residual heat in the system. The increasing slope indicates that the tilting time will be delayed which is beneficial for the recovery efficiency.

4.4 Sensitivity Analysis

In the previous two sections different designs of MPPWs were simulated to test the potential of counteracting the effect of different magnitude of buoyancy flow. This resulted in two proposed designs for the reference scenario.

- MPPW with two screens with lengths $Le = Li = 0.25H$
- MPPW with four screens controlled by control approach 1 (Case d.1) based on monitoring data at $r = R_{th}$ from the well location.

In this analysis the sensitivity of these two designs were tested for various conditions. The aim of this section was to find the answer to the following research question

How is the performance of HT-ATES systems with MPPWs affected by the storage volume, aquifer thickness, and magnitude of buoyancy flow?

Three parameters were varied with respect to the reference scenario (Table 3.3): aquifer thickness, storage volume and injection temperature. In Subsection 4.4.1 the results are presented for larger aquifer thickness ($H = 105m$, scenario 4) and smaller aquifer thickness ($H = 35m$, scenario 5). This is followed by the results of scenario 6 were a smaller storage

volume of $V = 450.000m^3$ was simulated. This section closes with an overview of the results of scenario 1-6 as proposed in Table 3.3.

4.4.1 Scenario 4 & 5: Aquifer thickness

The thermal recovery efficiency for H=70 (scenario 1), $H = 105m$ (scenario 4) and $H = 35m$ (scenario 5) are plotted in Figure D.26. In the first recovery cycle the scenario with the large aquifer thickness (H=105m) performs worse than scenario 1 with H=70m. This is a cause of how the control approach d.1 is developed. As the heat is retarded due to thermal retardation, cold water is extracted. The monitoring points record the decrease in temperature but this is assumed to be the bottom screens. Meaning that the top screen keeps the highest part of the total discharge while Figure 4.20b illustrates that it is rather the top screen that needs to be closed.

(a) Scenario 1: $H = 70$ m   (b) Scenario 4: $H = 135$ m

(c) Scenario 5: $H = 35$ m
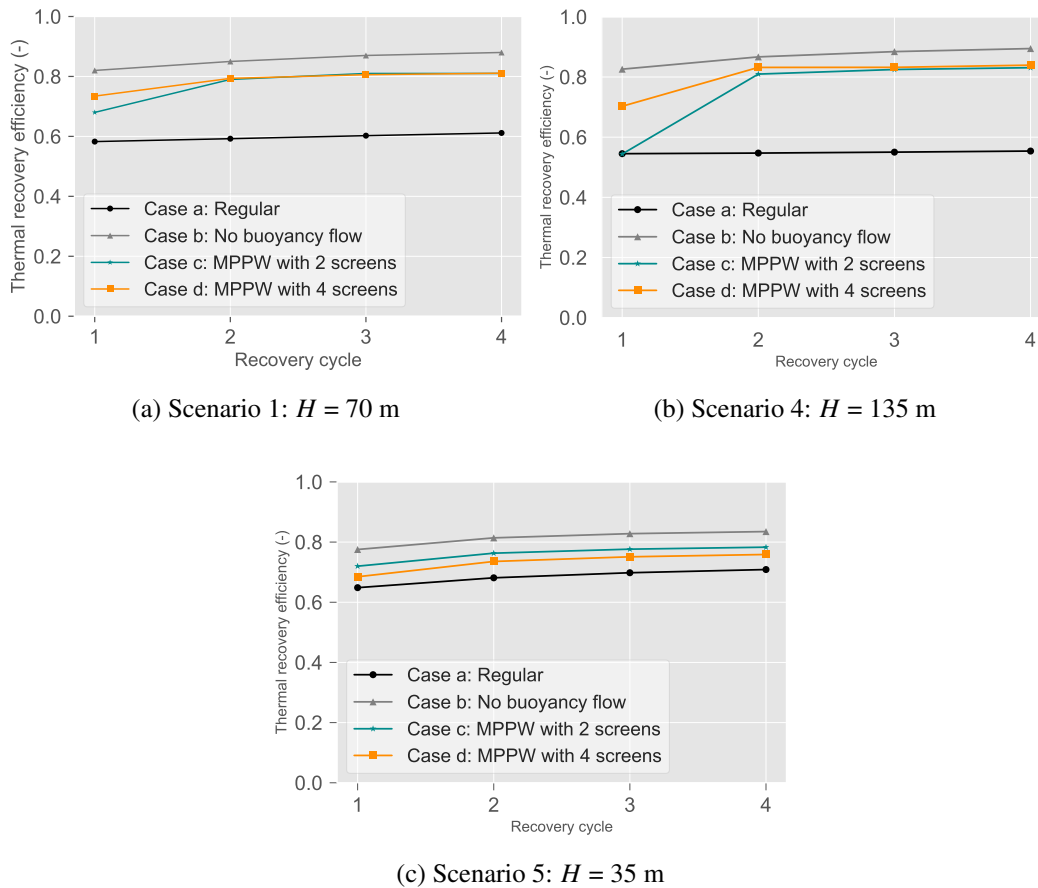
Figure 4.19: The thermal recovery efficiency over the first four recovery cycles for all four HT-ATES cases (a-d.1).

For larger aquifer thickness (H=105m, scenario 4), the heat loss due to buoyancy increases when using a fully penetrating well (Case a) with respect to the reference scenario. However, when applying MPPW with four screens that are monitored as discussed in this section the results are positively affected when compared to the results of the reference scenario (scenario 1) for controlled well screens. This is due to the fact that the buoyant water has more space to travel till reaching the top of the aquifer and induce tilting.

This also occurs for scenario 1 where H=70m but in lesser extent (Figure 4.20a). In this

(a) Aquifer thickness H=70m

(b) Aquifer thickness H=105m
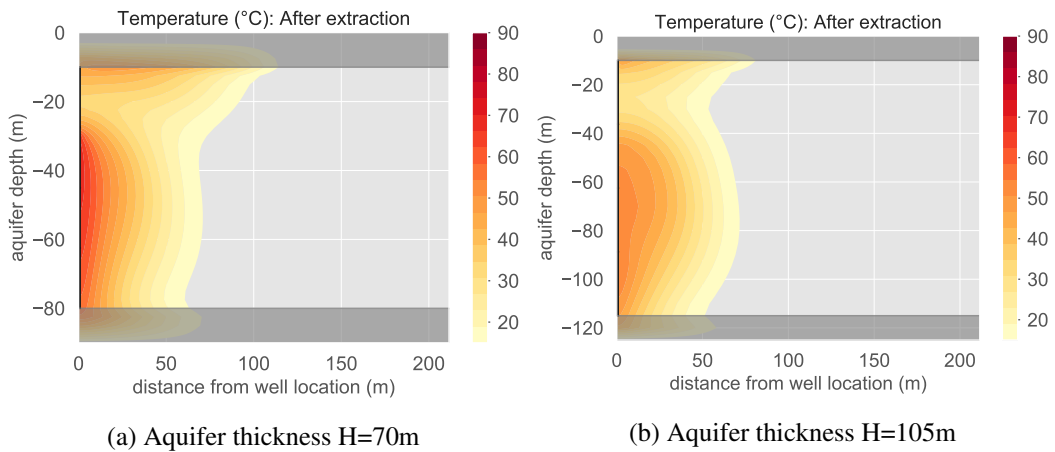
Figure 4.20: The temperature spread over the aquifer after the extraction period of the first recovery cycle.

scenario the travel distance of the heat is smaller. This is resumed after the first recovery cycle and all three aquifer thickness scenarios show the same trend for the following recovery cycles (Figure 4.19).When the aquifer thickness is reduced to 35m (-50% of 70m of reference scenario) control of the system has barely effect, see Figure 4.21b.

The aquifer thickness affects the results of the control approach. The effect in terms of improvement in thermal recovery efficiency is higher for larger aquifer thickness. In small aquifers the distance that MPPW can create for the water to travel is limited and therefor not very effective as was shown in this section. This can however have more effect if the storage periods are shorter. Velocity is defined as distance that is bridged over a certain time. In order to decrease the effect of buoyancy flow one can either look for larger aquifers or decrease the storage time.

4.4.2 Scenario 6: Storage Volume

The sensitivity of a MPPW design for an HT-ATES system was investigated for a smaller injection volume. Figure 4.21 presents the thermal recovery efficiency of the first four recovery cycles for the reference scenario (Figure 4.21a) and for scenario 6 where 50% less storage volume was simulated (Figure 4.21b).

(a) Scenario 1: $V = 900,000$ m^3

(b) Scenario 6: $V = 450,000$ m^3
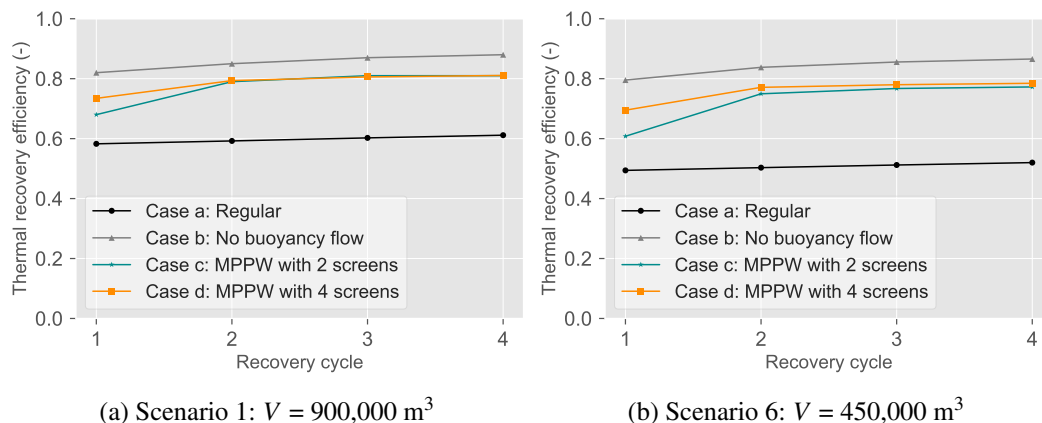
Figure 4.21: The thermal recovery efficiency over the first four recovery cycles for all four HY-ATES cases (a-d.1).

For small injection volumes, the overall surface area of the storage volume will be relatively large compared to the thermal volume. This results in relatively higher conduction losses. On top of that, the thermal front is closer to well as the thermal radius R_{th} is smaller for smaller injection volume. Consequently, thermal front tilting resulted in large amounts cold water extraction at the lower part of the screen for a regular HT-ATES systems. Therefore, the increase in thermal recovery by using MPPW is large in this scenario (+ 0.26). The two MPPWs designs (Case c, d) are barely sensitive to smaller injection volume as the performance is very close to the reference scenario. The use of two screens without control show smaller thermal recovery efficiency for the first recovery cycle with respect to a controlled four screen MPPW system. This is because the use of control enables more compactness of the storage volume resulting in that the conduction losses are minimized already in the first recovery cycle. In this case of a MPPW with two screen the conduction losses are high in the first year but reduce the subsequent cycles as the residual heat from the previous cycle reduces the temperature difference between the injected water and ambient groundwater.

4.4.3   Overview of scenarios

The best performing case with four wells for each scenario was compared to a regular HT-ATES (Case a), an HT-ATES without buoyancy (Case b) and the best Le/Li combination as found in the previous section. The thermal recovery efficiency for the fourth recovery cycle for all the scenarios are plotted in Figure 4.22. This figure illustrates that for all scenarios simulated, the performance of an HT-ATES is improved when applying MPPW. The performance is at it best for a low injection temperature. However, the loss due to buoyancy flow is only 0.17 for this scenario. The largest improvement is for the scenario with the large aquifer thickness. where 85% of the buoyancy flow is counteracted.

The result show the trend that the buoyancy flow counteraction is for all scenario except for the low injection temperature, at least 50%. So, this approach is for these scenarios a steady solution. This comparison also shows that a MPPW with four or two screen show almost the same result. Meaning that two wells is sufficient to counteract buoyancy flow. This answers the research question tackled in this section.
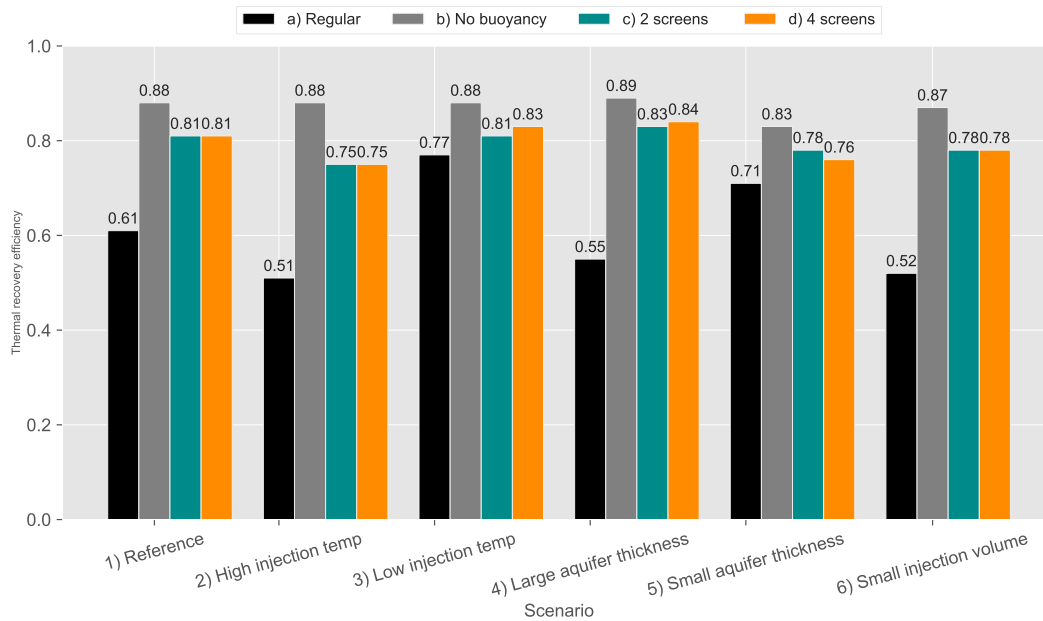
Figure 4.22: Thermal recovery efficiency for the fourth recovery cycle for all scenarios and cases.

The counteraction of the effect of buoyancy flow is calculated for the best performing MPPW design for each scenario. The values are presented in Table 4.3.

Table 4.3: Maximum counteraction of the effect of buoyancy flow as defined in Equation 3.20 for all scenarios (See Figure 4.22)

Scenario					
1	2	3	4	5	6
74%	65%	45/%	85%	58%	74%

The values as presented in this section are for one MPPW design with two screens and one MPPW design with four screens.

Extraction temperature

The extraction temperature shows for the same thermal recovery efficiency the same trend in the investigated phases. Figure 4.23 depicts the extraction temperature for scenario 2 for all the four cases that were used in the sensitivity analysis.
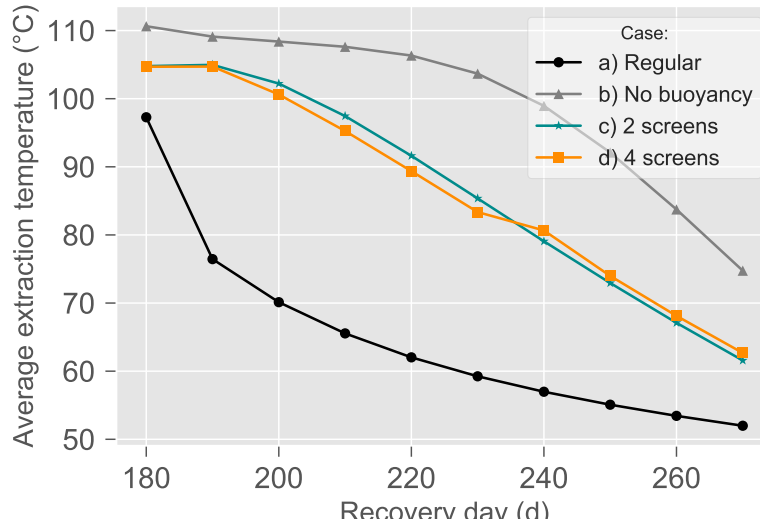
Figure 4.23: Extraction temperature during the fourth recovery cycle for Case a-d. for scenario 2.

A little jump is noticeable for Case d. This is the result of turning of a screen. This shows that the control approach works.

4.5 Circulation during storage

The results for scenario 7, where water is injected of 150°C are presented in this section. The aim of this section is test the possibility of vertical circulation to counteract the effect of buoyancy flow in the storage period.

(a) Thermal recovery efficiency

(b) Extraction temperature 4th recovery cycle
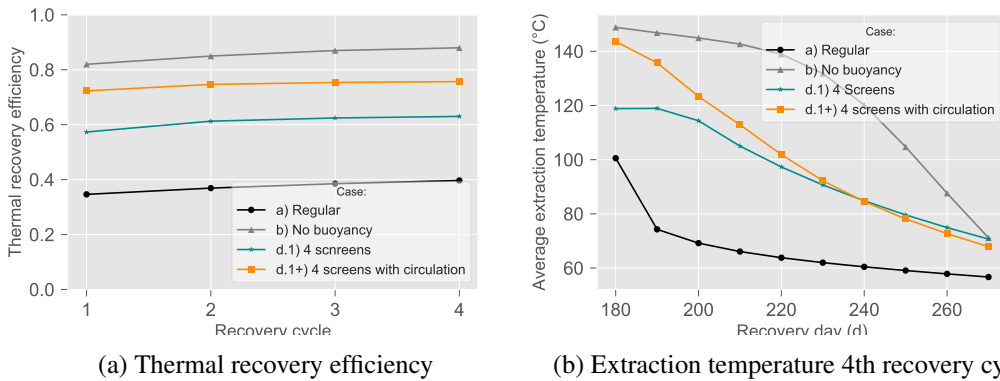
Figure 4.24: Results for scenario 7 (T_{inj} = 150 °C) with addition of vertical circulation during the storage phase (Section 3.4.1

The thermal recovery efficiency (see Figure 4.24a) is approximately 0.10 higher for all recovery cycles when there is vertical circulation in the storage period. When observing the extraction temperature depicted in Figure 4.24b, it shows higher extraction temperatures till day 60 of the extraction period. After this point, the performance is similar to d.1 without circulation. Figure 4.25 depicts the temperature spread in the aquifer after storage in the fourth recovery cycle for the case without ((Figure 4.25a) and with (Figure 4.25a) circulation.

It shows that the control of the system during storage was able to keep the water with the highest temperature in the entire aquifer. For Case d.1, the water with highest temperature are all located at the top of the aquifer. This explains why the extraction temperature is so much higher for the case with circulation.
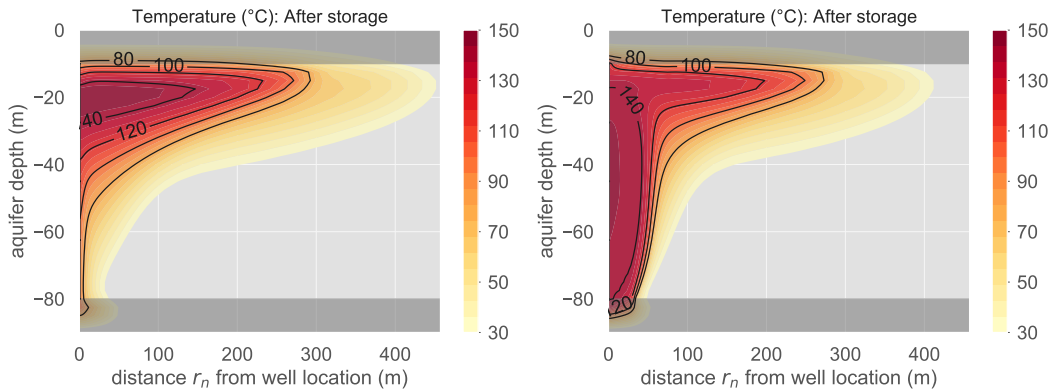
(a) Case d.1: Without circulation during storage   (b) Case d.1x: With circulation during storage

Figure 4.25: The temperature distribution of scenario 7 (T_{inj} = 150 °C) after storage for Case d.1 (a) and Case d.1x (b).

This result shows that vertical circulation is beneficial in terms of thermal recovery efficiency and extraction temperature when there is a large buoyancy flow.

It should be noted that pumping this water around needs additional energy. This energy requirement is dependent on the hydraulic head difference. This is significantly smaller than injection from and extraction to the surface as the pumping only occurs within the aquifer.

4.6   Applicability Analysis

In this section the results are presented for the applicability analysis as to awnser the following research question

Under what conditions does application of MPPWs increase the recovery efficiency of HT-ATES systems?

All the results of the conducted simulations are illustrated in Figure 4.26. The difference in thermal recovery efficiency between an HT-ATES system with MPPW (with two stacked screen of 0.5H) and a regular HT-ATES system (with one fully penetrating screen) is plotted for a range of buoyancy flow q_z (see Equation 3.14). The lines in the graph represent the result for a particular H/R_{th}. The results are for the second recovery cycle as the first recovery cycle is the most unstable cycle (Sauty et al. 1982). The following cycles continue with the same trend and therefore wont change the outcome of this analysis
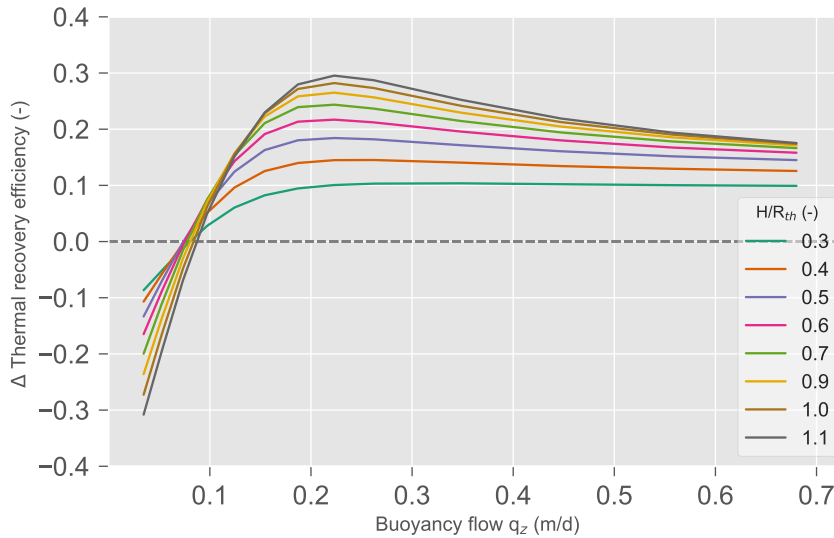
Figure 4.26: Difference in thermal recovery efficiency between MPPW with two screens and a regular HT-ATES system for various H/R_{th}

The positive values mean that thermal recovery efficiency is higher when using MPPW in comparison to a regular HT-ATES with a fully penetrating screen. The results show that for all H/R_{th} there is one buoyancy flow that acts as the turning point in which MPPW is beneficial. This is between $q_z = 0.073$-0.085 m/d. So this result shows that for all H/R_{th} the use of a two screen MPPW is beneficial if the buoyancy flow is above 0.085 m/d.

The lines also show a peak where after the benefit of MPPW decreases and all result converge to an absolute increase of 0.1 of the thermal recovery efficiency. This peak may indicate the maximum that this MPPW design can counteract in these conditions. As found in the previous sections, when buoyancy flow is becoming larger, smaller screen length and more gap is needed between the two screens. So, the design needs to be adjusted.

In H/R_{th}, the storage volume and aquifer thickness is incorporated. In q_z this is the (vertical) hydraulic conductivity and the injection and ambient groundwater temperature this. Figure 4.27 gives the value of the buoyancy flow q_z for a range of injection temperature and vertical hydraulic conductivity as can be found in the Netherlands (Bloemendal and Hartog 2018). The dotted red line is the the transition point as found in Figure 4.26. All the combinations above this line will benefit from applying MPPW.
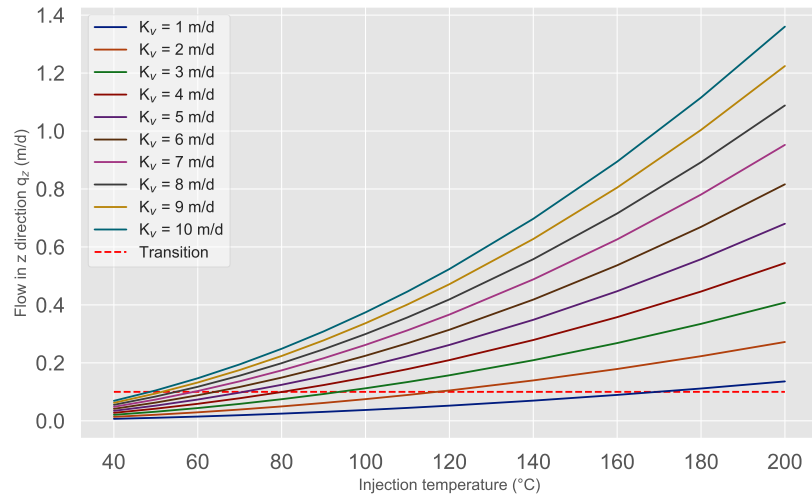
Figure 4.27: buoyancy flow for different vertical hydraulic conductivity (K_c) and injection temperature (T)

This result gives the possibility to give a first order estimation on the effect of applying MPPW. Further screen length and operational optimization will be the next step in the design process.

4.6.1 Conclusion: Applicability

The conclusion that can be drawn from this result is that in a large range of buoyancy flow (larger than 0.1 m/d) and ratio of the aquifer thickness over the thermal radius (larger than 0.3), the application of MPPW increases the thermal recovery efficiency. This result can be used in a preliminary design phase of HT-ATES systems to easily find whether the application of MPPW is beneficial in terms of thermal recovery efficiency. This can for example be done in the following order.

II
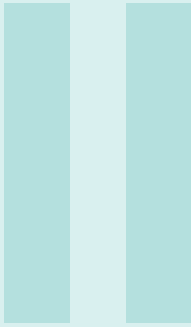
Reflection

The chapters contained in this part aim to reflect on the conducted research and main presented findings. This will be done in three chapters.

The discussion is presented in Chapter 5 and will discuss the used approach. The results will be interpreted, their limitations will be discussed and the added value compared to results from previous studies will be given and discussed.

In Chapter 6 the main research objective will be evaluated, supported by the results presented in this report. Recall that the objective as stated in the introduction of this report reads:

To design, develop, control, and assess the impact of the application of multiple partially penetrating wells on the performance of high temperature aquifer thermal energy storage systems in terms of thermal recovery efficiency.

In Chapter 7 recommendations will be given for possible future studies expanding on the research as presented in this thesis document.

5. Discussion

This research has shown a significant increase in thermal recovery efficiency of HT-ATES systems for the available hydraulic conductivity and aquifer thickness values in the Netherlands, when applying MPPWs as a method to counteract the effect of buoyancy flow. However, the use of a MPPW with two or four screens did not show a profound difference in terms of thermal recovery efficiency. The results as presented in this thesis demonstrate the practical possibilities of MPPWs for the realisation of an HT-ATES systems and therefore the added value of this research.

This chapter is focused on the discussion of the obtained and presented results. This is done by discussing three topics related to the research;

- Used methodology (Section 5.1)
- Limitations of this study (Section 5.2)
- Comparative analysis with results of other studies (Section 5.3)

5.1 Used methodology

In the following section several points are discussed related on the method applied in this study which may be argued in terms of reliability.

Cut-Off temperature

Throughout this research the thermal recovery efficiency was determined by assuming that the extraction volume is equal to the injection volume. In practice there may be a desire to maintain a certain minimum extraction temperature. This would result in smaller extraction periods as extraction stops when this temperature is reached.

The results also showed higher extraction temperatures for an HT-ATES system with a MPPW compared to a regular fully penetrating well. When a minimum extraction temperature is set, the increase in thermal recovery efficiency will be higher when using a MPPW as more water can be extracted at higher temperature.

Flow regime

The function that was used to represent the seasonal flow was a block function with equal injection, storage, extraction and rest periods of 90 days for one recovery cycle. In practice it is not realistic as there are **1)** fluctuations in heat demand and supply and **2)** no distinct storage and rest period tending the flow into more of sinusoidal form rather than a block function.

Fluctuating head demand and supply will have effect on the thermal recovery efficiency as this is defined as the total energy extracted over the total energy injected. So when the demand is smaller than the supply this will lead to low thermal recovery efficiency for that cycle. This leads to more residual heat in the aquifer for the following recovery cycle inducing less thermal loss in that following year, thus a higher thermal recovery efficiency.

In this presumable case, these fluctuation are harder to intercept when either two or four screens with a fixed discharge distribution are used. The use of four (or more) screens that are controlled based on monitored data are likely to be more efficient. The use of four screens delivers more flexibility when there are fluctuations.

The slope of the thermal front is found to be changing linearly in the injection and storage phase for a fully penetrating well and shows a bump in the injection phase for a case with MPPW where after it also decreases linearly. Meaning that decreasing or even diminishing the storage phase by increasing the injection phase won't have much effect as the tilting of the thermal front is happening at the same rate during injection and storage. So, it is predicted that the thermal recovery efficiency would be very similar when using a sinusoidal function.

Remaining losses

The theoretical maximum, which is the thermal recovery efficiency that results when buoyancy flow is neglected so that the loss is solely the result of conduction and dispersion losses, is used as the target value. As shown in the results, this target value was approached but not reached for the investigated MPPWs designs. It is argued if it realistic to achieve this target thermal recovery efficiency.

One reason for the remaining losses can be that the design of the MPPWs and control methods are not optimal. However, the difference in thermal recovery efficiency of the different tested design approaches were very small. It is therefore predicted that different design and control strategies are not likely to have significant effect on the performance. Another reason can be that there are additional losses when MPPWs are applied. When using smaller screen lengths, thus smaller area, to inject or extract the same discharge the water velocity will be higher. Caljé (2010) and Bloemendal and Hartog (2018) showed that dispersion losses increase along the top and bottom confining layers when velocities are higher. This seems to be confirmed by the fact that for the reference scenario the thermal recovery efficiency was converging such that more distance between the screens did not lead to additional efficiency. On the other hand, when the scenario with a larger aquifer thickness was simulated and thus more distance between the screens was created, the efficiency was closer to the theoretical maximum of the corresponding scenario (to take into account the decrease in conduction losses). This argues whether the theoretical maximum can be achieved with MPPW in certain scenarios as losses like dispersion increase as a result of higher velocities.

Nonetheless, this does not take away that the use of MPPW improves the performance of an HT-ATES system significantly in terms of increase of the thermal recovery efficiency and therefore won't change the main outcome of this thesis.

5.2   Limitations of research

In this section the main limitations of this study are discussed.

Homogeneous aquifer

The scope of this research was limited to solely the analysis of an anistropic homogeneous aquifer. This means that the hot water volume is not disrupted and the location of this water after storage can be predicted and the use of more than two screens seemed superfluous. However, it is not likely that this is the case in practice as it is more likely that the aquifer will be heterogeneous. On top of that, determining the complete subsurface layout and properties

is a challenge and often impossible. Heterogeneity of the aquifer causes hot water plumes to arise due to hampering of the storage volume by for example intervening clay layers and local velocity differences due to local heterogeneity. In these cases the use of more screens that operate based on monitoring data at a certain distance from the well will deliver more flexibility. It is predicted that this will change the results of this research such that the use of more than two monitored and controlled screens will be favorable in terms of increase in thermal recovery efficiency. Sommer et al. (2013) studied the effect of heterogeneity in low temperature ATES systems where buoyancy flow can be neglected (Doughty et al. 1982). Sommer et al. (2013) showed that over multiple recovery cycles the effect is limited as the system stabilizes. This was also explained by Vandenbohede et al. (2009), that because heat is not only transferred via the pore water but also the soil particles. The range of values for thermal properties of different soil materials is limited. This smooths the temperature differences resulting in a far more homogeneous medium. For HT-ATES systems with MPPW it is expected that also in case of heterogeneity the system will converge to one set of control sequence with the same discharge distribution each year.

Practical implementation

The practical limitations or regulations are not considered in this research. This is a field that still needs to be developed as application of MPPW has never been realized for HT-ATES systems. The only reference projects are in the field of freshwater storage in coastal aquifers and these are also limited. Zuurbier and Dooren (2019) suggest certain design regulations for MPPW in ASR systems. An important design regulation is that there has to be a meter between two screens, and between a screen and confining layer. This would mean less deep injection and and less shallow extraction. On a aquifer of 70 m that was simulated, it would not have significant effect.

Other practical design criteria are developed for low temperature ATES systems (NVOE 2006). Mono-wells for LT-ATES systems can in principle be categorized as multiple partially penetrating wells as there two screens positioned on top of each other in one borehole. An important aspect that needs to be considered is the minimal screen length required to achieve a desired pump rate. Equation 2.8 and Equation 2.9 are guidelines for the design velocity on the surface of the well during injection and extraction. These design velocities can be translated in to a screen length to achieve the desired hydraulic capacity by dividing it by the total surface area of the screen where the water is injected or extracted. The hydraulic capacity needed to inject water in a aquifer is larger than for extracting water. For the reference scenario a screen length of 142 m is required for injection and 80 m for extraction according to Equation 2.8 and Equation 2.9. The results of this research showed that smaller extraction screen lengths are more beneficial than smaller injection screen length. When considering the MPPW design with two screens that had an injection screen length of half the aquifer thickness ($Li = 70/2 = 35$ m) and an extraction screen length of a quarter of the aquifer thickness ($Le = 70/4 = 17.5$ m), would mean that at least both five injection and extraction screens are needed to inject and extract 5,000 m^3/d. The number of boreholes needed is mostly dependent on the injection screen length. This research found that the thermal recovery efficiency is more sensitive to the extraction screen length. This implicates that the increase in costs of an HT-ATES project by applying MPPW can be limited as larger injection screens can be used since the performance of the system is less sensitive to the injection depth.

Regardless of the arguments mentioned above, practical guidelines for the application of HT-ATES systems and MPPWs could still affect the complexity and the total costs of a

project and therefore needs to be considered in future research.

Monitoring location

In this thesis, the location of the monitoring wells were always at a certain distance from the well. It should be studied if it is an option to measure in the well which will mean that no monitoring wells need be drilled which will reduce the cost of a project. There are some concerns that need to be carefully considered when using this approach;

1. During injection the water that is infiltrated is measured instead of the actual temperature in the aquifer. This results in that the system will not or barely be controlled as no temperature gradient over the aquifer is used for control feedback.
2. During extraction the tilted thermal front is underestimated as closer to the well the temperature gradient is less profound. This becomes a negative effect because of the thermal retardation. Water moves faster than heat due to the thermal retardation. So, when the pumping scheme is based on the temperature measured in the well, the actual temperature of the extracted water can be lower. This effect is exaggerated when using partially penetrated wells which is used in this study, where also vertical flow is induced.

It is a challenge to use only information from the well to control the system. A proposed method can be to locate the residual heat plumes by the temperature gradient measured in the well. The screens where least residual heat is fount can be used to inject most of the water in the following recovery cycle. The screens where most residual heat was located can be used extract a larger portion of the the recovery water. So, the information in the well is not very representative for the state in the aquifer but a better system can be achieved by using the information of the previous year.

5.3   Comparative analysis of the results with other studies

In this section the results of this study are compared to the results and conclusion of comparable studies.

Density difference compensation with saline water

Lopik et al. (2016) study showed that the density difference between injection water and ambient groundwater can be compensated by using saline water as the injection water to decrease the density difference between the storage water and ambient ground water. The reference scenario (q_z = 0.18 (m/d)) of their study showed an increase of 0.29 in thermal recovery efficiency over the fourth recovery cycle. Where in this research the reference scenario (q_z = 0.15 (m/d)) presented an increase of 0.20 in the thermal recovery efficiency. This may look like a significant difference between the two methods but the percentage of the buoyancy flow that is counteracted in Lopik et al. (2016) is 78% while 74% in this study, making the results of the two methods comparable. Though, in the study of Lopik et al. (2016) the density difference is completely compensated and in this study the buoyancy flow is mitigated, both show strong resemblance in outcome. The preference of a method can be different for a particular scenario with certain geo-hydrological and operational properties. For example, for large systems in large aquifers the use MPPW can be preferred as the use of saline water that is extracted from deep brackish aquifers or seawater to compensate for the whole storage volume can result in significant salt accumulation at the bottom of the aquifer since the research of Lopik et al. (2016) showed that salt recovery is lower for scenarios

with small thermal radius (i.e, large aquifer small storage .For systems in small aquifers with large buoyancy flow, compensation of the density difference with saline water can be preferred as MPPW is less effective in small aquifers as there is not enough space to be used to mitigate the buoyancy flow. But when this system is placed in an area where it is not preferred to disturb the salinity of the ambient groundwater MPPW can be considered as a useful application with minimal extraction screen length. A combination of both can be a subject for further research.

MPPW in Aquifer Storage and Recovery

Beside this research there is one other study conducted to research the impact of using MPPW to counteract buoyancy flow in the groundwater. Zuurbier et al. (2014) researched how the recovery efficiency is affected by using MPPW in aquifer storage and recovery (ASR) systems where freshwater is buoyant due to the difference in density between the brackish groundwater. The main conclusion of the study complements the results of this research where MPPW proves to be an liable solution to counteract buoyancy flow in the groundwater. Zuurbier et al. (2014) showed an absolute increase of 0.25 in terms of freshwater recovery compared to a fully penetrating screen over the third recovery cycle. The difference between the study of Zuurbier et al. (2014) and this study is that this research is purely synthetic while the study of Zuurbier et al. (2014) is based on a real-world MPPW application. The target aquifer was heterogeneous and the discharge of the screens where adjusted throughout the cycles to improve performance. For freshwater recovery, the quality of the water is important. So, there is a strict threshold value which indicates when recovery stops. This can be compared to a cut-off temperature in heat storage systems that was discussed earlier in this chapter. Despite difference in heat and salt transport in the subsurface, the main issue in the systems which is buoyancy flow is the same expression. So, it is expected that practical application of MPPWs for HT-ATES systems will give benefits similar to the benefits discussed in this thesis.

6. Conclusion

In the current design of HT-ATES systems, either one fully penetrating or partially penetrating screen is used. This well design has low thermal recovery efficiency in case of large buoyancy flow. In this thesis it has been investigated if the use of multiple partially penetrating wells (MPPWs) are able to counteract the effect of buoyancy flow to increase the thermal recovery efficiency. The research objective is achieved as a design of MPPW is proposed and assessed in terms of thermal recovery.

Multiple partially penetrating wells have shown to be a promising solution for HT-ATES systems to counteract the effect buoyancy flow that is induced by the density difference between the injected water and the ambient groundwater.

Based on the analysis of four types of HT-ATES systems for multiple scenarios, this research shows that HT-ATES systems with a MPPWs can counteract up to 85% of the thermal loss due to the effect of buoyancy flow. For example, calculations of the reference scenario of this study resulted in a thermal recovery efficiency of 0.61 for a regular HT-ATES system, while the use of MPPWs gave an efficiency of 0.81.

Looking at the global performance of the MPPWs in terms of thermal recovery efficiency, it hereby does not make noticeable difference if two screens or four screens are used. Provided that the optimal screen lengths are used for the two screened MPPW.

Despite small difference in thermal recovery efficiency, the use of four screens showed to be more stable throughout all recovery cycles. It enabled mores division of the discharge over the screens and thus the entire aquifer. The use of four screens also has more flexibility which is more practical in reality where there is heterogeneity in the aquifer and variations in heat demand and supply.

Application of three control approaches with control feedback of temperature in the aquifer for a MPPW with four screens, points out that placing the monitoring points at a distance of one time the thermal radius gives the best results in the fourth recovery cycle.

For large magnitude of buoyancy flow (i.e. high hydraulic conductivity or high injection temperature) the application of a control method that predicts buoyancy flow is preferred. For small magnitude of buoyancy either no control is needed or the control needs to be solely based on concurrent measurements.

This research has pointed out that in general the application of MPPWs is beneficial if the buoyancy flow, what is defined as the vertical hydraulic conductivity times the density ratio of the ambient groundwater and injection water (Equation 3.14), is larger than 0.1 meters per day.

7. Recommendations

Looking at the results of this research on the application of MPPW in HT-ATES systems, it shows promise as a method to optimize the performance in terms of thermal recovery efficiency. Based on the results and other studies it is recommended to use MPPW when realising a HT-ATES system in large aquifers with significant buoyancy flow. However, there are more aspects that contribute to the feasibility of HT-ATES systems that are not studied in this thesis but create room for further research in this field.

Using the findings obtained over the course of this research some recommendation for more specific future research topics are listed below:

Real case

As this study was a synthetic study simplification of the system were implemented that presumably won't appear in reality. This can be in terms of hydro-geological properties such as the heterogeneity of the aquifer and operational properties like fluctuating heat demand/supply or a minimum extraction temperature requirement. It is therefore recommended to do this research on a real case study with representative hydro-geological and operational requirements which will bring the studies closer to reality. The results as found in this research and following numerical models used for synthetic studies are not a guarantee that this will occur in reality as validating groundwater models is not possible (Konikow and Bredehoeft 1992). In the end realising a project and monitor the system intensively is recommended to deliver more knowledge on these systems. Such research will bring the impact of HT-ATES systems with MPPWs to reality and will help improve future projects and studies.

Combination methods

Both application of MPPW and addition of salt to compensate the buoyancy flow (Lopik et al. 2016) has shown significant improvement in the performance of a HT-ATES system. The difference in approaches hint to the possibility to combine these two solutions. Salt can be used to increase the density but not fully compensate the injected water. The resulting buoyancy flow can be counteracted with MPPW. In this way **1)** lower salinity values will be needed and less accumulate of salt will take place at the bottom of the aquifer. **2)** larger screens can be be used which means less wells need to be drilled. The optimization of combining these two methods will be a valuable research topic.

Circulation during storage

This study had briefly researched the effect of circulating the storage volume during storage to minimize energy loss in this phase of the recovery cycle. The outcome was very positive for a system with very large buoyancy flow (see Section 4.5). The glimpse of the potential of this approach is encouraging for future research. It would be an interesting follow up to research the potential and challenges of vertical circulation of storage water with MPPWs in

HT-ATES systems.

Multi-criteria optimization

This study was mainly focused on optimizing the thermal recovery efficiency of HT-ATES systems by using MPPW. Additional factors that affect the feasibility need to be taken into account before realization. An important aspect is the costs of such systems. How does the gain in thermal recovery efficiency relate to increase in construction and operation costs? This needs to be investigated, since the system needs to be economically profitable. Another aspect is the environmental impact of HT-ATES systems in general and with MPPWs. In contemporary engineering it is not enough to have a brilliant idea, one must investigate and be aware of the possible risks and impact on the environment and society. How is the the subsurface environment affected by HT-ATES wells and what can be done to minimize these effects? In conclusion, multi-criteria optimization research is recommended that takes into account technological, environmental and economical aspects in order to guarantee it's feasibility.

Bibliography

Bakker, Mark, Vincent Post, Joseph Hughes, Christian Langevin, Alain Francés, and Jeremy White (2013). "Enhanced FloPy scripts for constructing and running MODFLOW-based models". In: *MODFLOW and More 2013: Translating Science and Practice*.

Bloemendal, JM (2018). "The hidden side of cities: Methods for governance, planning and design for optimal use of subsurface space with ATES". In:

Bloemendal, Martin and Niels Hartog (2018). "Analysis of the impact of storage conditions on the thermal recovery efficiency of low-temperature ATES systems". In: *Geothermics* 71, pp. 306–319.

Bloemendal, Martin and Theo Olsthoorn (2018). "ATES systems in aquifers with high ambient groundwater flow velocity". In: *Geothermics* 75, pp. 81–92. ISSN: 0375-6505. DOI: https://doi.org/10.1016/j.geothermics.2018.04.005. URL: http://www.sciencedirect.com/science/article/pii/S0375650518300117.

Buscheck, Thomas A, Christine Doughty, and Chin Fu Tsang (1983). "Prediction and analysis of a field experiment on a multilayered aquifer thermal energy storage system with strong buoyancy flow". In: *Water Resources Research* 19.5, pp. 1307–1315.

Buscheck, Thomas Alan (1984). *Hydrothermal analysis of aquifer thermal energy storage*. Tech. rep. California Univ., Berkeley (USA).

Caljé, R (2010). "Future use of aquifer thermal energy storage in below the historic centre of Amsterdam, Hydrology". In: *Delft University of Technology, Delft*.

Doughty, Christine, Göran Hellström, Chin Fu Tsang, and Johan Claesson (1982). "A dimensionless parameter approach to the thermal behavior of an aquifer thermal energy storage system". In: *Water Resources Research* 18.3, pp. 571–587.

ECN, Energie-Nederland, and Netbeheer Nederland (2016). "Energietrends 2016". In: p. 92.

Engineering, ToolBox (2003). *Water - Density, Specific Weight and Thermal Expansion Coefficient*. URL: https://www.engineeringtoolbox.com/water-density-specific-weight-d_595.html.

Harbaugh, Arlen W, Edward R Banta, Mary C Hill, and Michael G McDonald (2000). "MODFLOW-2000, The U. S. Geological Survey Modular Ground-Water Model-User Guide to Modularization Concepts and the Ground-Water Flow Process". In: *Open-file Report. U. S. Geological Survey* 92, p. 134.

Hartog, Niels, Martin Bloemendal, Stijn Beermink, and Gerard van den Berg (2018). *HEATSTORE*. English. URL: https://www.kwrwater.nl/en/projecten/heatstore/.

Hellström, Göran, Chin-Fu Tsang, and Johan Claesson (1988). "Buoyancy flow at a two-fluid interface in a porous medium: Analytical studies". In: *Water Resources Research* 24.4, pp. 493–506.

Konikow, Leonard F and John D Bredehoeft (1992). "Ground-water models cannot be validated". In: *Advances in water resources* 15.1, pp. 75–83.

Langevin, Christian D (2008). "Modeling axisymmetric flow and transport". In: *Groundwater* 46.4, pp. 579–590.

Langevin, Christian D, Daniel T Thorne Jr, Alyssa M Dausman, Michael C Sukop, and Weixing Guo (2008). *SEAWAT version 4: a computer program for simulation of multi-species solute and heat transport*. Tech. rep. Geological Survey (US).

Lopik, Jan H van, Niels Hartog, and Willem Jan Zaadnoordijk (2016). "The use of salinity contrast for density difference compensation to improve the thermal recovery efficiency in high-temperature aquifer thermal energy storage systems". In: *Hydrogeology Journal* 24.5, pp. 1255–1271.

Lopik, Jan H van, Niels Hartog, Willem Jan Zaadnoordijk, D Gijsbert Cirkel, and Amir Raoof (2015). "Salinization in a stratified aquifer induced by heat transfer from well casings". In: *Advances in water resources* 86, pp. 32–45.

Molz, FJ, JG Melville, O Güven, and Alfred D Parr (1983). "Aquifer thermal energy storage: an attempt to counter free thermal convection". In: *Water Resources Research* 19.4, pp. 922–930.

NVOE (2006). *Richtlijnen Ondergrondse Energieopslag, Design Guidelines of Dutch Branche Association for Geothermal Energy Storage*.

Oliphant, Travis (2006–). *NumPy: A guide to NumPy*. USA: Trelgol Publishing. [Online; accessed <today>]. URL: `http://www.numpy.org/`.

Olsthoorn, Th N et al. (1982). *The clogging of recharge wells, main subjects*. Keuringsinstituut voor Waterleiding Artikelen, KIWA, nv.

Sauty, JP, AC Gringarten, A Menjoz, and PA Landel (1982). "Sensible energy storage in aquifers: 1. Theoretical study". In: *Water Resources Research* 18.2, pp. 245–252.

Schaffer-Jin, Yulan (2014). "Investigations on groundwater dewatering by using vertical circulation wells: Numerical simulation method development and field validation". PhD thesis. Niedersächsische Staats-und Universitätsbibliothek Göttingen.

Schout, Gilian, Benno Drijver, and RJ Schotting (2016). "The influence of the injection temperature on the recovery efficiency of high temperature aquifer thermal energy storage: Comment on Jeon et al., 2015". In: *Energy* 103, pp. 107–109.

Sommer, Wijb, Johan Valstar, Pauline van Gaans, Tim Grotenhuis, and Huub Rijnaarts (2013). "The impact of aquifer heterogeneity on the performance of aquifer thermal energy storage". In: *Water Resources Research* 49.12, pp. 8128–8138.

Thorne, Danny, Christian D Langevin, and Michael C Sukop (2006). "Addition of simultaneous heat and solute transport and variable fluid viscosity to SEAWAT". In: *Computers & geosciences* 32.10, pp. 1758–1768.

Todd, David K and LW Mays (1980). "Groundwater hydrology. John Willey Sons". In: *Inc., New York* 535.

ToolBox, Engineering (2004a). *Water - Saturation Pressure*. URL: https://www.engineeringtoolbox.com/water-vapor-saturation-pressure-d_599.html.

– (2004b). *Water - Specific Heat*. URL: https://www.engineeringtoolbox.com/specific-heat-capacity-water-d_660.html.

Tsang, Chin Fu, Thomas Buscheck, and Christine Doughty (1981). "Aquifer thermal energy storage: a numerical simulation of Auburn University field experiments". In: *Water Resources Research* 17.3, pp. 647–658.

Vandenbohede, Alexander, Andy Louwyck, and Luc Lebbe (2009). "Conservative solute versus heat transport in porous media during push-pull tests". In: *Transport in Porous Media* 76.2, pp. 265–287.

Vandenbohede, Alexander, Andy Louwyck, and Nele Vlamynck (2014). "SEAWAT-Based Simulation of Axisymmetric Heat Transport". In: *Groundwater* 52.6, pp. 908–915.

Voss, Clifford I et al. (1984). *A finite-element simulation model for saturated-unsaturated, fluid-density-dependent ground-water flow with energy transport or chemically-reactive single-species solute transport*. Vol. 84. US Geological Survey Reston, VA.

Ward, James D, Craig T Simmons, and Peter J Dillon (2007). "A theoretical analysis of mixed convection in aquifer storage and recovery: How important are density effects?" In: *Journal of Hydrology* 343.3-4, pp. 169–186.

Zheng, Chunmiao and P Patrick Wang (1999). *MT3DMS: a modular three-dimensional multispecies transport model for simulation of advection, dispersion, and chemical reactions of contaminants in groundwater systems; documentation and user's guide*. Tech. rep. Alabama Univ University.

Zuurbier, Koen G, Willem Jan Zaadnoordijk, and Pieter J Stuyfzand (2014). "How multiple partially penetrating wells improve the freshwater recovery of coastal aquifer storage and recovery (ASR) systems: A field and modeling study". In: *Journal of hydrology* 509, pp. 430–441.

Zuurbier, Koen and Teun van Dooren (2019). *Technological and Economical guide for ASRCoastal application*. URL: http://www.subsol.org/uploads/deliverables/D1.7_-_Technological_and_Economical_guide_for_ASR-Coastal_application_.pdf.

III
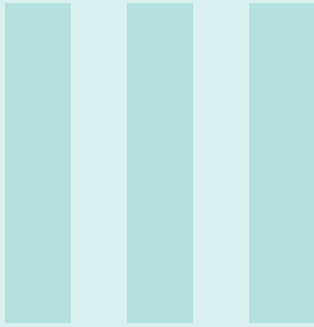
Appendices

A. Evaluation of Model

A.1 Approach

There are only a couple of HT-ATES systems operating and most of them without useful data. The data from (Buscheck et al. 1983) is used as the reference scenario of this research. It gives the opportunity to evaluate the outcomes of the simulation. The data is calibrated with the experimental results from the *Auburn University Pilot Study* (Molz et al. 1983).
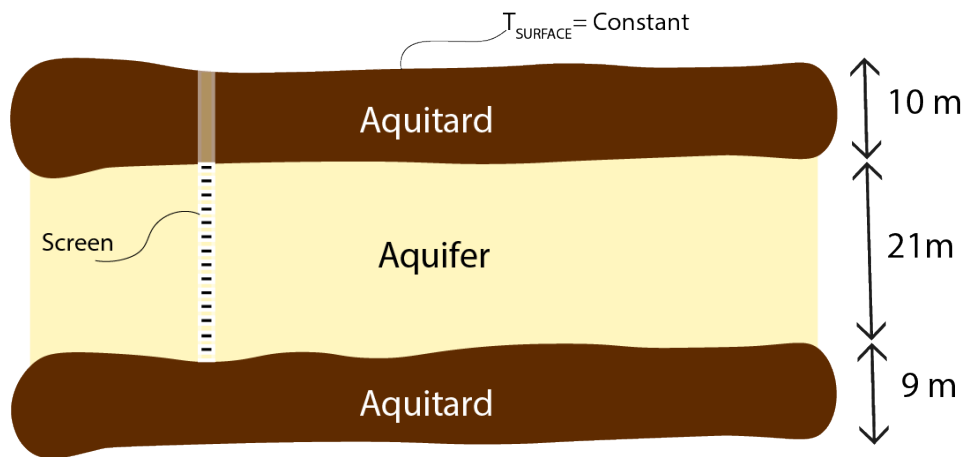
Figure A.1: Schematic overview of the systems

However, a homogeneous anistropic aquifer (see Figure A.1 is simulated instead of the heterogeneous aquifer described by, ditto to the research by (Lopik et al. 2016). The outer, upper and lower boundaries are assumed to have a constant head and temperature (20 °C). The characteristic of different layers are presented in Table A.1.

A.1.1 Grid Resolution

The model uses a logarithmic scale with a domain to 1000m. The smallest cell size is 0.5m and increases to the largest cell size of 50m in 100 steps. This amount of steps showed sufficient accuracy, The grid layer thickness Δz is 0.5m.

A.1.2 Flow regime

A block function is used to represent the course of the discharge over one recovery cycle. Each recovery cycle is 360 days function with four phases of 90 days. A time step of $\Delta t = 5d$ is used.

The injection volume V_{inj} is equal to the extraction volume V_{ex} for all the conducted simulations. It is therefore referred to as the storage volume V.

,

Properties	Values
Aquifer properties	
Specific storage	$S_s = 6*10^{-4}$ m^{-1}
Porosity	$\theta = 0.25$
Bulk density	$\rho_b = 1{,}950$ kg/m^3
Heat capacity	$c_{ps} = 696.16$ J/kg C
Thermal conductivity	$\lambda = 2.29$ W/m C
Thermal distribution coefficient	$K_{dt} = 1.66 *10^{-4}$ m^3/kg
Thermal retardation factor	$R_T = 2.29$
Bulk thermal diffusivity	$D_T = 0.189$ m^2/day
Horizontal hydraulic conductivity	$k_h = 53.4$ m/day
Vertical hydraulic conductivity	$k_v = 7.7$ m/day
Aquifer thickness	$H = 21$ m
Aquitard properties	
Specific storage	$S_s = 9*10^{-2}$ m^{-1}
Porosity	$\theta = 0.35$
Bulk density	$\rho_b = 1{,}690$ kg/m^3
Heat capacity	$c_{ps} = 696.16$ J/kg °C
Thermal conductivity	$\lambda = 2.56$ W/m / °C
Thermal distribution coefficient	$K_{dt} = 1.66 *10^{-4}$ m^3/kg
Bulk thermal diffusivity	$D_T = 0.151$ m^2/day
Horizontal hydraulic conductivity	$k_h = 53.4 * 10^{-6}$ m/day
Vertical hydraulic conductivity	$k_v = 7.7 * 10^{-6}$ m/day
Groundwater properties	
Heat capacity	$c_{pf} = 4{,}186$ J/kg °C
Thermal conductivity	$\lambda = 0.58 W/m/C$
Solute transport properties	
Longitudinal dispersion	$\alpha_l = 0.5$
Transversal dispersion	$\alpha_t = 0.05$

Table A.1: Properties of the layers of Auburn University field experiment. (Molz et al. 1983)

A.2 Results

As explained in the model that is used is validated with the results of (Lopik et al. 2016).
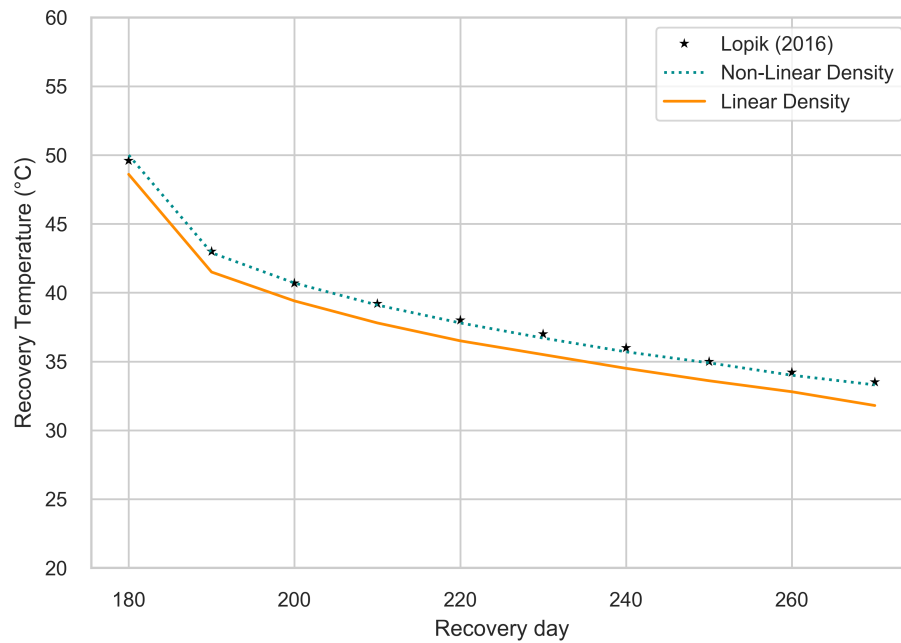
Figure A.2: Calculated extraction temperature for the fourth recovery cycle
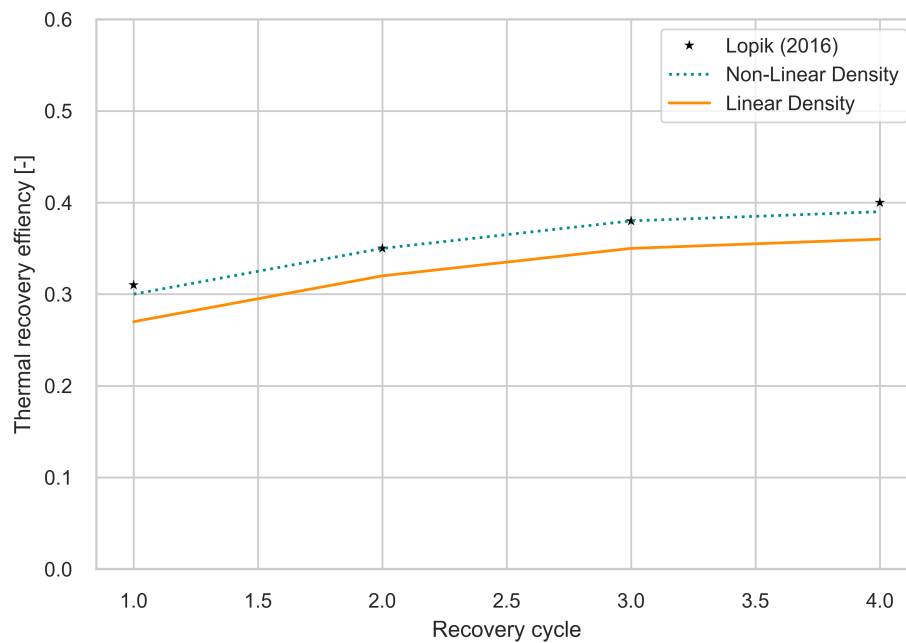
Figure A.3: Calculated thermal recovery efficiency per cycle

Figure A.2 show the the extraction temperature calculate by (Lopik et al. 2016) and the model used in this study. It shows quite identical results. The same goes for the calculated thermal recovery efficiency as can be seen in Figure A.3. Therefore, it can be concluded that

the model is representing the required processes in a good manner.
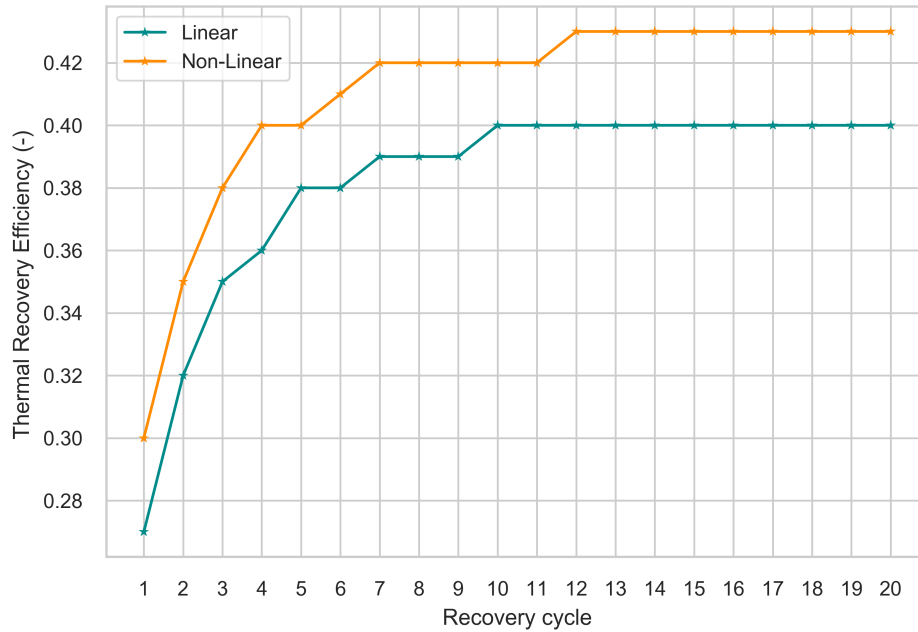
Figure A.4: Thermal recovery efficiency for 20 recovery cycles.

The figures also show that the use of a linear density equation causes some errors corresponding to both the extraction temperature and the thermal recovery efficiency.

When, plotting the thermal recovery efficiency for 20 recovery cycles, its shows the same trend (See Figure A.4.

B. Effect of Anisotropy

A material is called anisotropic if the the properties are not equal in each direction. If it is the same it is called isotropic. In this study most of the properties are assumed to be isotropic except for the hydraulic conductivity. This material property was set to be anisotropic for both the confining layers and the aquifer. As the characteristic tilting time expresses, both the vertical and hydraulic conductivity have effect of the tilting of the thermal front in HT-ATES system. Therefore different combinations of the vertical and hydraulic conductivity were simulated to research the effect of on the thermal recovery efficiency. Four different combinations were evaluated for a fully penetrating well and a MPPW with two screens of both a screen length of 50% of the aquifer thickness. Other system properties are kept constant to the reference scenario as described in Table A.1. The thermal recovery efficiency and the heat spread in the aquifer will be presented and discussed in the following sections.

B.1 Thermal recovery efficiency

The thermal recovery efficiency over four recovery cycles were determined for four different combinations of vertical and horizontal hydraulic conductivity. Figure B.1 presents the result for a regular HT-ATES system with a fully penetrating well. The thermal recovery
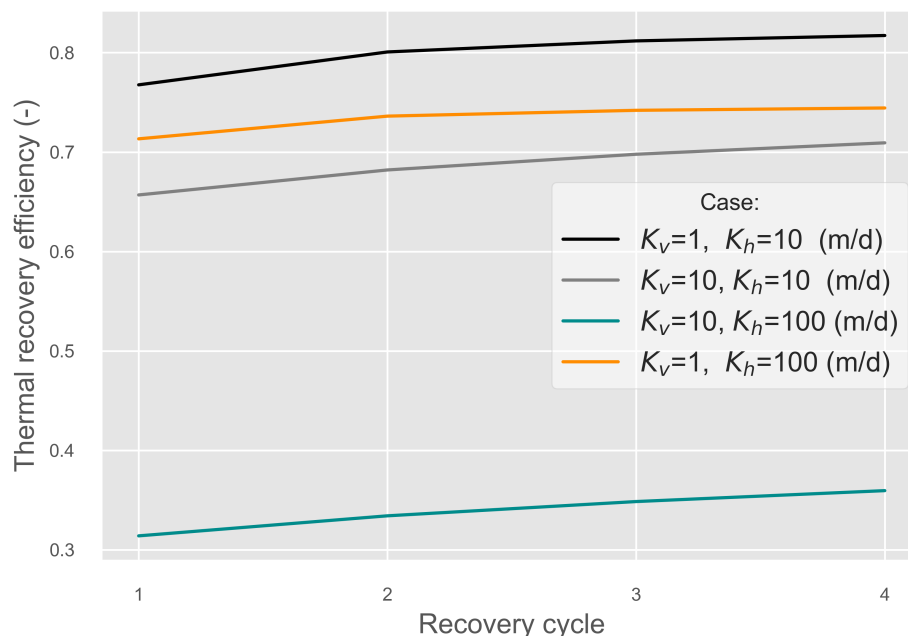
Figure B.1: Thermal recovery efficiency for different hydraulic conductivity combinations over four cycles and a fully penetrating wells

efficiency is mostly affected by the vertical hydraulic conductivity. For a large difference in horizontal hydraulic conductivity, respectively 10-100 m/d but equal small vertical hydraulic conductivity (Case 1 and 4) the absolute difference in efficiency around 5%. This is two times higher for Case 2, $K_v = K_h = 10m/d$. However, when $K_v = 10m/d$ and $K_h = 100m/d$ (Case 3) the performance of the system is very poor. This case reaches a maximum thermal recovery of only 0.36 in the fourth recovery cycle even-though it has the same anisotropy value as Case 1.

The same cases were also simulated for an HT-ATES with MPPW. The thermal recovery efficiency values are presented in Figure B.2.
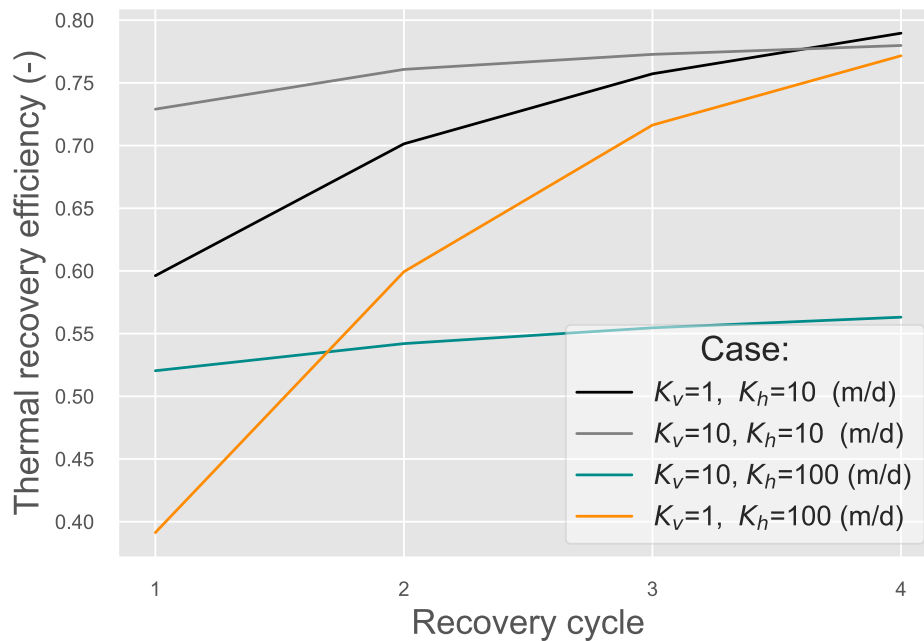
Figure B.2: Thermal recovery efficiency for different hydraulic conductivity combinations over four cycles MPPW

The results of the fourth recovery cycle for both HT-ATES systems are bundled in Figure B.2. For the cases where the vertical hydraulic conductivity is small (Case 1 and 4) the application of MPPW is not beneficial. The buoyancy flow in these cases is not enough to make the water reach the upper half of the aquifer before extraction. This effect on the thermal recovery efficiency is large for the first two recovery cycles. In the following cycles, the heat from previous cycles can be recovered which evens out the effect of anisotropy.

Table B.1: Overview of the tested scenarios and

				Thermal recovery efficiency (-)	
Case	Kv (m/d)	Kh (m/d)	Anistropy (Kh/Kv)	Fully penetrating	MPPW two screens Le = Li = 0.5H
1	1	10	10	0.82	0.79
2	10	10	1	0.71	0.78
3	10	100	10	0.36	0.56
4	1	100	100	0.74	0.77

The largest gain found is four Case 3. In this case, the buoyancy flow causes the hot storage water to end up at the top of the aquifer. The large horizontal conductivity spreads the water and induces tilting of the thermal front. The deep injection with MPPW ensures that hot water arrives later at the top of the aquifer, leaving less time for the water to move in horizontal direction. **??** shows the heat spread in the aquifer after each phase of the fourth recovery cycle. As this

B.2 Conclusion

The anisotropy value itself does not significantly influence the thermal recovery efficiency. The effect of high permeable aquifers in both vertical and horizontal direction has the largest influence on the thermal recovery efficiency. It is a combination of both conductivity's that can result in large losses as an result of the effect of the buoyancy flow.

(a) K_h/K_v=10/1 (m/d)   (b) K_h/K_v=10/10 (m/d)   (c) K_h/K_v=100/10 (m/d)   (d) K_h/K_v=100/1 (m/d)
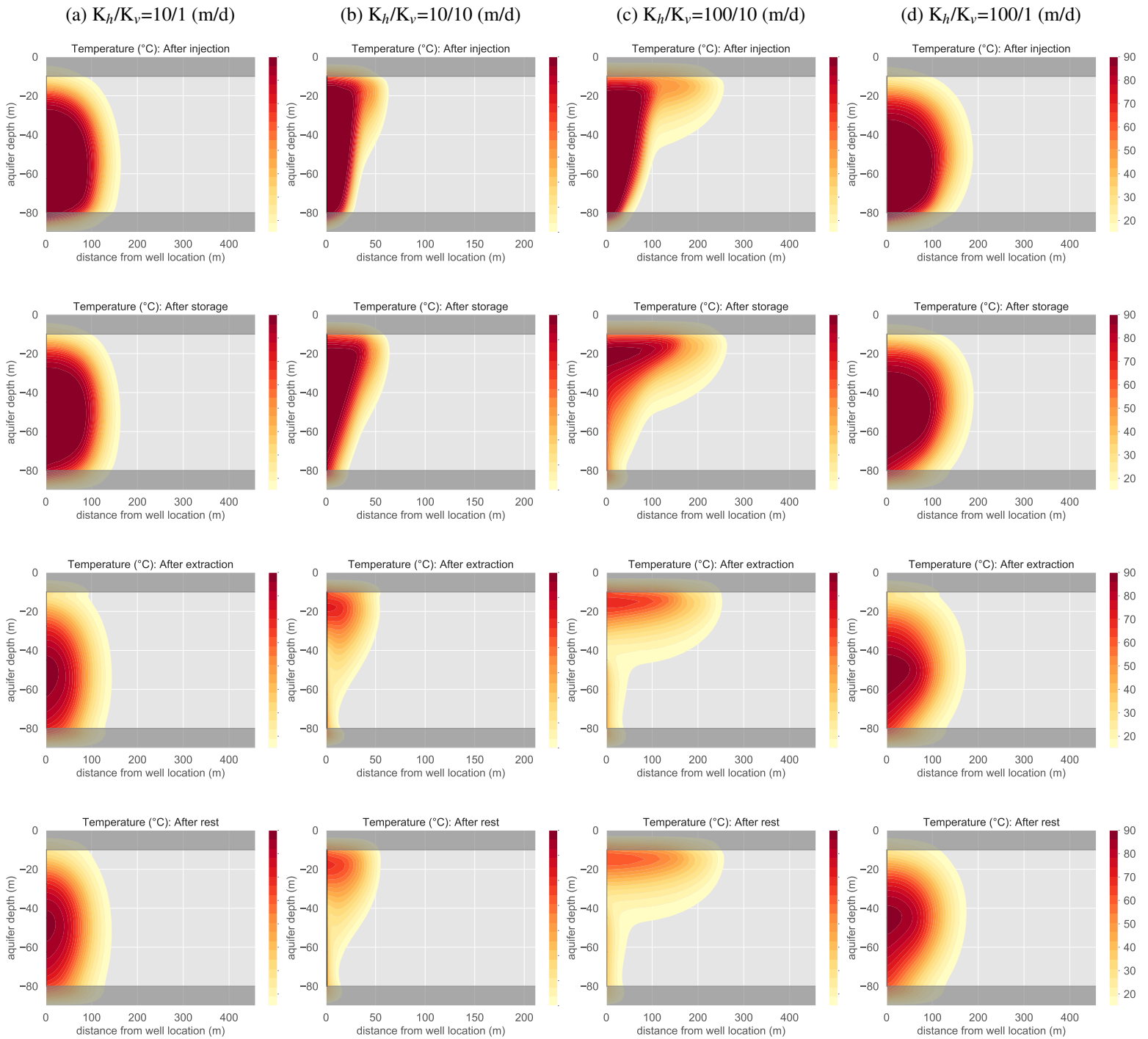
C. Efficiency cycle 1-3

C.1 Scenario 1: $T_{inj} = 90\,°C$

First recovery cycle
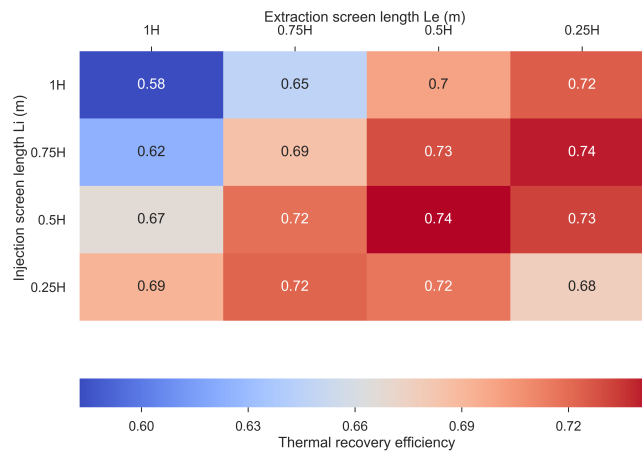
Figure C.1: Thermal recovery efficiency scenario 1 year 1

Second recovery cycle
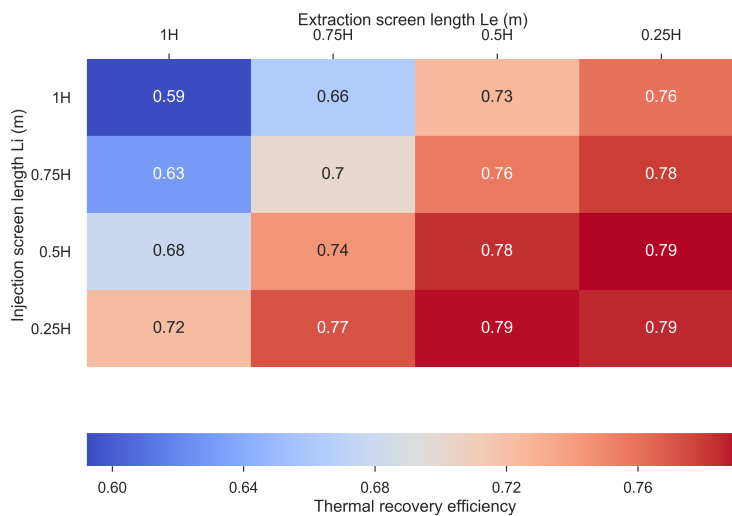
Figure C.2: Thermal recovery efficiency scenario 1 year 2

Third recovery cycle
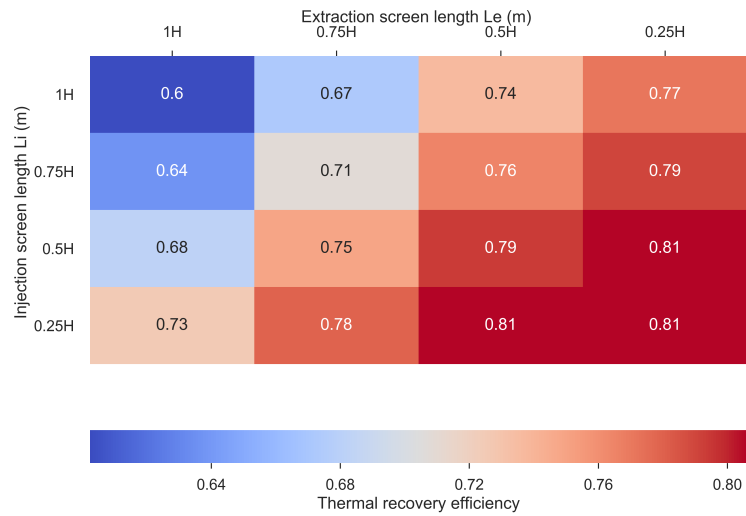
Figure C.3: Thermal recovery efficiency scenario 1 year 3

C.2   Scenario 2: $T_{inj} = 112\,°C$

First recovery cycle
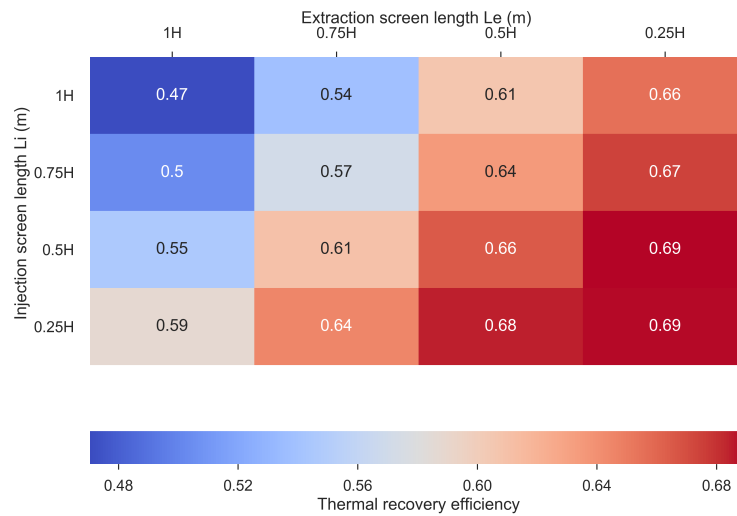
Figure C.4: Thermal recovery efficiency scenario 2 year 1

Second recovery cycle
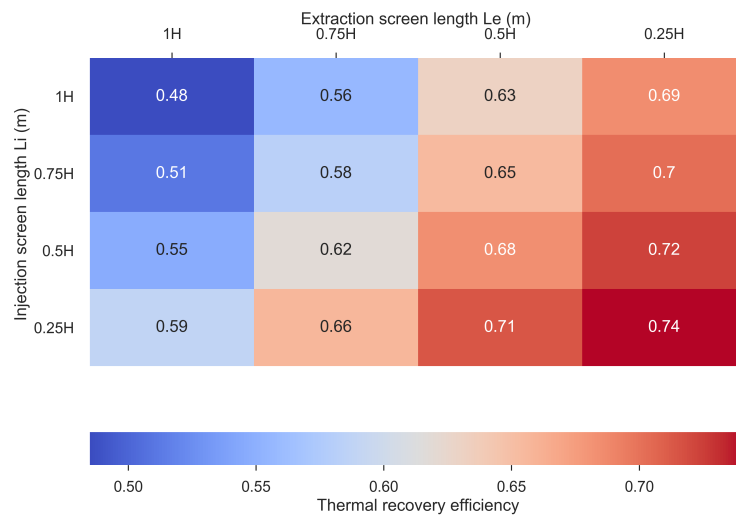
Figure C.5: Thermal recovery efficiency scenario 2 year 2

Third recovery cycle
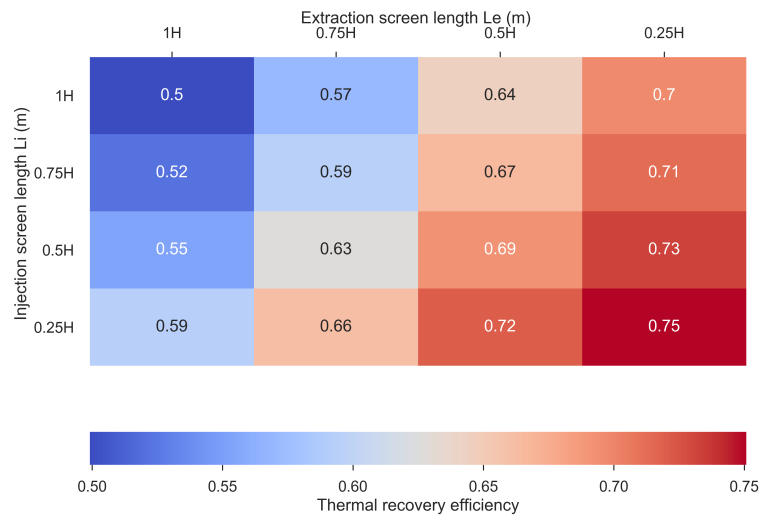
Figure C.6: Thermal recovery efficiency scenario 2 year 3

C.3 Scenario 3: $T_{inj} = 61\,°\text{C}$

First recovery cycle
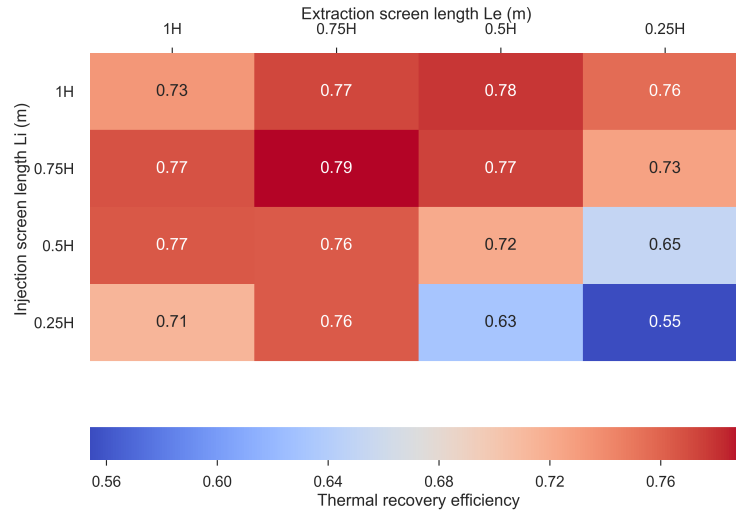
Figure C.7: Thermal recovery efficiency scenario 3 year 1

Second recovery cycle
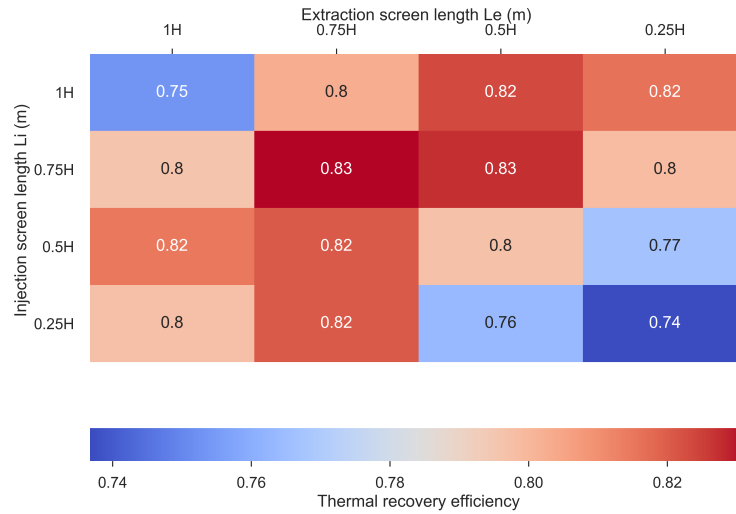
Figure C.8: Thermal recovery efficiency scenario 2 year 2

Third recovery cycle
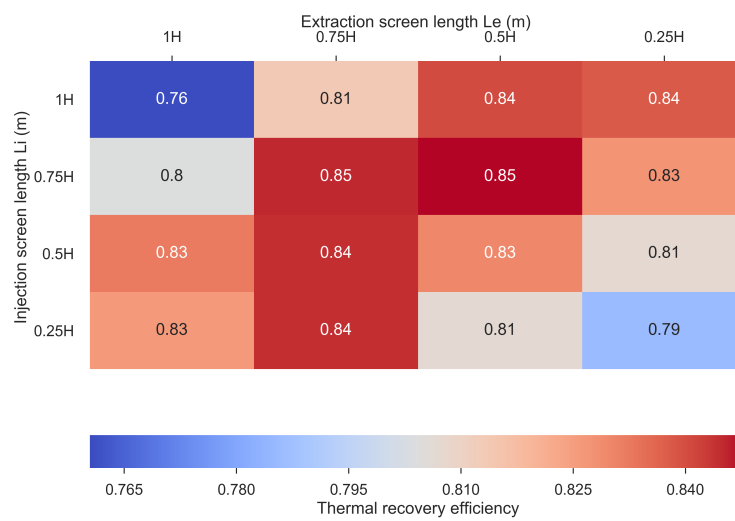
Figure C.9: Thermal recovery efficiency scenario 2 year 3

D. Parameter Research

D.1 Hydro-geological Properties

In order to determine in which geohydrological and operational conditions and it is useful to implement MPPW as a method to improve the performance of the system.

		H (m)	Kh (m/d)	Kv (m/d)	T (°C)	V |(m^3/yr)
		Parameters				
BASE 1	1	30	5	1	50	500000
	2	40	10	2	60	600000
	3	50	15	3	70	700000
	4	60	20	4	80	800000
BASE 2	5	70	25	5	90	900000
	6	80	30	6	100	1000000
	7	90	35	7	110	1100000
	8	100	40	8	120	1200000
	9	110	45	9	130	1300000
BASE 3	10	120	50	10	140	1400000

Table D.1: The ranges of the different parameters and the corresponding base cases.

As previous research has showed, the hydraulic conductivity of the aquifer and the aquifer thickness are geohydrological parameters that influence the buoyancy flow and the tilting of the thermal front. Other factors that influence the heat loss by variable density driven flow are the operational parameters; storage volume and injection temperature. In this analysis a wide range of these parameters are chosen based on the research of (Bloemendal and Hartog 2018). Each parameter is varied in 10 steps from the lower value to the upper value of the range, while the other parameters are kept constant. This procedure is done for three different cases. The first case uses the lower bound values of the parameters, the second the median and the third the upper bound values. An overview of the simulated cases is presented in Table D.1.

- **BASE 1:** - Lower bound of parameters
- **BASE 2:** - Median bound of parameters
- **BASE 3:** - Upper bound of parameters.

These simulations are all executed for the three HT-ATES systems as described above. The HT-ATES system with MPPW has two screens with both a screen length of half the aquifer thickness, like illustrated in Figure 3.9. The lower well is solely used for injection while the upper is only used for extraction.

D.2   Results: Parameter Research

In this section the results are presented of the parameter research. For each parameter the slope change in time for the three types of HT-ATES systems is presented and the resulting recovery efficiency. This is done for all the three base cases as presented in **??**. Subsequently, the efficiency results for the three base cases of each parameter are presented in one graph.

D.2.1   Injection Temperature

BASE 1
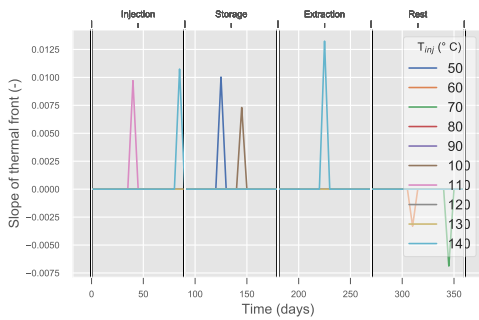
Figure D.1: No variable density flow.
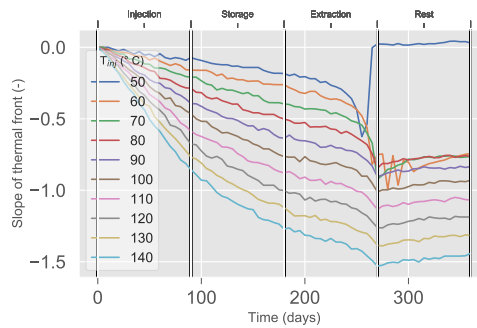
Figure D.2: Regular HT-ATES system.

Figure D.1 shows the slope change for the case where no density driven flow was considered. It is interesting to see that indeed the slope remains approximately zero for all cases. While 'Figure D.2 shows large changes in the slope of the thermal front. The change in slope is decreasing faster for higher temperatures.
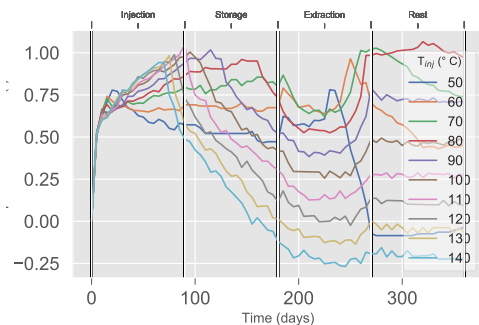
Figure D.3: MPPW
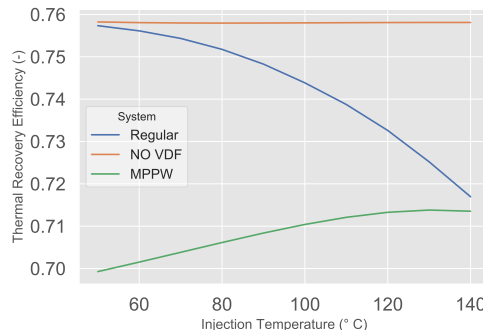
Figure D.4: Efficiency's

Figure D.3 presents the slope change for the case where the two well MPPW HT-ATES system was simulated. The slope show a small increase in the beginning of the injection period but eventually decreases again. The resulted efficiency of the different cases is shown in Figure D.4. It shows that for this base case the efficiency of the MPPW system does not improve the regular HT-ATES system. The regular HT-ATES system is performing close to the theoretical system with no buoyancy flow but decreases slowly with increasing temperature.

BASE 2
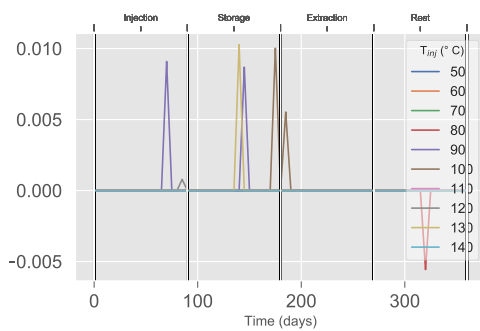
Figure D.5: No variable density flow.
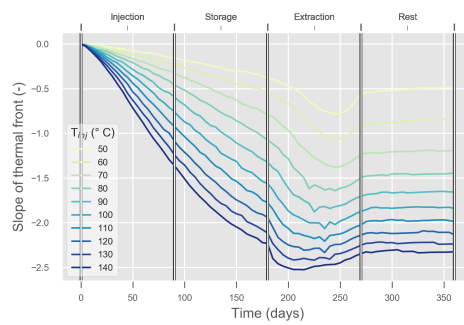
Figure D.6: Regular HT-ATES system.

Figure D.5 shows that for these cases the slope over time is zero when there is no density driven flow. Figure D.6 preents the slope over time of a regular HT-ATES system under average or moderate aquifer properties as found in the Netherlands. It shows an linear decrease in slope with the slope being steeper for higher temperatures.
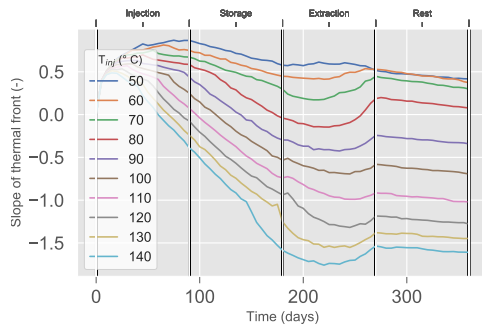
Figure D.7: MPPW
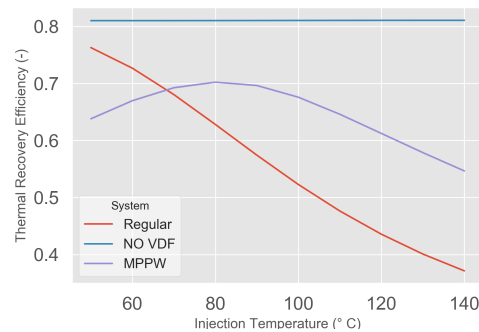
Figure D.8: Efficiency's

The slope for a system with mppw shows a small increase before decreasing. The decrease in slope starts earlier for higher temperatures, see Figure D.7. It can be noted that for the case where 80 is injected, the slope is around zero during extraction phase. When translating this to efficiency, the highest thermal energy recovery is found for this case as can be seen in Figure D.8. This is the case where adding two MPPW has the maximum thermal energy recovery efficiency. It can also be noted that between 100 C and 140 C the gain of MPPW is the highest compared to the regular system.

BASE 3
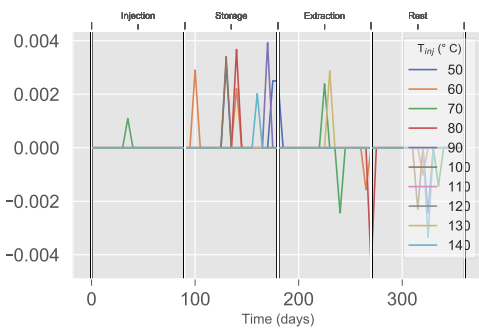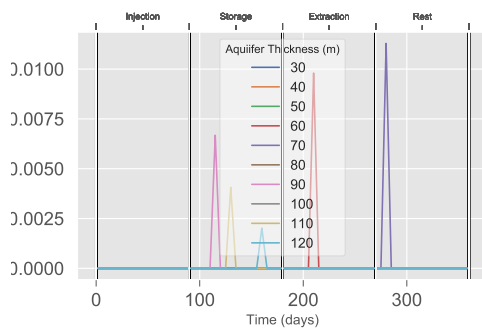

Figure D.9: No variable density flow.
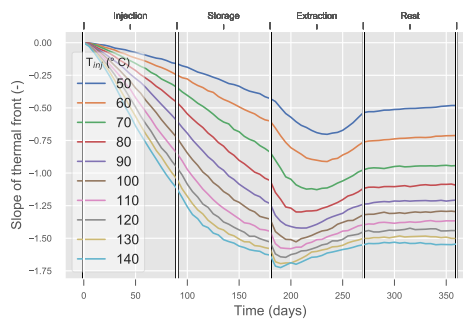
Figure D.10: Regular HT-ATES system.

Figure D.9 shows the slope over time for the case with high values of the aquifer and operation properties and no variable density driven flow. The slope remains approximately zero. For the regular HT-ATES system with density driven flow the slope is changing linearly for the first have of injection temperature. Thereafter. the slope change is showing a more exponential relation. The difference between the injection temperature is becoming smaller for higher temperatures. This is clearly notable at the end of the recovery cycle. Where the difference of slope for $T_{inj} = 50C$ and $T_{inj} = 60C$ is approxiametly 1, it is 0.2 for the difference between $T_{inj} = 130C$ and $T_{inj} = 140C$. This indicates that for these high aquifer properties and injection volume, it does not matter what temperature is injected for the buoyancy flow.
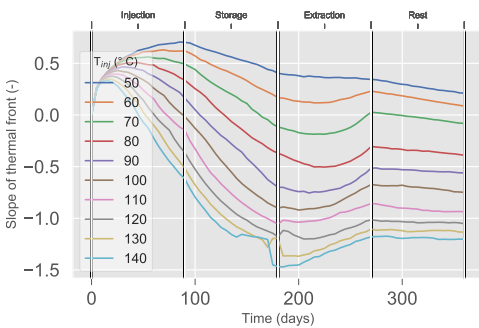
Figure D.11: MPPW
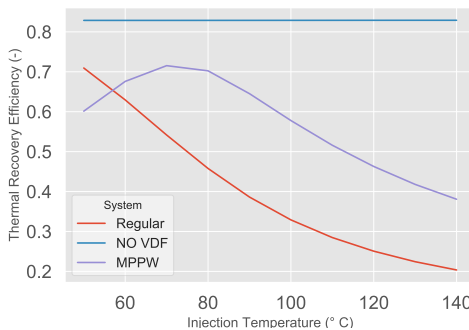
Figure D.12: Efficiency's

For the case where MPPW is applied, the slope shows initially an increase in slope Figure D.11. For the lower temperatures this increase occurs more gradually and for some show a sinus relation. But the higher the temperature, this increase is smaller and the following decrease is changing from more a sinus like relation to a linear relation. The efficiency of the MPPW is starting to be beneficial for temperature higher than 57.7 C, and has a maximum performance when 70 is injected. The largest benefit compared to a regular HT-ATES system is for the where 80 C is injected. This leads to a more than 20 % increase in thermal energy recovery.
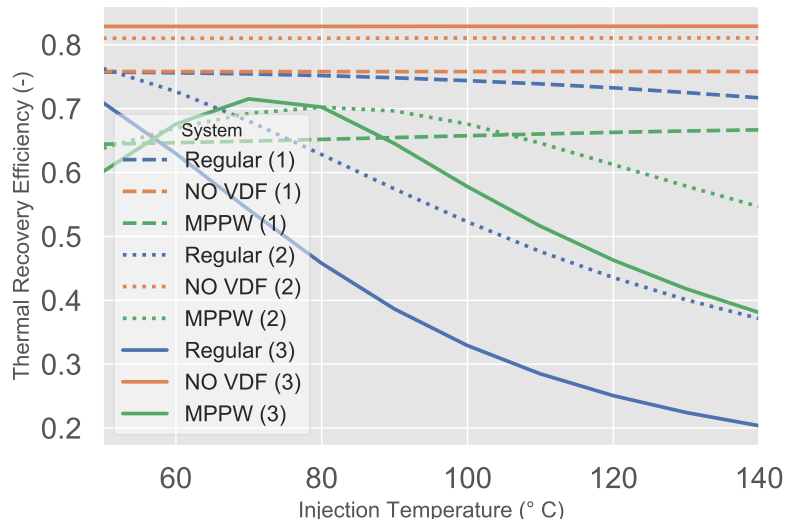
Figure D.13: Thermal recovery efficiency's for all cases.

Thermal Recovery Efficiency's

In Figure D.13 the thermal recovery efficiency for all the cases are plotted. It shows that a MPPW system under unfavorable aquifer properties for buoyancy flow performs similar to a regular HT-ATEs system under average properties. It can also be noted that for temperature between 60 C and C, it does not matter whether you have large or average hydraulic conductivity, storage volume and aquifer thickness.

D.2.2 Aquifer Thickness

BASE 1
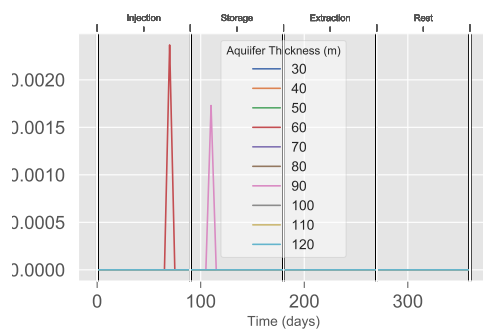
Figure D.14: No variable density flow.
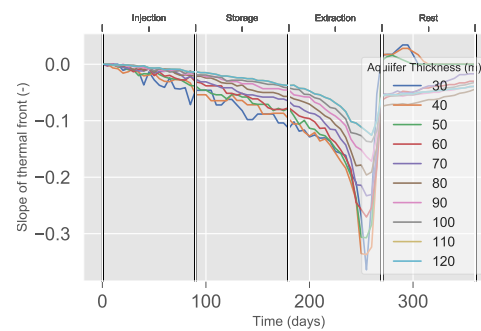
Figure D.15: Regular HT-ATES system.

Figure D.14 shows that the slope remains zero for all simulated aquifer thicknesses in this case where the operational and aquifer properties are low. Figure D.15 presents the slope over time for a regular HT-ATES system. The slope in the injection and extraction phase is linear. The slope of the slope change in time is steeper for smaller aquifer thicknesses. It can also be noted that the transition to the storage phase is smooth.
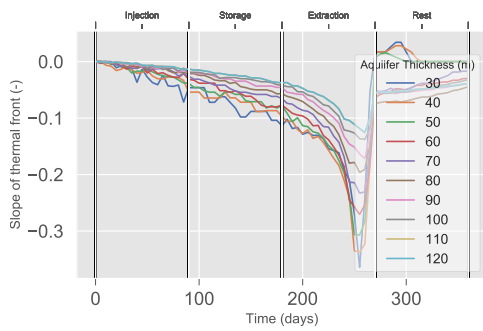
Figure D.16: MPPW
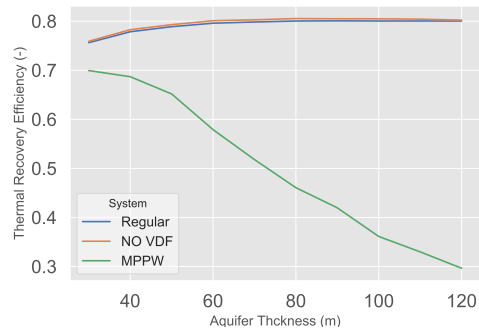
Figure D.17: Efficiency's

The slope increase is becoming less for increasing aquifer thickness for a system with two MPPW Figure D.16. It stabilizes in the storage to extraction period with very small changes in slope in time. However, the efficiency is decreasing when the aquifer thickness is increasing. This can be expected since the the hydraulic conductivity and injection temperature are low such that the what is not buoyant enough to reach the upper half of the aquifer. Figure D.17 shows the it is not beneficial to use MPPW for this case.

BASE 2
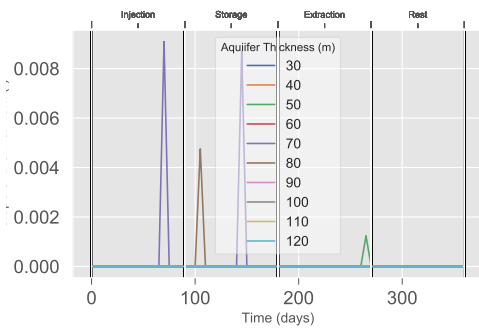
Figure D.18: No variable density flow.
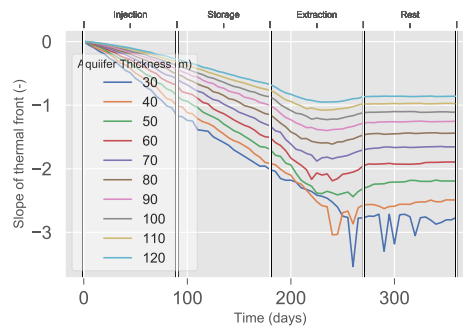
Figure D.19: Regular HT-ATES system.

Figure D.18 presents the slope over time for a system withou density driven flow. It presents that for this cases the slope of the thermal front is zero throughout the recovery cycle. The slope change in time for the regular case shows a linear relation, Figure D.19. The change of the slope in time is larger for smaller aquifer thicknesses in this case with average operational and aquifer properties.
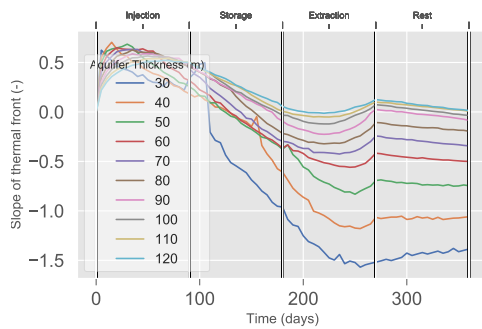
Figure D.20: MPPW
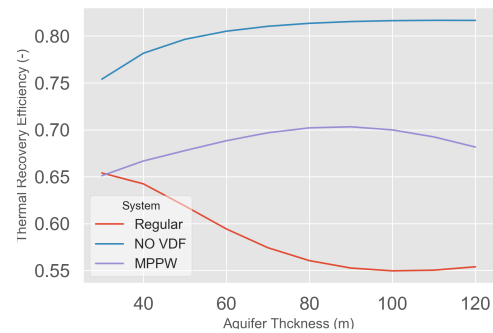
Figure D.21: Efficiency's

For a system with MPPW the slope is shows an increas in slope, the increase is steeper for smaller aquifer thickness. However, the decrease of slope is also steeper after it has reached it maximum slope. The efficiency of the regular HT-ATES system decreases with increasing aquifer thickness. While for a system with MPPW it initially increases with a maximum point at a thickness of 80m thereafter it decreases.

BASE 3

Figure D.22: No variable density flow.
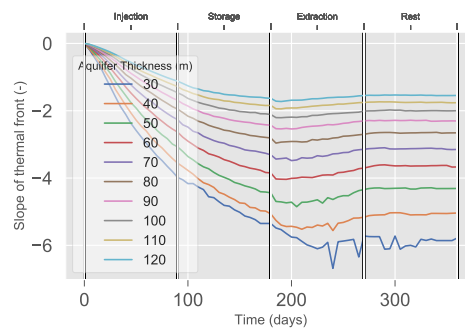
Figure D.23: Regular HT-ATES system.

Figure D.22 shows that the slope stays zero for this case with varying aquifer thickness. For the system with a regular HT-ATES system an exponential decrease of the slope can be found for in the injection and storage phase, see Figure D.23. This decay is faster for this case when the aquifer thickness is small. What can be noted is that when the extraction phase start the slope decay is stopped and the slope of the slope change is small, and almost zero for the three largest aquifer thickness. The difference between the relations is becoming smaller for larger aquifer thickness. This is especially notable in the rest phase.
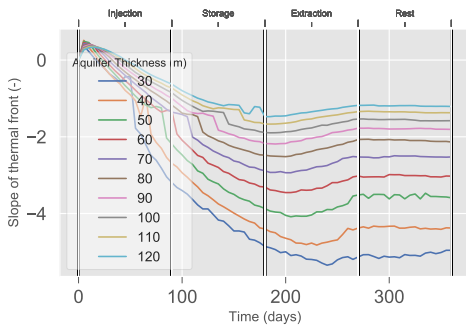
Figure D.24: MPPW
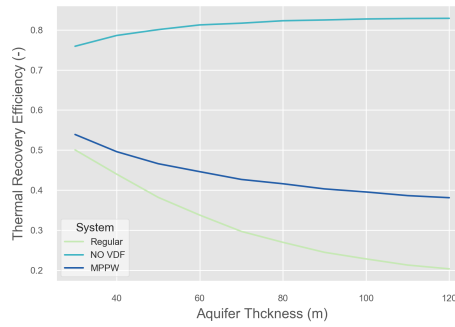
Figure D.25: Efficiency's

Figure D.24 presents the slope over time for a system with two MPPW. It shows a small increase in the slope before it decreases linearly. It shows a bump before decreasing more exponentially. Just like for the regular case, it can be seen that the slope change is smaller for larger aquifer thickness but the difference is becoming smaller. The efficiency of a regular HT-ATES system is decreasing with larger aquifer thickness, the same hold for a MPPW HT-ATES system whil for a theoretical system it increases. This is against the prospect that a smaller slope change leads to higher efficiency.

Thermal Recovery Efficiency's
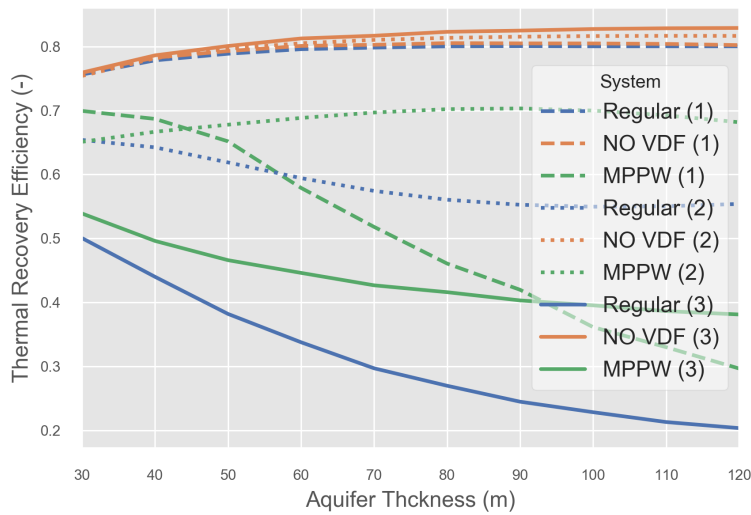
Figure D.26: Thermal recovery efficiency's for all cases.

Figure D.26 presents the thermal recovery efficiency for all three base cases and type of HT-ATES systems. It shows that the theoretical maximum for the systems start at the same point but diverge with the case of the large system leading the maximum followed by the average and the small system. This means that with a larger aquifer thickness the conduction losses decrease. For the last two base cases it shows an improvement of the system performance when implementing a two well MPPW.

D.2.3 Hydraulic Conductivity

BASE 1
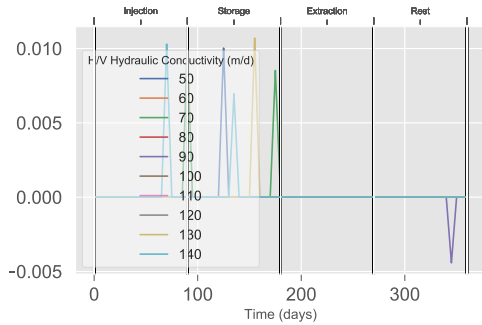
Figure D.27: No variable density flow
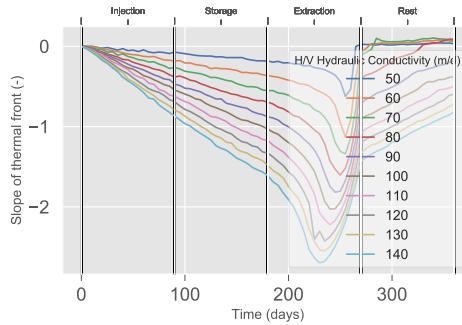
Figure D.28: Regular HT-ATES

Depicted in Figure D.27 is the slope for the case where no variable density driven flow is considered. In this case the slope stays zero throughout the recovery cycle. As can be seen in Figure D.28, the slope for a regular HT-ATES decreases linearly in the injection and storage phase. The decrease is faster for aquifers with larger hydraulic conductivity. In the extraction phase it continues decreasing until the minimum is reached and increases rapidly till the rest phase where it continues increasing but at a slower rate.
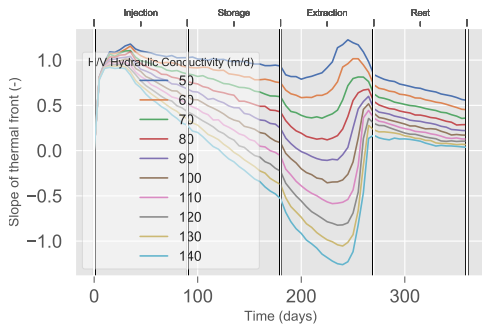
Figure D.29: MPPW
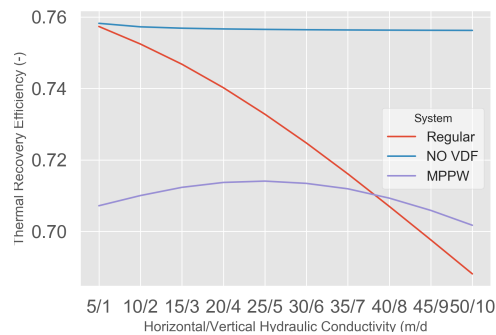
Figure D.30: Efficiency's

For the case where a system with MPPW is applied, the slope increases with the same shape as the rest phase of regular HT-ATES system with the wells reversed Figure D.29. Subsequently, it decrease linearly till the extraction phase where it shows a faster decrease till it increases again, after the linear decrease in the rest phase. The corresponding efficiency of these cases are presented in Figure D.30. It shows an intersection between the regular and the MPPW case between a hydraulic conductivity of 35 m/d and 40 m/d. Before this intersection the system with MPPW performed worse thant the regular system.

BASE 2
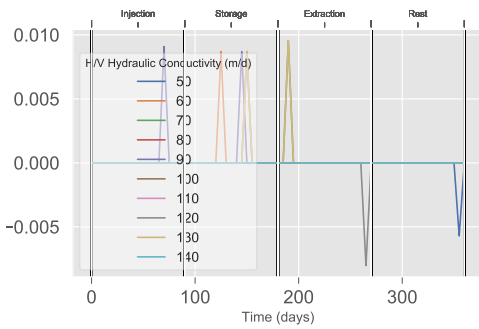
Figure D.31: No variable density flow
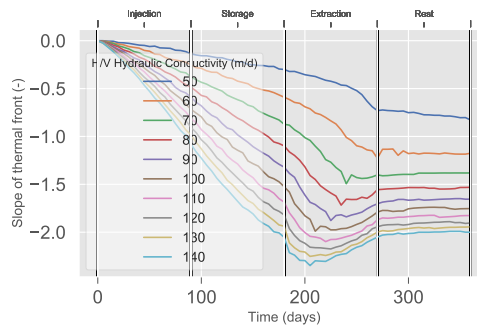
Figure D.32: Regular HT-ATES

For the average base case the slope of the system with no density driven flow is around zero for all hydraulic conductivity as can be seen in Figure D.31. Figure D.32 illustrates the slope for the regular HT-ATES system. The slope over time is decreasing linearly in the injection and storage phase. In the storage phase it continues the linear relation till it switches direction and becomes horizontal in the rest phase.
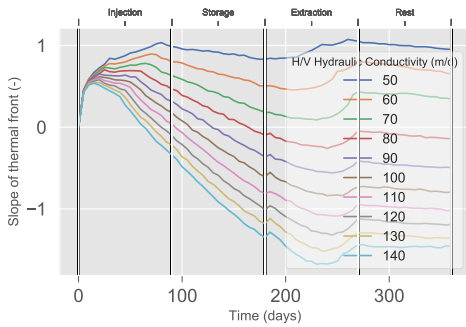
Figure D.33: MPPW
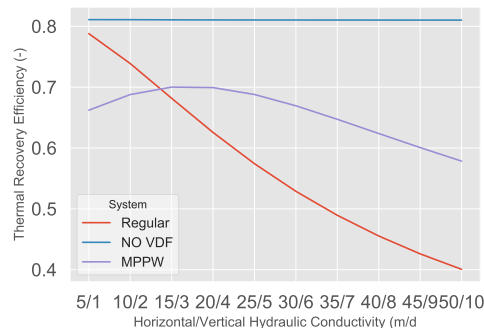
Figure D.34: Efficiency's

Figure D.33 presents the slope for the case with a MPPW HT-ASTES system. It can be noted that the slope initially increases before it starts decreasing. The cases where the hydraulic conductivity is low show a higher maximum positive slope. Another observation is the fact that the slope over time for the different cases are diverged compared to the regular system. The cases with a hydraulic conductivity of 15 m/d and 20 m/d are both close to a slope of zero. These two case have the highest recovery efficiency with a MPPW Figure D.34. The efficiency of a regular system decreases almost linearly with increasing hydraulic conductivity. However, for hydraulic conductivity between 5 m/d and 14 m/d a regular system shows a better performance with the lowest value approaching the theoretical maximum.

BASE 3
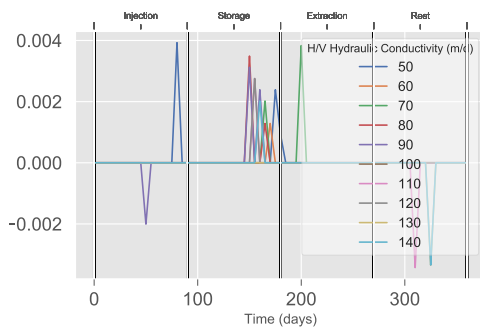
Figure D.35: No variable density flow
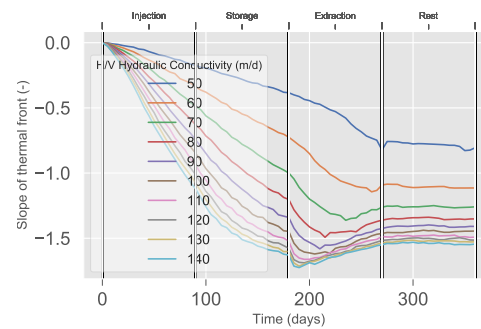
Figure D.36: Regular HT-ATES

The case where no variable density driven flow is considered the slope remains zero throughout the recovery cycle. This can be seen in Figure D.35. The regular HT-ATES system show a linear decreasing slope. However, this becomes more exponential with increasing hydraulic conductivity. The difference between the different cases is diminishing. It looks that this is also happening exponentially, see Figure D.36.
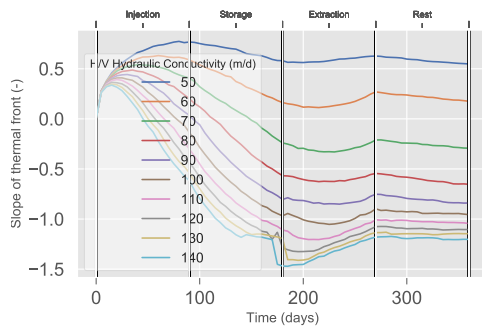
Figure D.37: MPPW
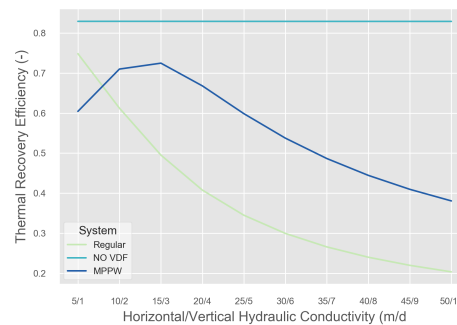
Figure D.38: Efficiency's

As can be seen in Figure D.37 the slope shows an increase in the beginning of the injection phase. The lower the hydraulic conductivity, the higher the maximum slope is before decreasing again. For the first two cases the decrease in slope happens in the storage phase. As for the regular case, the difference between the cases is decreasing with increasing hydraulic conductivity. The efficiency of this base case and varying hydraulic conductivity is presented in Figure D.38. As depicted the regular system has a higher efficiency in the beginning till the intersection. Following a maximum efficiency of the MPPW system at a hydraulic conductivity of 15 m/d. After this point the two lines show a same rate of decrease.

Thermal Recovery Efficiency

All the efficiency plots are merged in one plot presented in Figure D.39. It can be noted that the maximum point of BASE 3 with a MPPW is exceeding the other MPPW system and approaching the theoretical maximum of BASE 1.
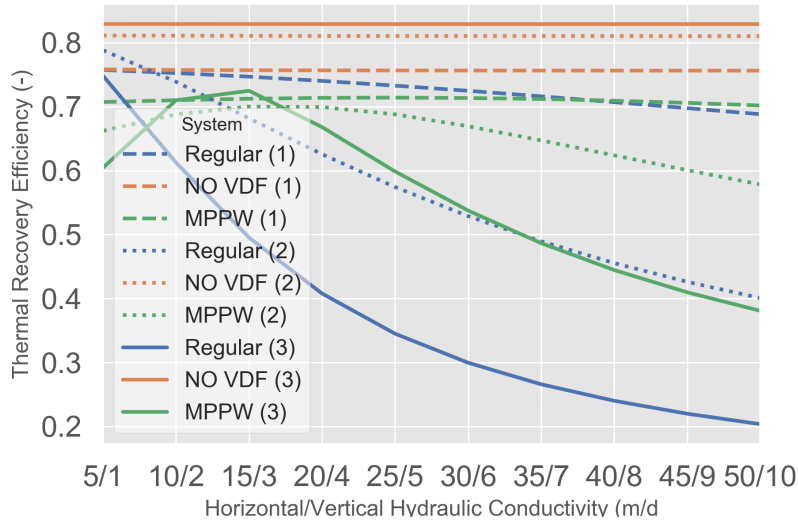
Figure D.39: Thermal recovery efficiency's for all cases.

D.2.4 Storage Volume

BASE 1
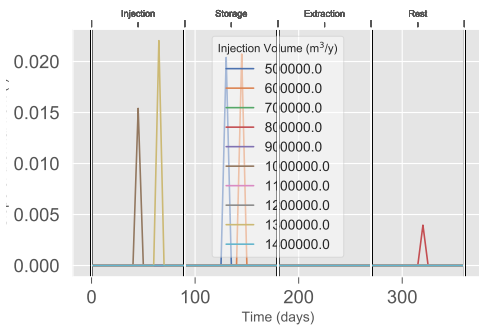
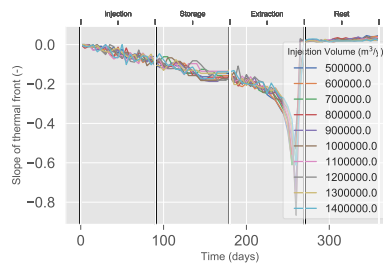Figure D.40: No variable density flow.

Figure D.41: Regular HT-ATES system.

The slope is zero throughout the recovery cycle for the case where no variable density drive flow is considered as can be seen in Figure D.40. The slope for the regular case decreases linearly over time in the injection and storage phase. It can be noted that the behaviour does not matter on the volume.
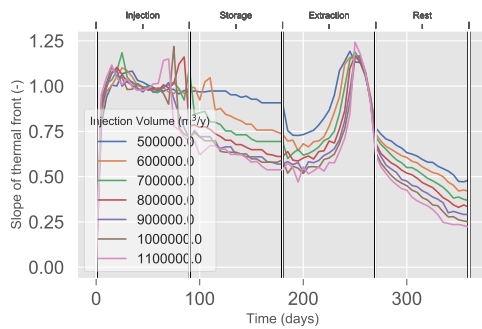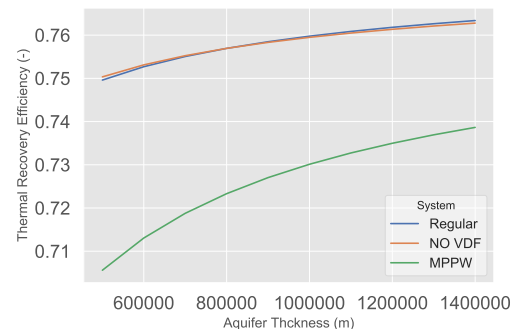
Figure D.42: MPPW

Figure D.43: Efficiency's

For the system with MPPW it does matter what volume is stored. However the difference for the different storage volumes decreases with increasing volume. It is interesting to notice that the slope does not become negative. The efficiency of the regular system is higher for all cases with the varying storage volumes. There is an increase however in the efficiency for higher volumes.

BASE 2
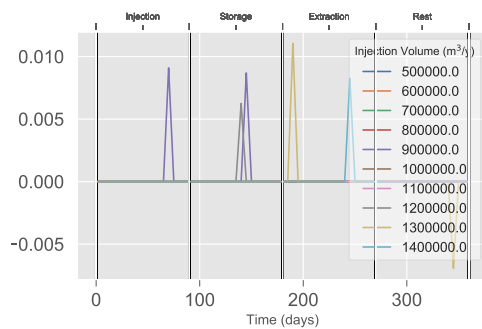
Figure D.44: No variable density flow.
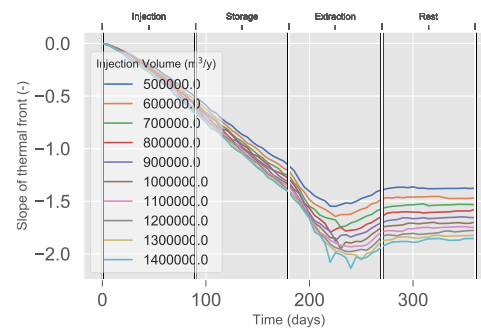
Figure D.45: Regular HT-ATES system.

The case with no variable density flow shows that the slope of the thermal front is zero (**??**). The regular cas, as shown in Figure D.45 shows aa linear decrease of the slope of the thermal front. It also shows that for this case the slope decrease until the storage does not matter on the storage.
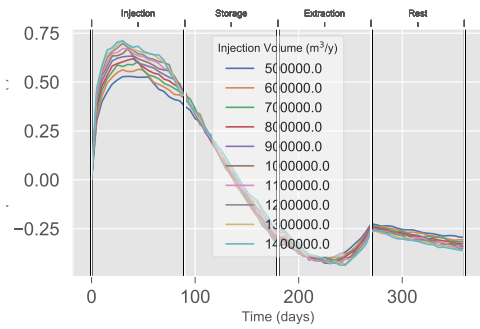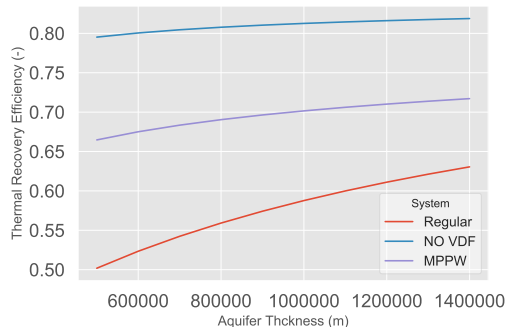
Figure D.46: MPPW

Figure D.47: Efficiency's

Figure D.46 presents the case for a system with MPPW. It shows a sinus relation, with a small increase and peak of the thermal front. The thermal recovery efficiency of the different cases are illustrated in Figure D.47. This plot shows that the performance of this base case is performing better in terms of efficiency than the regular case. However, it should be noted that the efficiency o the regular HT-ATES system increases faster for larger storage volumes than the system with MPPW.

BASE 3
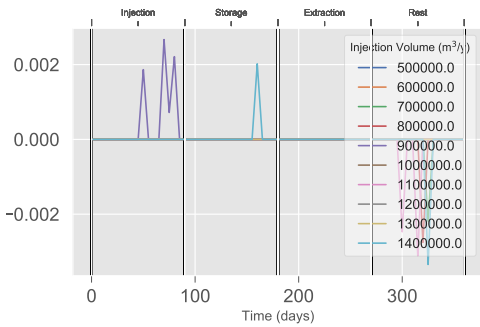
Figure D.48: No variable density flow.
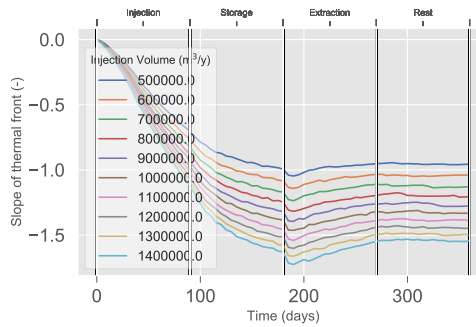
Figure D.49: Regular HT-ATES system.

As can be seen in Figure D.48 there is no slope for the theoretical system with no density driven flow. The regular system is shown in Figure D.49 and this shows that the slope is decreasing exponentially in time. The smaller volumes show a smaller slope decrease compared the larger storage volumes.
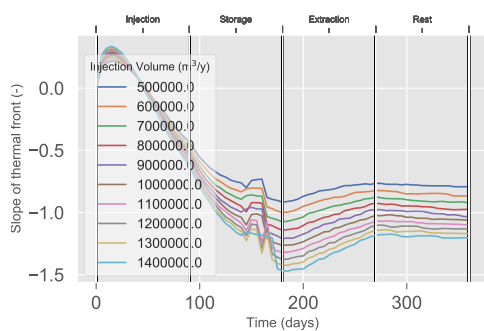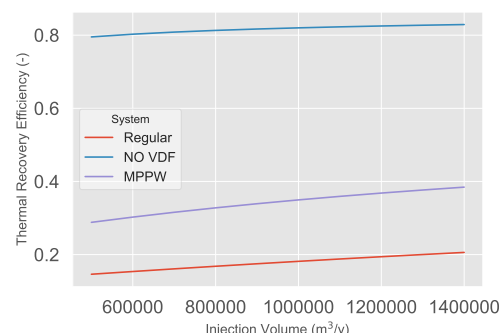
Figure D.50: MPPW

Figure D.51: Efficiency's

This is different for the case where MPPW is implemented which is illustrated in Figure D.50. During the injection and storage phase the slope changes are very similar for the different storage volumes. The efficiency for all three systems show a similar trend, with the MPPW system performing slightly better than the regular system
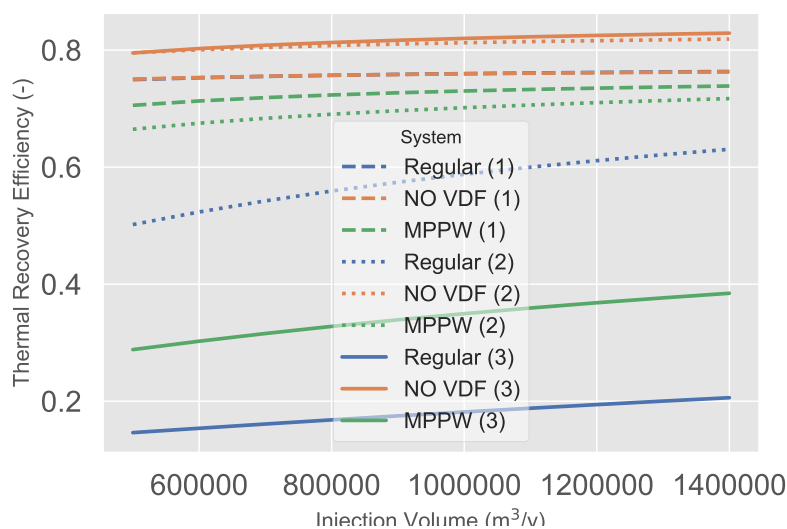

Figure D.52: Thermal recovery efficiency's for all cases.

Figure D.52 presents all the efficiency plots merged in one plot. It can be noted that all cases show the same trend for changing storage volumes.

D.2.5 Cases for Optimization

Table D.2 presents the cases for which the different monitoring and control methods were applied.

Table D.2: Efficiency of the extracted cases from Section D.2

Case	1	2	3	4	Worst Case
T_{inj}	**80**	140	90	90	140
H	120	120	**90**	70	120
k_{h}/k-{v}	50/10	**15/3**	25/5	25/5	50/10
V	1.4^-6	1.4^-6	9^-5	**5^{-5}**	1.4^{-6}
Regular	0.46	0.50	0.55	0.50	0.20
Theoretical Max.	0.83	0.83	0.81	0.80	
2 well no monitor	0.70	0.69	0.70	0.66	0.38
Monitor	0.73	0.75	0.74	0.70	0.51

As can be seen, for all the cases the eventual difference with the theoretical maximum is about 10 %.

E. Temp. dependent water properties

When using super-heated water (>100 °C) there needs to be sufficient pressure to keep it in the liquid phase. This is called the saturation pressure. Figure E.2 illustrates the required pressure for a certain temperature water. It shows that with the right pressure (around 1000 kPa) water of 300 °C can be reached in liquid phase.
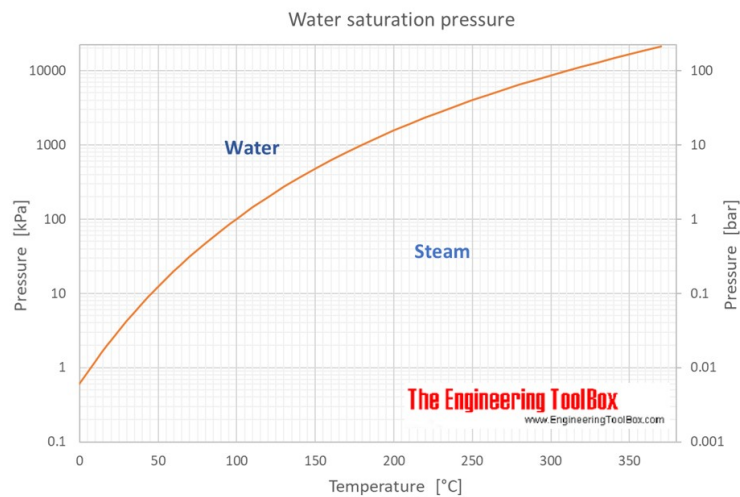

Figure E.1: Saturation pressure and temperature relation (ToolBox 2004a)
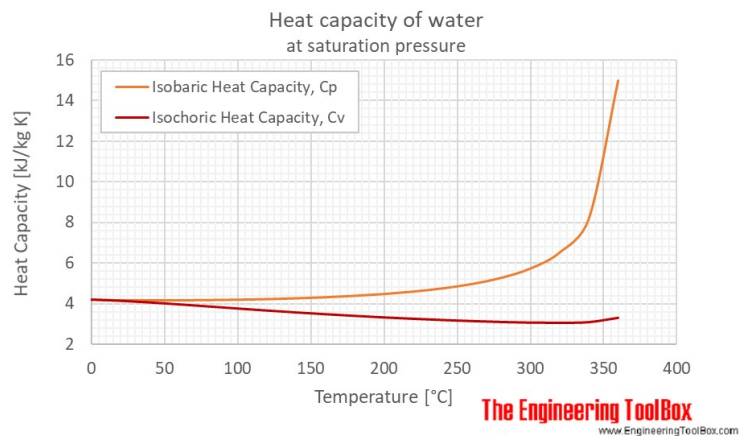
- 1 kPa = 0.1m of water

Figure E.2: Heat capacity and temperature relation (ToolBox 2004b)